A Species-Level Timeline of Mammal Evolution Integrating Phylogenomic Data

Sandra Álvarez-Carretero[†1,2], Asif U. Tamuri[†3,4], Matteo Battini[5], Fabrícia F. Nascimento[6], Emily Carlisle[5], Robert J. Asher[7], Ziheng Yang[2], Philip C. J. Donoghue[5], and Mario dos Reis[1].

† These authors contributed equally

Correspondence to: m.dosreisbarros@qmul.ac.uk and phil.donoghue@bristol.ac.uk.

[1] School of Biological and Behavioural Sciences, Queen Mary University of London, London, UK.
[2] Department of Genetics, Evolution, and Environment, University College London, London, WC1E 6BT, UK.
[3] Centre for Advanced Research Computing, University College London, Gower St, London, WC1E 6BT, UK.
[4] EMBL-EBI, Wellcome Genome Campus, Hinxton, Cambridgeshire, CB10 1SD, UK
[5] School of Earth Sciences, University of Bristol, Life Sciences Building, Tyndall Avenue, Bristol, BS8 1TQ, UK.
[6] MRC Centre for Global Infectious Disease Analysis, School of Public Health, Imperial College London, London, UK.
[7] Department of Zoology, University of Cambridge, Downing Street, Cambridge, CB2 3EJ, UK.

Abstract

High-throughput sequencing projects generate genome-scale sequence data for species-level phylogenies[1–3]. However, state-of-the-art Bayesian methods for inferring timetrees are computationally limited to small datasets and cannot exploit the deluge of new genomes[4]. In the case of mammals, molecular-clock analyses of limited datasets have produced conflicting estimates of clade ages with large uncertainties[5,6] and, thus, the timescale of placental mammal evolution remains contentious[7–10]. Here we develop a Bayesian molecular-clock dating approach to estimate a timetree of 4,705 mammal species integrating information from 72 mammal genomes. We show increasingly larger phylogenomic datasets produce diversification time estimates with progressively smaller uncertainties, facilitating precise tests of macroevolutionary hypotheses. For example, we confidently reject an explosive model of placental mammal origination in the Paleogene[8] and show crown Placentalia originated in the Late Cretaceous with unambiguous ordinal diversification in the Paleocene/Eocene. Our new Bayesian methodology facilitates analysis of complete genomes and thousands of species within an integrated framework, making it possible to address hitherto intractable research questions on species diversifications. As such, our approach can be used to tackle other contentious cases of animal and plant diversifications that require analysis of species-level phylogenomic datasets.

Main

High-throughput sequencing projects are generating hundreds[1] to thousands[2] of genome sequences, with imminent plans to sequence more than a million species[11]. However, the accumulation of sequenced genomes is now outpacing the analytical capacity of computer software and many of the tools required to extract information from these vast datasets are lacking[12]. This is particularly the case for Bayesian Markov Chain Monte Carlo (MCMC) molecular-clock methods that are used routinely to infer evolutionary timescales[4], for groups as diverse as pathogens[13], plants[14], and animals[15], but which are computationally expensive. Consequently, these methods have been limited in their application to datasets comprising dozens of genes for many species[5,16] or many genes for dozens of species[7,17], constraining the scope of evolutionary questions that can be addressed.

Although fast non-Bayesian clock-dating methods have been developed[18], these typically do not incorporate uncertainties on evolutionary branch lengths[19] or arbitrary fossil calibration densities[20,21]. On the other hand, the Bayesian approach, despite its computational expense, is appealing because it facilitates explicit integration of these uncertainties[4]. Furthermore, large genomic datasets allow inference of precise timelines that can be used to obtain correlations between diversification events and the geological and climatic evolution of our planet[4]. Although increased precision of estimates is not a guarantee the estimates will be more accurate (particularly if errors in fossil calibrations or in the clock model are present, in which case the estimates may be biased[21,22]), statistical theory shows that, when the prior and model are appropriate, Bayesian estimates of clade ages using genomic data will converge to a limiting distribution centred on their true values[20,22,23].

The limitations of Bayesian molecular-clock analyses on small datasets have become starkly apparent in studies of mammal diversification. Bayesian estimates using few genes typically have uncertainties so large that credibility intervals on the ages of ordinal crown-groups straddle a mid-Cretaceous to Paleogene interval[5,6,24,25], despite a decidedly post-K-Pg fossil record of ordinal crown groups[26–29]. Critically, these Bayesian estimates cannot help to discriminate among competing scenarios of mammal diversification with respect to the K-Pg mass extinction[30–32]. Although Bayesian analyses have been carried out on genome-scale datasets[7,33,34], only a small number of taxa have been used and, therefore, the increased precision of phylogenomic analyses has not been propagated through to species-level mammal phylogenies. Thus, despite several decades of research, the precise timeline of mammal evolution remains unresolved[5–9,34].

Furthermore, efforts to incorporate species-level alignments into the Bayesian analysis of mammals have been unsatisfactory. For example, in the backbone-and-patch approach, a limited number of genes is used to estimate divergence times on a main tree of few species[6]. Divergence times for key nodes are then used to calibrate the root of densely sampled subtrees, resulting in a species-level phylogeny. However, the backbone-and-patch method is not a valid Bayesian approach because the loci used in subtree estimation are the same loci used to estimate the main tree, resulting in duplicate use of the same data and a squaring of the likelihood[35]. In Bayesian clock-dating, likelihood squaring leads to convergence to the wrong limiting distribution of node ages[23,36].

Sequential Bayesian dating of subtrees

Here we overcome the limitations of previous Bayesian clock-dating studies on small datasets by developing the Bayesian sequential-subtree approach (Fig. 1), which we use to infer a timetree of 4,705 mammal species. First, a genome-scale alignment (15,268 one-to-one orthologs, 33.2M aligned bases) and a suite of 32 fossil calibrations are used to infer the timetree for 72 species. The resulting posterior distribution of node ages is then used, together with a further set of 60 fossil calibrations, to date 13 subtrees encompassing 4,705 species with new alignments (182 loci, up to 5.33 x 10^5 aligned bases), thus avoiding data duplication in the likelihood (see Methods). Our approach is feasible because we use the approximate likelihood calculation[37], which provides a 1,000x speed-up over traditional MCMC timetree inference without loss of accuracy[37,38]. This facilitates analysis of more taxa and much longer alignments than has been possible previously (Table 1). By using the flexible Skew-*t* and Skew-normal distributions to model the posterior time estimates from the 72-genome analysis, we accurately transfer information from the genome-scale analysis into the subtree analysis[35], augmented by the additional subtree-specific fossil calibrations. Our fossil calibrations restrict the minimum ages of clades based on the oldest unequivocal members of crown groups and, in most cases, also their maximum age through consideration of the presence and absence of stem and sister groups, their palaeoecology, palaeobiogeography, and comparative taphonomy[39] (see Supplementary Information).

Analyses of small phylogenies[36] and simulated data[23,36] indicate that genome-scale data should lead to asymptotic reduction of uncertainty in divergence time estimates. We demonstrate this for our mammal data by performing random sampling of loci and calculating divergence times on the 72-species phylogeny. By increasing the number of loci analysed from 1 to 15K, uncertainties in time estimates are progressively reduced irrespective of the relaxed-clock model used (Fig. 2a). Average relative uncertainty on node ages stabilises at 23.6%-25.0% for the 15K loci. This means that, for each 1 Myr of divergence, ~250 Kyr of uncertainty is added to the width of the credibility intervals, which is substantially less than previous Bayesian analyses based on a limited number of genes[5,6] (Table 1). Although reduction in uncertainty is modest beyond 1,000 loci (Fig. 2a), the analysis of the full dataset comes with little extra computational cost because the approximate likelihood calculation depends on the number of taxa, not the alignment length[37].

We next assessed the fit of the relaxed-clock models by using the stepping-stones integrator[40]. This is critical because the competing autocorrelated (geometric Brownian motion or GBM[23,41]) and independent log-normal (ILN[23,42]) rate models can produce dramatically different time estimates when using the same fossil calibrations[35]. Clock-model testing has not previously been conducted at large scale because marginal likelihood inference requires expensive exact likelihood calculation. We overcame this problem by implementing stationary block resampling[43] to obtain reliable estimates of the standard error of the log-marginal likelihood estimates. In this way, we can guarantee the MCMC sample is large enough to obtain an acceptable error for calculating the posterior probabilities of the clock models. We find that, for 71.3% of the 645 loci analysed (Fig. 2b), GBM has a posterior probability >95%, whereas ILN has a posterior >95% for only 10.7% of loci.

Some topological relationships among major groups of mammals, such as the placement of the placental root, the position of Scandentia with respect to Primates and Glires, and the position of several major groups within Laurasiatheria (Carnivora, Perissodactyla, Chiroptera

and Artiodactyla), have been difficult to resolve[32,33,44]. We selected seven re-arrangements of these major groups and estimated the divergence times using the 15K loci and the 72-species phylogeny. We find these topological re-arrangements have a marginal effect on estimated divergence times (Fig. 2c), apparently because these topological uncertainties are characterised by small internal branches.

High-resolution timeline of mammal evolution

Using the results from the 72-genome analysis, we then proceeded with the sequential-subtree approach to date the 4,705-species phylogeny using the GBM rate model. The resulting species-level timetree (Fig. 3a) provides a high-resolution timeline for the diversification of mammals, a timeline with substantially less uncertainty than has been characteristic of previous Bayesian studies, facilitating tests of competing models of ordinal diversification. With this timetree, we have effected the advances set out by Murphy and colleagues[32] to improve the estimated timescale of mammalian evolution, viz. (a) 'more contiguous and accurate genome alignments that improve upon detection of orthologous sequences'[45], (b) 'improvements in the calibration of nodes with fossils'[21,35], and (c) 'improvements in relaxed-clock methodologies'[35,43]. Furthermore, we have also assessed asymptotics and topological uncertainty to address their impact on the estimated timescale. Generally, we find that, in comparison to previous analyses, clade age estimates are younger and more precise. It appears unlikely, given our asymptotic results (Fig. 2a), that a further increase in precision could be achieved simply by greater sampling of sequence data. Instead, more precise fossil constraints will have a material impact here.

Our results, in comparison to previous studies, show a greater proximity between the origination of ordinal level crown-groups and the K-Pg event (Fig. 3a, Extended Data Fig. 1-2), implying a late Cretaceous prehistory to 'modern mammals' with diversification that continued into the Paleogene (Fig. 3b). This timescale is incompatible with previous scenarios positing a deep-Cretaceous origin of ordinal level crown placental groups[46], and also incompatible with the explosive model, which envisages crown Placentalia originating in the Paleogene[8]. Among proposed mammal diversification models[32], our timetree appears compatible with the soft explosive[10] and long fuse[31] models. However, discriminating among these is challenging because, as formulated[32], these hypotheses lack taxonomic precision. We find crown Placentalia diverged 83.3-77.6 Ma, while the fundamental clades (Boreoeutheria, Laurasiatheria, and Euarchontoglires) diverged within the last ~10 Myr of the Cretaceous. Furthermore, 17 out of 18 crown placental orders and all crown marsupial orders originated after the K-Pg (Fig. 2a), indicating the bulk of extant mammal ordinal diversity is a post-K-Pg phenomenon. In terms of inter-ordinal diversity, our results are compatible with both (i) an origin of placental inter-ordinal crown clades following the profound K-Pg extinction in which few lineages survived; and (ii) diverse inter-ordinal stem-lineage representatives surviving the K-Pg extinction, but with this diversity later pared back (due to later extinctions) to the current crown-clades which diverged after the K-Pg. Reconciling these competing hypotheses will require integrated co-analysis of living and fossil species[47], to reveal the diversification dynamics that resulted in extant mammal diversity.

Efficient computing in the genomics era

The species-level MCMC sampling required about 80K hours of computing time in a high-performance computing cluster and released ~16.7K metric tonnes of CO_2[48]. Without the technological improvements used here, these analyses would have required hundreds of years of CPU time and emitted over 1.9M tonnes of CO_2 (see Supplementary Information). By using existing tools and combining them in a novel way within the sequential-subtree approach, we have demonstrated that hierarchical Bayesian analysis of species-level timetrees integrating genomes is now feasible. Thus, the methodology developed here can be used to tackle other contentious cases of species diversification that, so far, have been analysed using limited datasets. By integrating our method with the million and more genomes currently planned for sequencing[11], the prospect of obtaining a reliable evolutionary timescale for the entirety of the tree of life now appears within reach.

Code availability

A repository containing instructions to reproduce the analyses is available at http://github.com/sabifo4/mammals_dating (DOI: 10.5281/zenodo.5736629). The MCMCtree software and mcmc3r R package are freely available from http://abacus.gene.ucl.ac.uk/software/paml.html and https://github.com/dosreislab respectively.

Data availability

All data required to reproduce the analyses are available at DOI: 10.6084/m9.figshare.14885691.

Acknowledgements

We thank James Gilbert and Chris G Faulkes for help with the Rodentia subtrees. This work used computing resources from Queen Mary's Apocrita HPC and University College London Myriad HPC facilities. This work was supported by Biotechnology and Biological Sciences Research Council, UK, awards BB/T01282X/1, BB/T012951/1, and BB/T012773/1.

Author contributions

M.d.R. conceived the work. M.d.R, Z.Y., P.C.J.D., S.A.C. and A.U.T. designed the analysis. S.A.C., A.U.T., R.J.A., P.C.J.D., M.B., E.C. and F.F.N. compiled, processed and verified the molecular and fossil data. S.A.C., A.U.T. and M.d.R. analysed the data. M.d.R. and P.C.J.D. wrote the paper with input from all authors.

Competing Interests

The authors declare no competing interests.

Corresponding Authors

Correspondence to M.d.R. m.dosreisbarros@qmul.ac.uk and P.C.J.D. phil.donoghue@bristol.ac.uk.

References

1 Zoonomia Consortium. A comparative genomics multitool for scientific discovery and conservation. *Nature* 2020; **587**: 240–245.

2 Feng S, Stiller J, Deng Y, Armstrong J, Fang Q, Reeve AH *et al.* Dense sampling of bird diversity increases power of comparative genomics. *Nature* 2020; **587**: 252–257.

3 Harvey MG, Bravo GA, Claramunt S, Cuervo AM, Derryberry GE, Battilana J *et al.* The evolution of a tropical biodiversity hotspot. *Science* 2020; **370**: 1343–1348.

4 dos Reis M, Donoghue PCJ, Yang Z. Bayesian molecular clock dating of species divergences in the genomics era. *Nat Rev Genet* 2016; **17**: 71–80.

5 Meredith RW, Janečka JE, Gatesy J, Ryder OA, Fisher CA, Teeling EC *et al.* Impacts of the Cretaceous Terrestrial Revolution and KPg extinction on mammal diversification. *Science* 2011; **334**: 521–524.

6 Upham NS, Esselstyn JA, Jetz W. Inferring the mammal tree: Species-level sets of phylogenies for questions in ecology, evolution, and conservation. *PLoS Biol* 2019; **17**: e3000494.

7 dos Reis M, Inoue J, Hasegawa M, Asher RJ, Donoghue PCJ, Yang Z. Phylogenomic datasets provide both precision and accuracy in estimating the timescale of placental mammal phylogeny. *Proc Biol Sci* 2012; **279**: 3491–3500.

8 O'Leary MA, Bloch JI, Flynn JJ, Gaudin TJ, Giallombardo A, Giannini NP *et al.* The placental mammal ancestor and the post-K-Pg radiation of placentals. *Science* 2013; **339**: 662–667.

9 dos Reis M, Donoghue PC, Yang Z. Neither phylogenomic nor palaeontological data support a Palaeogene origin of placental mammals. *Biol Lett* 2014; **10**: 20131003.

10 Phillips MJ. Geomolecular Dating and the Origin of Placental Mammals. *Syst Biol* 2016; **65**: 546–557.

11 Lewin HA, Robinson GE, Kress WJ, Baker WJ, Coddington J, Crandall KA *et al.* Earth BioGenome Project: Sequencing life for the future of life. *Proc Natl Acad Sci U S A* 2018; **115**: 4325–4333.

12 Siepel A. Challenges in funding and developing genomic software: roots and remedies. *Genome Biol* 2019; **20**: 147.

13 Faria NR, Rambaut A, Suchard MA, Baele G, Bedford T, Ward MJ *et al.* The early spread and epidemic ignition of HIV-1 in human populations. *Science* 2014; **346**: 56–61.

14 Ramírez-Barahona S, Sauquet H, Magallón S. The delayed and geographically heterogeneous diversification of flowering plant families. *Nat Ecol Evol* 2020; **4**: 1232–1238.

15 Whelan NV, Kocot KM, Moroz TP, Mukherjee K, Williams P, Paulay G *et al.* Ctenophore relationships and their placement as the sister group to all other animals. *Nat Ecol Evol* 2017; **1**: 1737–1746.

16 Misof B, Liu S, Meusemann K, Peters RS, Donath A, Mayer C *et al.* Phylogenomics resolves the timing and pattern of insect evolution. *Science* 2014; **346**: 763–767.

17 Jarvis ED, Mirarab S, Aberer AJ, Li B, Houde P, Li C *et al.* Whole-genome analyses resolve early branches in the tree of life of modern birds. *Science* 2014; **346**: 1320–

1331.

18 Tao Q, Tamura K, Kumar S. Efficient Methods for Dating Evolutionary Divergences. In: Ho SYW (ed). *The Molecular Evolutionary Clock: Theory and Practice*. Springer International Publishing: Cham, 2020, pp 197–219.

19 Thorne JL, Kishino H. Estimation of divergence times from molecular sequence data. In: Nielsen R (ed). *Statistical methods in molecular evolution*. Springer Verlag, 2005, pp 235–256.

20 Yang Z, Rannala B. Bayesian estimation of species divergence times under a molecular clock using multiple fossil calibrations with soft bounds. *Mol Biol Evol* 2006; **23**: 212–226.

21 Inoue J, Donoghue PCJ, Yang Z. The impact of the representation of fossil calibrations on Bayesian estimation of species divergence times. *Syst Biol* 2010; **59**: 74–89.

22 dos Reis M, Zhu T, Yang Z. The impact of the rate prior on Bayesian estimation of divergence times with multiple Loci. *Syst Biol* 2014; **63**: 555–565.

23 Rannala B, Yang Z. Inferring speciation times under an episodic molecular clock. *Syst Biol* 2007; **56**: 453–466.

24 Springer MS, Murphy WJ, Eizirik E, O'Brien SJ. Placental mammal diversification and the Cretaceous-Tertiary boundary. *Proc Natl Acad Sci U S A* 2003; **100**: 1056–1061.

25 Hasegawa M, Thorne JL, Kishino H. Time scale of eutherian evolution estimated without assuming a constant rate of molecular evolution. *Genes Genet Syst* 2003; **78**: 267–283.

26 Alroy J. The fossil record of North American mammals: evidence for a Paleocene evolutionary radiation. *Syst Biol* 1999; **48**: 107–118.

27 Benton MJ. Early origins of modern birds and mammals: Molecules vs. morphology. *Bioessays* 1999; **21**: 1043–1051.

28 Hunter JP, Janis CM. Spiny Norman in the Garden of Eden? Dispersal and early biogeography of Placentalia. *J Mamm Evol* 2006; **13**: 89–123.

29 Luo ZX. Transformation and diversification in early mammal evolution. *Nature* 2007; **450**: 1011–1019.

30 Cooper A, Fortey R. Evolutionary explosions and the phylogenetic fuse. *Trends Ecol Evol* 1998; **13**: 151–156.

31 Archibald JD, Deutschman DH. Quantitative analysis of the timing of the origin and diversification of extant placental orders. *J Mamm Evol* 2001; **8**: 107–124.

32 Murphy WJ, Foley NM, Bredemeyer KR, Gatesy J, Springer MS. Phylogenomics and the Genetic Architecture of the Placental Mammal Radiation. *Annu Rev Anim Biosci* 2021; **9**: 29–53.

33 Tarver JE, dos Reis M, Mirarab S, Moran RJ, Parker S, O'Reilly JE *et al.* The interrelationships of placental mammals and the limits of phylogenetic inference. *Genome Biol Evol* 2016; **8**: 330–344.

34 Liu L, Zhang J, Rheindt FE, Lei F, Qu Y, Wang Y *et al.* Genomic evidence reveals a radiation of placental mammals uninterrupted by the KPg boundary. *Proc Natl Acad Sci U S A* 2017; **114**: E7282–E7290.

35 dos Reis M, Gunnell GF, Barba-Montoya J, Wilkins A, Yang Z, Yoder AD. Using phylogenomic data to explore the effects of relaxed clocks and calibration strategies on divergence time estimation: Primates as a test case. *Syst Biol* 2018; **67**: 594–615.

36 dos Reis M, Yang Z. The unbearable uncertainty of Bayesian divergence time estimation. *J Syst Evol* 2013; **51**: 30–43.

37 dos Reis M, Yang Z. Approximate likelihood calculation on a phylogeny for Bayesian estimation of divergence times. *Mol Biol Evol* 2011; **28**: 2161–2172.

38 Battistuzzi FU, Billing-Ross P, Paliwal A, Kumar S. Fast and slow implementations of relaxed-clock methods show similar patterns of accuracy in estimating divergence times. *Mol Biol Evol* 2011; **28**: 2439–2442.

39 Donoghue PCJ, Yang Z. The evolution of methods for establishing evolutionary timescales. *Philos Trans R Soc Lond B Biol Sci* 2016; **371**: 20160020.

40 Xie W, Lewis PO, Fan Y, Kuo L, Chen M-H. Improving marginal likelihood estimation for Bayesian phylogenetic model selection. *Syst Biol* 2011; **60**: 150–160.

41 Thorne JL, Kishino H, Painter IS. Estimating the rate of evolution of the rate of molecular evolution. *Mol Biol Evol* 1998; **15**: 1647–1657.

42 Drummond AJ, Ho SYW, Phillips MJ, Rambaut A. Relaxed phylogenetics and dating with confidence. *PLoS Biol* 2006; **4**: 699–710.

43 Politis DN, Romano JP. The Stationary Bootstrap. *J Am Stat Assoc* 1994; **89**: 1303–1313.

44 Nishihara H, Maruyama S, Okada N. Retroposon analysis and recent geological data suggest near-simultaneous divergence of the three superorders of mammals. *Proc Natl Acad Sci U S A* 2009; **106**: 5235–5240.

45 Wheeler TJ, Eddy SR. nhmmer: DNA homology search with profile HMMs. *Bioinformatics* 2013; **29**: 2487–2489.

46 Bininda-Emonds OR, Cardillo M, Jones KE, MacPhee RD, Beck RM, Grenyer R *et al.* The delayed rise of present-day mammals. *Nature* 2007; **446**: 507–512.

47 Louca S, Pennell MW. Extant timetrees are consistent with a myriad of diversification histories. *Nature* 2020; **580**: 502–505.

48 Zwart SP. The ecological impact of high-performance computing in astrophysics. *Nature Astronomy* 2020; **4**: 819–822.

49 Springer MS, Stanhope MJ, Madsen O, de Jong WW. Molecules consolidate the placental mammal tree. *Trends Ecol Evol* 2004; **19**: 430–438.

50 The Paleobiology Database. https://paleobiodb.org/.

Table 1. Comparison of molecular-clock dating studies of mammal divergences.

Study[a]	Taxa in molecular alignment[b]	Genes[c]	Alignment length[d]	Crown Mammalia[e]	Placentalia[e]	No. placental crown orders originating in K / in Pg
Bininda-Emonds et al. (2007)[46]	2,182	66	51,089	166.2 (fixed)	108.7–93.9	9/7
Meredith et al. (2011)[5]	**164**	**26**	**35,603**	**238.2–203.3**	**116.8–92.1**	**7/10**
dos Reis et al. (2012)[7]	**274 (36)**	**12 (14,632)**	**7,370 (20.6×10^6)**	**191.9–174.1**	**90.4–87.9**	**2/10**
O'Leary et al. (2013)[8]	46	27	36,860	167.7–164.7	64.85 (fixed)	0/14
Upham et al. (2019)[6]	**4,098**	**31**	**39,099**	**210.9–166.7**	**105.0–77.4**	**9/9**
This study	**4,705 (72)**	**182 (15,268)**	**> 10^4 (33.2×10^6)**	**251–165**	**83.3–77.6**	**1/17**

a. Bayesian studies are shown in bold typeface.
b,c. Numbers in brackets are the number of complete genomes in the alignment (b), and number of genes for the genome-scale part of the alignment (c).
d. Numbers in brackets are the number of nucleotide sites for the genome-scale part of the alignment. In this study, subtree alignment lengths range from 5.11×10^4 to 5.33×10^5 bases. Missing data range from 46% to 60% in the genomic partitions and from 17% to 99% in the subtree partitions (see Methods).
e. Age in Mega annum (Ma) given as the 95% credibility/confidence interval.

Figure 1. Summary of the Bayesian sequential subtree dating approach. The pipeline is divided into molecular data preparation (blue), dating step 1 (green) and dating step 2 (orange). Number of taxa ranges from 10 to 72 among genomic loci (50% of loci have at least 67 taxa and 90% at least 53 taxa), and from 48 to 3,986 in the 182 gene set. A hidden-Markov model (HMM)[45] was used to detect homology and construct the subtree alignments, thus bypassing unreliable homology annotations (see Methods). SN and ST: Skew-normal and Skew-*t* distributions.

Figure 2. Bayesian estimation of mammal divergence times. a, Relative uncertainty in Bayesian estimates of node ages (defined as 95% credibility interval width divided by the posterior mean) is plotted against the number of loci for two relaxed-clock models. Sets of n = 1, 10, 30, 50, 100, and 1,000 loci were sampled randomly from the full set of 15K loci (also included) and grouped into four partitions (except for n = 1), with times estimated using approximate likelihood calculation in MCMCtree. **b**, Among the 15K loci, 645 loci have all 72 species present. These loci were used to estimate posterior probabilities for the two relaxed-clock models using exact likelihood and the stepping-stones integrator. The histogram of Pr(GBM | D) is shown with black outline, and the 95% confidence interval of the histogram, obtained using the stationary block bootstrap, are shown in a blue shade. Vertical black bars are results for individual loci. **c**, Seven dated variations of the mammal topology. T1-T5 have the Atlantogenata rooting of Placentalia[44,49].

Figure 3. Timetree of 4,705 mammal species. a, Times are estimated with MCMCtree[23] using approximate likelihood[37]. Black bars indicate the 95% HPD CI of node ages (in Ma), with nodes plotted at the posterior means. **b**, Lineages through time plot (black line) with 95% CI (dotted lines),

number of extinct mammal species, mammal genera, and eutherian genera through time (mined from PaleoDB[50]) are shown.

Extended Data Figure 1. Comparison of prior and posterior times. a, Prior distribution of node ages generated by MCMC sampling without the molecular alignment. **b**, Posterior distribution of node ages when the 72-genome alignment is included during MCMC sampling. In both **a** and **b**, nodes are plotted at their posterior mean ages. The blue horizontal bars indicate the 95% credibility intervals of node ages.

Extended Data Figure 2. Impact of fossil calibration strategies on node age estimates. The posterior of node ages for the 72-taxon phylogeny is estimated using two additional fossil calibration strategies (y-axis) and plotted against the main estimates using best practice in calibration choice[39] (x-axis). In all cases the fossil minima are the same, but the calibration maxima changes. In the first strategy (black dots), calibration densities are narrow and close to the fossil ages. A truncated-Cauchy with a short tail (using $p = 0$ and $c = 0.001$, which extends the tail to about 110% of the fossil age) is used[21]. This strategy assumes the fossil record is a good indicator of the true node ages. In the second strategy (red dots), a truncated-Cauchy with a heavy tail (using $p = 0.1$ and $c = 1$, which extends the tail to over 900% of the fossil age) is used[21]. This strategy ignores the presence and absence of stem and sister groups, their palaeoecology, palaeobiogeography, and comparative taphonomy[39]; and instead, assumes the node ages can be arbitrarily old. Dots are plotted at the posterior mean ages and vertical and horizontal bars indicate 95% CIs. The solid line is the $x = y$ line. The dashed lines are the regression lines for the corresponding data points.

METHODS

Data Collection and Filtering

Dataset 1: 72-genome alignment

We downloaded the set of one-to-one protein-coding orthologs for the 72 mammal genomes available in Ensembl release 98 (http://www.ensembl.org, accessed 2019/11/15) using `EnsemblBioMarts`[51] (https://m.ensembl.org/biomart/martview). Sequences that did not meet the following requirements were removed from further analysis: (i) present in both human and mouse, (ii) not containing internal stop codons or gene/transcript mismatches, (iii) present in at least 10 species, and (iv) at least 100 codons in length. This left a total of 15,569 orthologs, which we partitioned into two data blocks: (i) first and second codon positions (12CP) and (ii) third codon positions (3CP). For each ortholog, an alignment was built with `PRANK` v140603[52] and the best-scoring maximum-likelihood (ML) trees were inferred with `RAxML` v8.2.10[53]. Note we used only the alignments with the 12CP-partition in the subsequent Bayesian molecular-clock analyses.

We further filtered the dataset using the estimated best-scoring ML trees for each gene to identify those having a branch length larger than 60% of the total tree length (the sum of all branch lengths). The relative branch length test is useful to detect misaligned or misidentified orthologs in the alignments[7,54], which may result in unusually long branch lengths. Let b_{ij} be the *i*-th branch length for gene tree *j* , and let *n* be the number of branches in the tree, then the relative branch length is

$$r_{ij} = b_{ij} / \sum_{i=j}^{n} \quad b_{ij}. \quad (1)$$

We identified 133 ortholog alignments associated with at least one relative branch length larger than 60%. These ortholog alignments were removed from further analyses.

Then, we estimated the pairwise distance between each ortholog in *Mus musculus* and *Homo sapiens* using the R (v3.5 to v4.0) function `ape::dist.dna`[55] v5.5. There were 4 genes (ENSG00000132185, ENSG00000204544, ENSG00000120937, and ENSG00000236699) for which the distances were returned as `NaN` or were larger than 0.75 for at least one of the substitution models used (i.e., TN93, JC69, and raw). Furthermore, when we plotted the percentage of the tree length inferred for each ortholog alignment versus the corresponding largest branch length (also in percentage), we found an outlier (ENSG00000176973, see Figure S1). We removed these 5 ortholog alignments, resulting in 15,431 orthologous gene alignments. Of those, 163 orthologs were removed as they are used in the construction of dataset 2 (see below). This filtering step resulted in 15,268 ortholog alignments (Table S1).

The 15,268 ortholog alignments were sorted from fast- to slow-evolving according to the pairwise-distance estimates and grouped into four partitions with the same number of genes. Each of the four partitions contained the concatenated 12CP of the orthologs for the partition (Table S2). The rationale for this partitioning strategy is as follows. In previous work[35,56], we tested phylogenomic data partitioning according to locus rate, principal component analysis of relative branch lengths, and amino acid composition at loci. However, those analyses showed no noticeable differences in posterior time estimates across the partitioning strategies[35,56]. On the other hand, we have shown that uncertainty in time estimates is sensitive to the number of partitions used[7,22], with more partitions producing more precise estimates, but at the cost of additional computation time. It appears four partitions give a reasonable trade-off between computational speed and precision of estimates. For example, twenty partitions would produce slightly more precise estimates but at 5 times the computational cost.

Dataset 2: Alignments of 4,705 taxa

We downloaded 832 complete mammal mitochondrial genomes from NCBI RefSeq (accessed: 2016/01/14). Twelve extinct and two redundant entries were removed, leaving

818 genomes. Twelve protein-coding genes (all but *ND6*) and the two non-coding RNA genes were extracted from each genome. The overlapping region in *ATP8* (position 95 to end) and overlapping codons at the end of *ND4L* were deleted.

To increase the nuclear and mitochondrial datasets, we mined sequences deposited in the European Nucleotide Archive (ENA, https://www.ebi.ac.uk/ena). The GenBank taxonomy (ftp://ftp.ncbi.nih.gov/pub/taxonomy/) was used to search for non-Ensembl mammalia species (this taxonomy is only used for ENA searches and not for any other analyses). A total of 7,188 taxa were found, 83 of which were extinct. The GenBank identifiers were used to reference the corresponding taxa in the ENA, from which all matching coding and non-coding sequences for non-Ensembl mammal taxa were downloaded (accessed: 2016/01/17): we found 6,453 taxa with coding sequences and 3,239 taxa with non-coding sequences (6,606 distinct taxa).
This project started in early 2016. At the time, we downloaded 15K nuclear orthologous gene alignments for 43 mammal taxa from Ensembl 83 and used these orthologs to create HMM sequence profiles with `HMMER`[57]. The HMM profiles were then used to identify orthologs for additional taxa from GenBank (https://www.ncbi.nlm.nih.gov/genbank/), bypassing unreliable GenBank homology annotations, and thus allowing reliable construction of large mammal subtrees. In late 2019, we updated the 15K orthologs to 72 genomes using Ensembl 98 (see above), but the HMM profiles and corresponding homology searches were based on the 2016 mining of Ensembl. HMM profiles were also created for mitochondrial protein-coding and non-coding genes and used for taxa extension of the corresponding alignments. DNA homology searches were performed with `nhmmer`[45] using the following match criteria:

- Sequences with E-value $< 1e^{-100}$ for a single gene were collected (i.e., sequences with multiple low E-values for different genes were removed).
- Matched sequences had to be at least 70% as long as the shortest Ensembl sequence in the alignment because many deposited sequences are partial sequences.
- Matches from hybrid/cross species were removed.
- Unspecified species (sp.) were excluded, unless no other member of the genus was represented (4 taxa included).
- Unconfirmed species (cf.) were excluded, unless no other member of the genus was represented (1 taxa included).
- Coding sequences were checked for correct open reading frame and translation.

Nuclear genes resulting in an expanded set of at least 50 taxa were selected, resulting in a set of 168 nuclear genes. These 168 genes correspond to 163 genes in the 2019 Ensembl mining (5 genes did not pass filtering criteria for the 72 taxa, but they did pass the criteria with the 43 taxa). Thus, dataset 1, based on the 2019 Ensembl mining, was reduced from 15,431 genes to 15,268 (Table S1) to avoid data duplication in the sequential dating approach. For new mined taxa, sequence annotations were extracted, sorted, and visually inspected to help verify homology. Alignments were then extended with homology-matched sequences using `PAGAN` v0.61[58]. Sequences were added in order of decreasing length (i.e., longest sequences were added to the alignment first). Table S3 gives summaries of the numbers of taxa and alignment lengths for datasets 1 and 2.

We then used `RAxML` to estimate the topology for each one of the 182 loci (168 nuclear + 14 mitochondrial) under the GTR+G model. We then manually inspected the trees and further filtered taxa following these criteria:

- Remove taxa that did not share genes with their order, family, and genus. This is done to avoid unidentifiable positioning of taxa in the subtrees: if a species does not share genes with its close relatives, then several positionings of the species within the subtree will have the same likelihood (a.k.a. “likelihood terraces”).

- Keep only one member of each species while maintaining maximum locus coverage, that is, remove redundant subspecies. Many subspecies slow the analysis down and are not informative about deep divergences (e.g., *Rangifer tarandus tarandus*). Also, subspecies annotations are missing for many loci, leading to integrity problems when resolving tips.
- Outdated taxonomic names according to the literature were removed.
- Remove taxonomically mismatched or mislabelled taxa.
- Flag taxa with large topological placement discrepancy with the literature.
- Outliers with unusually long branches in estimated trees were removed (three sequences in two genes).

Taxa were subdivided according to the following taxonomic groups: Afrotheria, Xenarthra, Marsupialia, Euarchonta, Lagomorpha, Laurasiatheria, and Rodentia. Laurasiatheria, Rodentia and Chiroptera, which are species-rich, were further divided into additional subsets to speed-up the dating analysis. Monotremata was added as an outgroup to all subtrees. The final dataset has 4,705 taxa and 182 loci divided into 13 subtree alignments. Each alignment was divided into five-partitions: (i) mitochondrial 12CP, (ii) mitochondrial 3CP, (iii) mitochondrial RNA, (iv) nuclear 12CP, (v) nuclear 3CP (Tables S4-S7). A `RAxML` analysis (GTR+G) was then run on each subtree with the genome-scale tree used as a backbone constraint. The final phylogeny has two manual adjustments. In the original tree, tenrecs are a sister clade to the rest of Afrotheria but, following recent work[6,33], we adjusted tenrecs as a sister clade to chrysochlorids. In the original tree, *Dromiciops* is placed as sister to *Notoryctes* but, following recent work[59], we placed *Dromiciops* basal to the rest of Australidelphia.

Divergence Time Estimation

All divergence-time estimation analyses were carried out with the `MCMCtree` v4.9h/i dating software from the `PAML` package[60]. The following analyses were carried out: (1) asymptotic analysis of uncertainties in time estimates as a function of number of loci, (2) Bayesian selection of relaxed-clock model, and (3) analysis of time estimates for seven topological re-arrangements of the mammal tree. Analyses 1-3 were carried out on the 72-taxon dataset. Last, we ran the (4) sequential-subtree analysis, which is divided into two parts: (i) estimation of times in 72-taxon tree, and (ii) estimation of times for the set of subtrees (4,705 taxa) using the time posterior of step I as the time prior.

(1) Asymptotic analysis of uncertainty in time estimates

To evaluate how our phylogenomic-scale data leads to asymptotic reduction of uncertainty in divergence time estimates, we randomly sampled data subsets with n = 1, 10, 30, 50, 100, and 1,000 loci from dataset 1, and grouped them into four partitions with roughly the same number of genes (except for n = 1). We then estimated the divergence times using the approximate likelihood calculation in `MCMCtree`, under both the independent log-normal (ILN) and the autocorrelated (geometric Brownian motion or GBM) rate models for each data subset (see 3 below for details on approximate likelihood method). Then, for each subset, we calculated the ratio of the 95% credibility interval width over the posterior mean of the node age. The uncertainty ratios across all 71 node ages were then averaged. This provides us with a measure of the average uncertainty in posterior node ages. For example, if the ratio is 20%, it means that, on average, the CI width is equivalent to 20% of the node age, or alternatively, that 20 My of uncertainty are added to the CI width for every 100 My of divergence.

(2) Bayesian rate model selection

We assessed adequacy of the ILN against the GBM rate models by using the stepping-stones approach[40]. Because an MCMC sample is a stationary time series, the stationary bootstrap[61] can be used to estimate the standard error of the log-marginal likelihood estimate while accommodating the autocorrelation of the MCMC. Let log $\mathbf{L}_i$ be the vector of

log-likelihood values sampled from the *i*-th power posterior. We sample, with replacement, blocks of observations from log $\mathbf{L}_i$, and the random blocks are stitched together to form a bootstrap sample log $\mathbf{L}_i$*. The size of the blocks has a geometric distribution with mean equal to 10% of the length of log $\mathbf{L}_i$. The procedure is repeated for each power-posterior sample and the log-marginal likelihood is then calculated using the stepping-stones formula[40]. The procedure is repeated 100 times to obtain 100 bootstrap estimates of the marginal-log likelihood, which are then used to estimate the standard error of the estimate. We validated the algorithm by comparing bootstrap standard error estimates against those obtained from brute-force re-calculation of the marginal likelihood, the latter being very computationally expensive as it involves running many independent stepping-stones analyses.

We used the 645 genes that were present in all the 72 taxa. Analyses were carried out using exact likelihood because the approximation is not good in the tails of the likelihood function, and tail values have a large impact on the marginal likelihood estimates. The age of the root was set to have a prior mean of 1 using the gamma density $\Gamma(100,100)$. We used diffuse gamma priors on the mean rate, $\mu \sim \Gamma(2,40)$ and $\sigma_2 \sim \Gamma(1,10)$. The birth and death prior was set to $\lambda = \mu = 1$, and $\rho = 0.1$, which generates an approximately uniform density[20]. Analyses were carried out using the main tree topology (Figure S2 b, T2). Each gene was analysed separately under the HKY85+G5 nucleotide substitution model[62–64], and sampling was done over 32 beta points in the power posterior. Choice of beta points, application of the stepping-stones formula, and bootstrap block-sampling were done with the `mcmc3r` v0.4.3 package[35]. In total, rate model selection required 41,280 MCMC chains (645 genes x 2 rate models x 32 beta points), totalling four months of wall time (2M hours or >200 years of CPU time) in a high-performance computer cluster.

We also carried out a maximum likelihood ratio test of the strict molecular clock[65]. The strict clock was rejected in 642 out of 645 loci (after false-discovery rate correction at the 5% level).

(3) Time estimation on topological rearrangements for 72-taxa

The seven tree topologies used are shown in Figure S2 (a-g). Time estimation was carried out using dataset 1 under approximate likelihood calculation. All analysis setups were as in step I of the sequential Bayesian approach (see below).

(4) Sequential Bayesian approach: from genomes to subtrees

Hessian calculation to approximate the likelihood on 72 taxa

We use the approximate likelihood method to speed up computation during MCMC sampling[37]. This involves obtaining the maximum-likelihood estimates (MLEs) of the branch lengths, **b**, on a partition, together with the gradient, **g**, and Hessian, **H**, of the log-likelihood evaluated at the MLEs. Then **b**, **g**, and **H** are used to approximate the likelihood during MCMC sampling (see [66] for a tutorial). We used `BASEML`[60] v4.9h/i to calculate **b**, **g**, and **H** for each of the 4 partitions in the 72-genome alignment using the HKY+G5 substitution model[62,63]. We tested 7 different topological relationships among mammals (Figure S2), with each tree topology requiring calculation of its own set of **b**, **g**, and **H**.

Divergence-time estimation on the 72-taxon tree

Nodes are calibrated using uniform distributions based on the fossil record. The distributions have soft bounds, that is, there are probabilities, p_L and p_U, that the node age falls outside lower and upper calibration bounds. Here we tested two approaches for setting these probabilities: (1) using $p_L = p_U = 0.025$, and (2) $p_L = 0.001$ and $p_U = 0.1$. The second approach assumes the probability of violation of the minimum bound is very small (i.e., assuming fossil placement and dating are accurate), while allowing for a larger upper-bound probability. We find that choice of p_L and p_U have a small impact on time estimates on the 72-genome phylogeny (Figure S3). However, for the second analysis step (subtree time estimation), we find that, when $p_L = 0.001$ and $p_U = 0.1$, the fitted Skew-*t* calibration densities are too asymmetrical and with heavy tails, leading to convergence problems in the MCMC

(e.g., see [67] for a discussion of convergence on distribution tails). Thus, we favour the use of Skew-*t* calibrations based on the posterior using $p_L = p_U = 0.025$ for the rest of the analyses (see below for details on Skew-*t* distribution fitting).

Table S8 lists the fossil calibrations used for the 72-species phylogeny. Our fossil calibrations include previously published constraints on clade age[33,68], plus new calibrations that we have formulated following established best practice[69]. Briefly, minima are based on the oldest unequivocal member of a crown group and we follow the youngest age interpretations. Maxima are more challenging to establish since absence of fossil evidence cannot simply be interpreted as evidence of the absence of a lineage at a given time interval. Hence, we use evidence of the presence of outgroup lineages with comparable ecology and taphonomy to serve as evidence of the absence of ingroup lineages since, were they present, the preservation of outgroup relatives demonstrates that they should be preserved[39]. However, there remains a non-zero probability that lineages existed before our maxima and hence we implement them as soft constraints, which allows the analysis to explore older ages for the origination of a calibrated clade but at low prior probability. Detailed justifications for all calibrations are provided in the Annex of the Supplementary Information. We note our fossil calibrations were set at the project beginnings in 2016. Table S8 provides the latest geochronological updates (Sep 2021). The old calibrations are used for the asymptotic and topology variation analyses, while the updated calibrations are used in the sequential dating approach. The calibration updates are very small, usually below the sampling error of the MCMC, and thus have little effect on time estimates (Figure S4).

The birth and death process[23], used to specify the time prior for nodes with no calibrations, was set to $\lambda = \mu = 1$, and sampling fraction to $\rho = 0.1$, which gives an approximately uniform kernel. The GBM rate model is used with a gamma-Dirichlet prior[56] on the mean *i*-th partition rate, $\mu_i \sim \Gamma(2,40)$, and on the relaxed-clock parameter, $\sigma_i^2 \sim \Gamma(1,10)$. This setting gives a diffuse prior on the rate that is roughly centered on the average substitution rate of nuclear genes in mammals[56,66].

We ran `MCMCtree` without data to sample from the time prior. This is done to verify the prior is sensible and not in conflict with the calibration densities used[21,70]. To ensure MCMC convergence and increase effective sample size (ESS), we ran several MCMC chains of sufficient length. We used `Tracer`[71] v1.7 and the `coda::effectiveSize`[72] v0.19.4 to make sure the ESS was larger than 200 for all estimated parameters (Table S9). We also used the R function `rstan::monitor`[73] v2.21.2 to calculate the ESS for bulk and tail quantiles and the potential scale reduction factor on rank normalised split chains (Rhat). Values over 100 for the former are considered good, while *Rhat* values need to be either smaller than or equal to 1.05 to show chain convergence. We further explored chain convergence by visually plotting the distributions of the different chains ran in `MCMCtree` with the R package `MCMCtreeR` [74] v1.1 (see Figure S5). Figure S6 shows the convergence plots for each tree hypothesis, which show excellent convergence.

Fitting of Skew-t distributions to posterior times

We used the posterior time estimates sampled during the MCMC runs under the GBM model to fit Skew-*t* (ST) distributions to the 71 internal nodes of the 72-species tree. This was done with the R function `sn::st.mple`[75] v2.0.0 under the BFGS method for parameter optimisation. To check if the fitted ST distributions were sensible, we sampled, using `MCMCtree`, from the new ST-based prior (i.e., without the alignment data), and checked whether the sampled prior distributions matched the original ST distributions. This is necessary because of the constraint that nodes are younger than their parents. This means ST calibrations on adjacent nodes could suffer from truncation effects and the resulting prior could be in conflict with the ST densities. We did not observe any such conflict (see Figure S7). For the crown-lagomorpha node, however, the corresponding ST calibration caused convergence problems when dating the lagomorpha subtree (dataset 2). This ST calibration, which has a heavy tail, was replaced by an essentially equivalent Skew-normal calibration,

which has a light tail, thus solving the convergence problem.

Time estimation on the 4,705-taxon phylogeny

Hessian and gradient calculation for each partition on each subtree were done using the HKY+G5 substitution model, as for dataset 1. Subtrees were calibrated using the fitted ST densities and 60 additional soft-bound calibrations (Tables S10-S11). These calibrations are also updated according to new geochronology. The same rate and birth-death model priors as in step I were used. For each subtree, we ran 32 independent MCMC chains to check convergence and ensure enough samples were collected to approximate the posterior (see Figure S8 and Tables S12-13), although some of those did not pass quality filters and were not included (see Figure S8).

We ran `MCMCtree` without data to sample from, and verify the integrity of, the prior. We repeated this analysis twice: once including only the ST calibrations and a second time with both ST and soft-bound calibrations in the subtrees. This was necessary to assess whether the soft bounds were in conflict with the ST densities, producing truncation problems. In a few cases, after examining the prior, we observed conflict between the ST densities and the soft bounds. In such cases, calibrations were adjusted so that the resulting prior CI limits were within ~5% of the original ST density quantiles. Adjustments included either nudging the maximum age of a soft-bound calibration or nudging the ST calibration densities themselves.

Assembly of the 4,705-taxon timetree

Time calibrated subtrees were attached to the corresponding node in the 72-species mammal phylogeny using a custom Python (v3.8.5) script. Outgroup (Monotremata) and any marker taxa were removed before merging the subtrees into the main tree. Marker taxa were needed in the Rodentia and Laurasiatheria subtrees to guarantee integrity of ST-calibrated nodes. That is, when splitting these large subtrees for divergence times estimation, some nodes shared with the main 72-species tree would disappear in some subtrees. Consequently, marker taxa (shared with a sister subtree) were added back into the corresponding subtree to retain the calibrated node and guarantee integrity during merging (see supplementary data). The result of the subtree merging is the fully-dated 4,705-taxon phylogeny. We verified integrity of time estimates by repeating analyses on subsets of shared data cross partitions (see Supplementary Information, Fig. S9).

Mining of PaleoDB for fossil mammal taxa

The fossil data were downloaded from the Paleobiology Database (https://paleobiodb.org/, accessed March 2021), using the API service with resolution set to genus level, excluding uncertain genera, only body fossil taxa (i.e., no ichnotaxa), and accepted names only. The data were cleaned by removing individual stratigraphic occurrences that had an age range greater than 20 million years, as this suggests the dating of the occurrence is uncertain or incorrect on the database. The higher clade classifications were added to the genera, and some manual corrections to the fossil classifications were made. The maximum and minimum ages for each genus were extracted, as well as whether the genus is extant or extinct. The genera with age ranges approaching or equal to 0 million years were double checked against the literature to ensure the extinct/extant status was correct. The number of extinct species for each genus was also extracted from the Paleobiology Database[50] and added to the dataset.

References for Methods

51 Kinsella RJ, Kähäri A, Haider S, Zamora J, Proctor G, Spudich G *et al.* Ensembl BioMarts: a hub for data retrieval across taxonomic space. *Database* 2011; **2011**. doi:10.1093/database/bar030.

52 Löytynoja A. Phylogeny-aware alignment with PRANK. *Methods Mol Biol* 2014; **1079**: 155–170.

53 Stamatakis A. RAxML version 8: a tool for phylogenetic analysis and post-analysis of large phylogenies. *Bioinformatics* 2014; **30**: 1312–1313.

54 Springer MS, Gatesy J. On the importance of homology in the age of phylogenomics. *Syst Biodivers* 2018; **16**: 210–228.

55 Paradis E, Claude J, Strimmer K. APE: analyses of phylogenetics and evolution in R language. *Bioinformatics* 2004; **20**: 289–290.

56 dos Reis M, Thawornwattana Y, Angelis K, Telford MJ, Donoghue PCJ, Yang Z. Uncertainty in the timing of origin of animals and the limits of precision in molecular timescales. *Curr Biol* 2015; **25**: 2939–2950.

57 Eddy SR. Profile hidden Markov models. *Bioinformatics* 1998; **14**: 755–763.

58 Löytynoja A, Vilella AJ, Goldman N. Accurate extension of multiple sequence alignments using a phylogeny-aware graph algorithm. *Bioinformatics* 2012; **28**: 1684–1691.

59 Mitchell KJ, Pratt RC, Watson LN, Gibb GC, Llamas B, Kasper M *et al.* Molecular phylogeny, biogeography, and habitat preference evolution of marsupials. *Mol Biol Evol* 2014; **31**: 2322–2330.

60 Yang Z. PAML 4: phylogenetic analysis by maximum likelihood. *Mol Biol Evol* 2007; **24**: 1586–1591.

61 Politis DN, Romano JP. The stationary bootstrap. *J Am Stat Assoc* 1994; **89**: 1303–1313.

62 Hasegawa M, Kishino H, Yano T. Dating of the human-ape splitting by a molecular clock of mitochondrial DNA. *J Mol Evol* 1985; **22**: 160–174.

63 Hasegawa M, Yano T-A, Kishino H. A new molecular clock of mitochondrial DNA and the evolution of hominoids. *Proc Japan Acad Ser B* 1984; **60**: 95–98.

64 Yang Z. Maximum likelihood phylogenetic estimation from DNA sequences with variable rates over sites: approximate methods. *J Mol Evol* 1994; **39**: 306–314.

65 Felsenstein J. Evolutionary trees from DNA sequences: a maximum likelihood approach. *J Mol Evol* 1981; **17**: 368–376.

66 dos Reis M, Yang Z. Bayesian molecular clock dating using genome-scale datasets. In: Anisimova M (ed). *Evolutionary Genomics: Statistical and Computational Methods*. Springer New York: New York, NY, 2019, pp 309–330.

67 Rannala B, Zhu T, Yang Z. Tail paradox, partial identifiability, and influential priors in Bayesian branch length inference. *Mol Biol Evol* 2012; **29**: 325–335.

68 Benton MJ, Donoghue PCJ, Vinther J, Asher RJ, Friedman M, Near TJ. Constraints on the timescale of animal evolutionary history. Palaeontologia Electronica. 2015.

776 doi:10.26879/424.

777 69 Parham JF, Donoghue PCJ, Bell CJ, Calway TD, Head JJ, Holroyd PA *et al.* Best
778 practices for justifying fossil calibrations. Systematic Biology. 2012; **61**: 346–359.

779 70 Warnock RCM, Parham JF, Joyce WG, Lyson TR, Donoghue PCJ. Calibration
780 uncertainty in molecular dating analyses: there is no substitute for the prior evaluation of
781 time priors. *Proc R Soc B* 2015; **282**: 20141013.

782 71 Rambaut A, Drummond AJ, Xie D, Baele G, Suchard MA. Posterior Summarization in
783 Bayesian Phylogenetics Using Tracer 1.7. *Syst Biol* 2018; **67**: 901–904.

784 72 Plummer M, Best N, Cowles K, Vines K. CODA: convergence diagnosis and output
785 analysis for MCMC. *R News* 2006; **6**: 7–11.

786 73 Stan Development Team. *Stan Development Team (2020). RStan: the R interface to*
787 *Stan. R package*. 2020https://mc-stan.org (accessed 25 Jun2021).

788 74 Puttick MN. MCMCtreeR: functions to prepare MCMCtree analyses and visualize
789 posterior ages on trees. *Bioinformatics* 2019; **35**: 5321–5322.

790 75 Azzalini A. *The R package 'sn': the skew-normal and related distributions such as the*
791 *skew-t*. 2019http://azzalini.stat.unipd.it/SN/ (accessed 25 Jun2021).

792
793

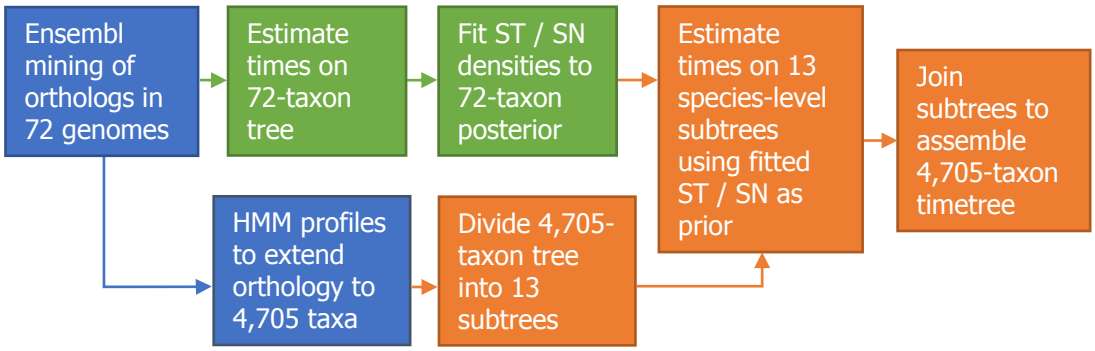
Ensembl mining of orthologs in 72 genomes
Estimate times on 72-taxon tree
Fit ST / SN densities to 72-taxon posterior
Estimate times on 13 species-level subtrees using fitted ST / SN as prior
Join subtrees to assemble 4,705-taxon timetree
HMM profiles to extend orthology to 4,705 taxa
Divide 4,705-taxon tree into 13 subtrees

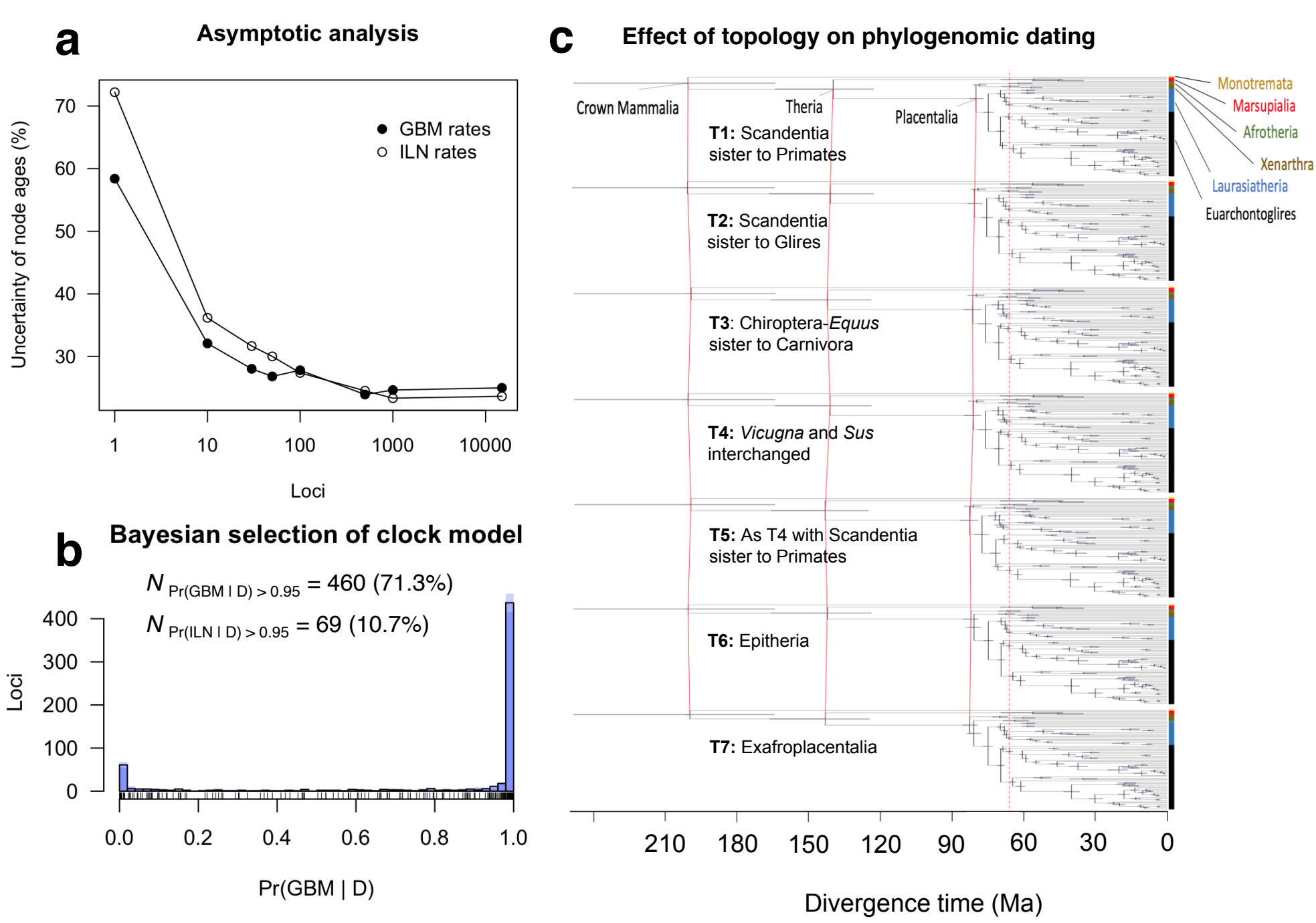
a
Asymptotic analysis
Uncertainty of node ages (%)
70
60
50
40
30
GBM rates
ILN rates
1
10
100
1000
10000
Loci
b
Bayesian selection of clock model
N Pr(GBM I D) > 0.95 = 460 (71.3%)
N Pr(ILN I D) > 0.95 = 69 (10.7%)
Loci
400
300
200
100
0
0.0
0.2
0.4
0.6
0.8
1.0
Pr(GBM | D)
c
Effect of topology on phylogenomic dating
Crown Mammalia
Theria
Placentalia
T1: Scandentia sister to Primates
T2: Scandentia sister to Glires
T3: Chiroptera-Equus sister to Carnivora
T4: Vicugna and Sus interchanged
T5: As T4 with Scandentia sister to Primates
T6: Epitheria
T7: Exafroplacentalia
Monotremata
Marsupialia
Afrotheria
Xenarthra
Laurasiatheria
Euarchontoglires
210
180
150
120
90
60
30
0
Divergence time (Ma)

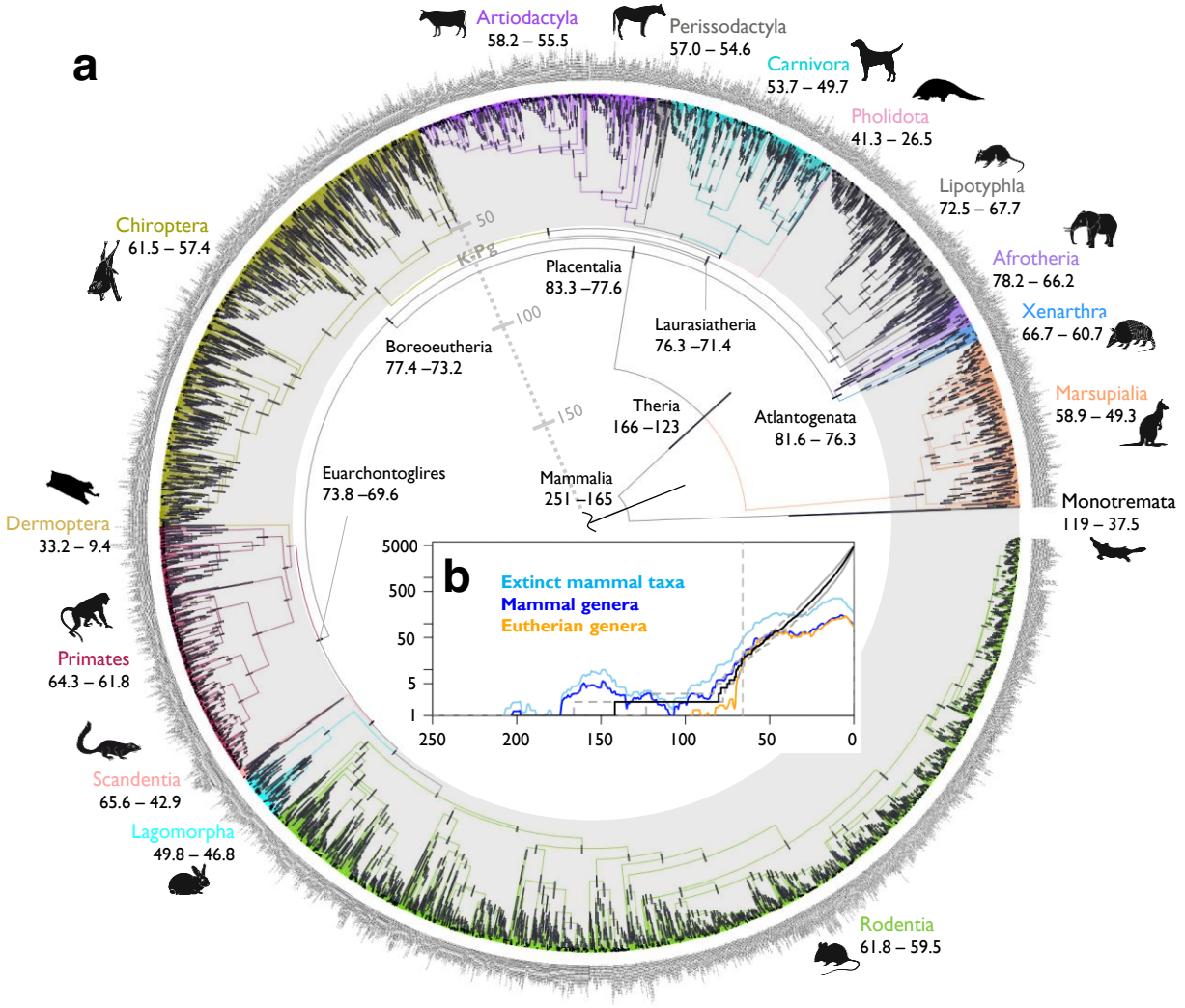
a
Artiodactyla
58.2 – 55.5
Perissodactyla
57.0 – 54.6
Carnivora
53.7 – 49.7
Pholidota
41.3 – 26.5
Lipotyphla
72.5 – 67.7
Afrotheria
78.2 – 66.2
Xenarthra
66.7 – 60.7
Marsupialia
58.9 – 49.3
Monotremata
119 – 37.5
Rodentia
61.8 – 59.5
Lagomorpha
49.8 – 46.8
Scandentia
65.6 – 42.9
Primates
64.3 – 61.8
Dermoptera
33.2 – 9.4
Chiroptera
61.5 – 57.4
50
K-Pg
100
150
Placentalia
83.3 –77.6
Laurasiatheria
76.3 –71.4
Boreoeutheria
77.4 –73.2
Theria
166 –123
Atlantogenata
81.6 – 76.3
Euarchontoglires
73.8 –69.6
Mammalia
251 –165
b
Extinct mammal taxa
Mammal genera
Eutherian genera
5000
500
50
5
1
250
200
150
100
50
0

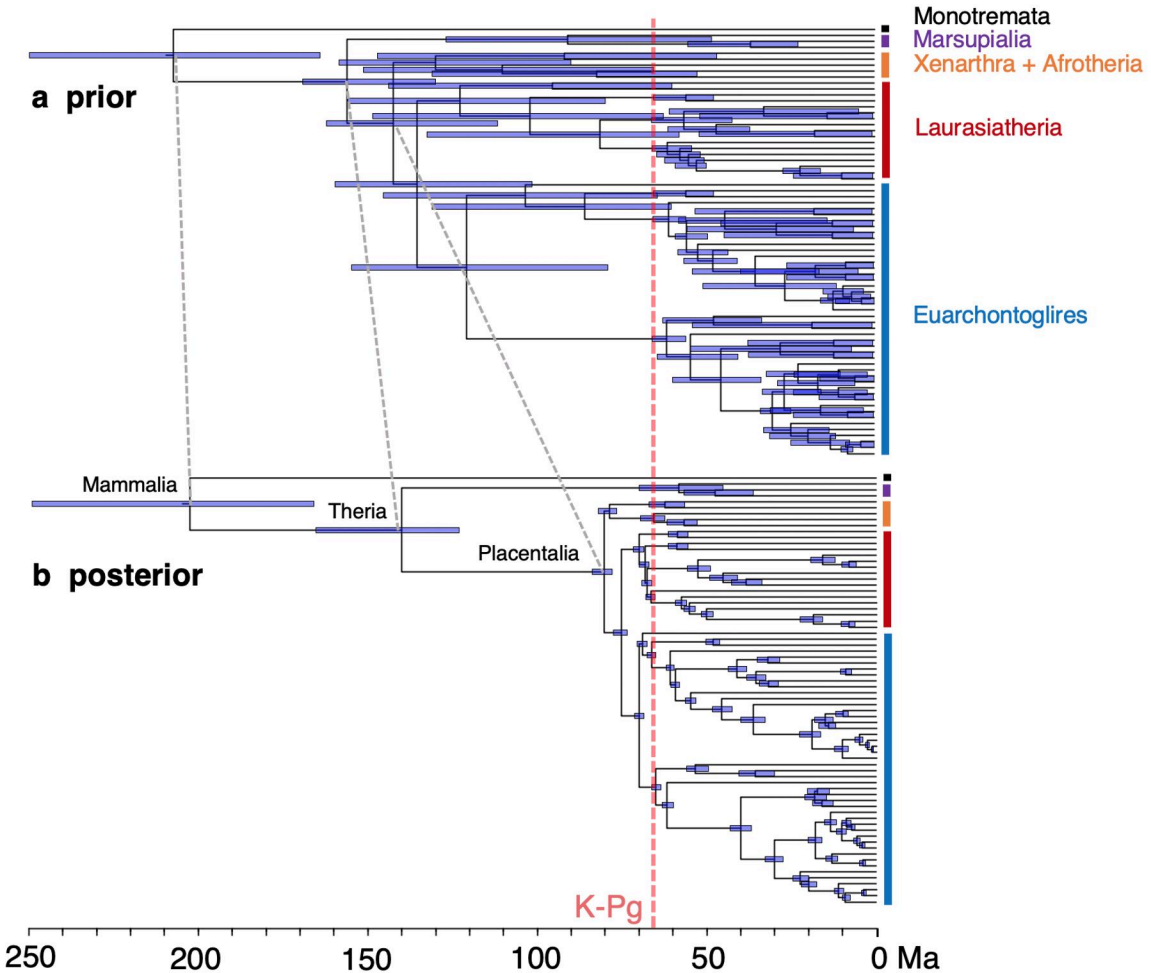
Monotremata
Marsupialia
Xenarthra + Afrotheria
Laurasiatheria
Euarchontoglires
a prior
Mammalia
Theria
Placentalia
b posterior
K-Pg
250
200
150
100
50
0 Ma

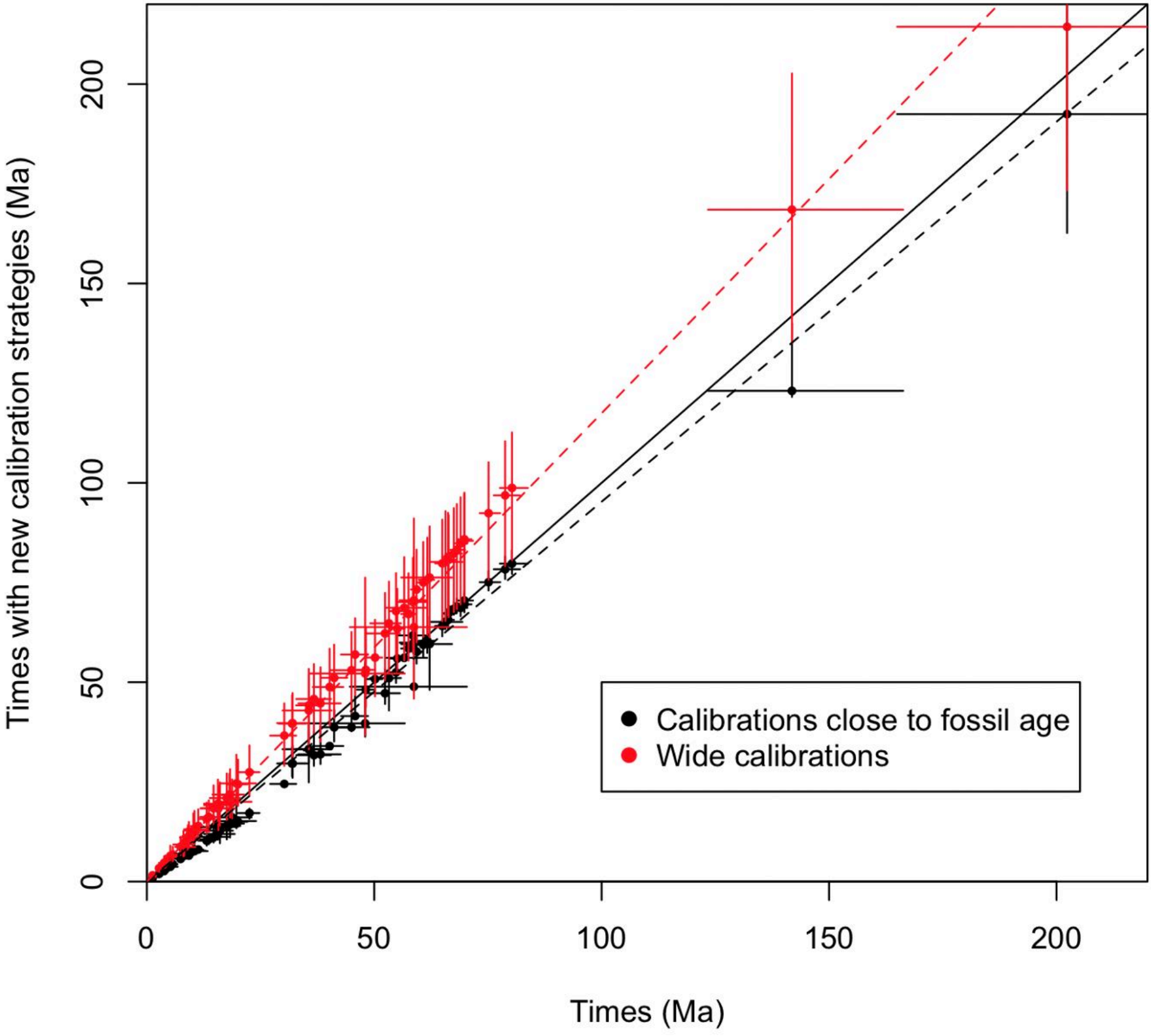
Times with new calibration strategies (Ma)
0
50
100
150
200
Times (Ma)
Calibrations close to fossil age
Wide calibrations

Supplementary Information for
A Species-Level Timeline of Mammal Evolution Integrating Phylogenomic Data

Sandra Álvarez-Carretero[†,1,2], Asif U. Tamuri[†,3,4], Matteo Battini[5], Fabrícia F. Nascimento[6], Emily Carlisle[5], Robert J. Asher[7], Ziheng Yang[2], Philip C.J. Donoghue[*5], and Mario dos Reis[*1].

[1] School of Biological and Behavioural Sciences, Queen Mary University of London, London, UK.
[2] Department of Genetics, Evolution, and Environment, University College London, London, WC1E 6BT, UK.
[3] Centre for Advanced Research Computing, University College London, Gower St, London, WC1E 6BT, UK.
[4] EMBL-EBI, Wellcome Genome Campus, Hinxton, Cambridgeshire, CB10 1SD, UK
[5] School of Earth Sciences, University of Bristol, Life Sciences Building, Tyndall Avenue, Bristol, BS8 1TQ, UK.
[6] MRC Centre for Global Infectious Disease Analysis, School of Public Health, Imperial College London, London, UK.
[7] Department of Zoology, University of Cambridge, Downing Street, Cambridge, CB2 3EJ, UK.

[†] Contributed equally to this work
* Corresponding authors

Table of Contents

Data Collection and Filtering

Tables and Figures cited in the “Methods” section *“Data Collection and Filtering”* can be found below. They are shown in the same order in which they are cited in the corresponding subsections.

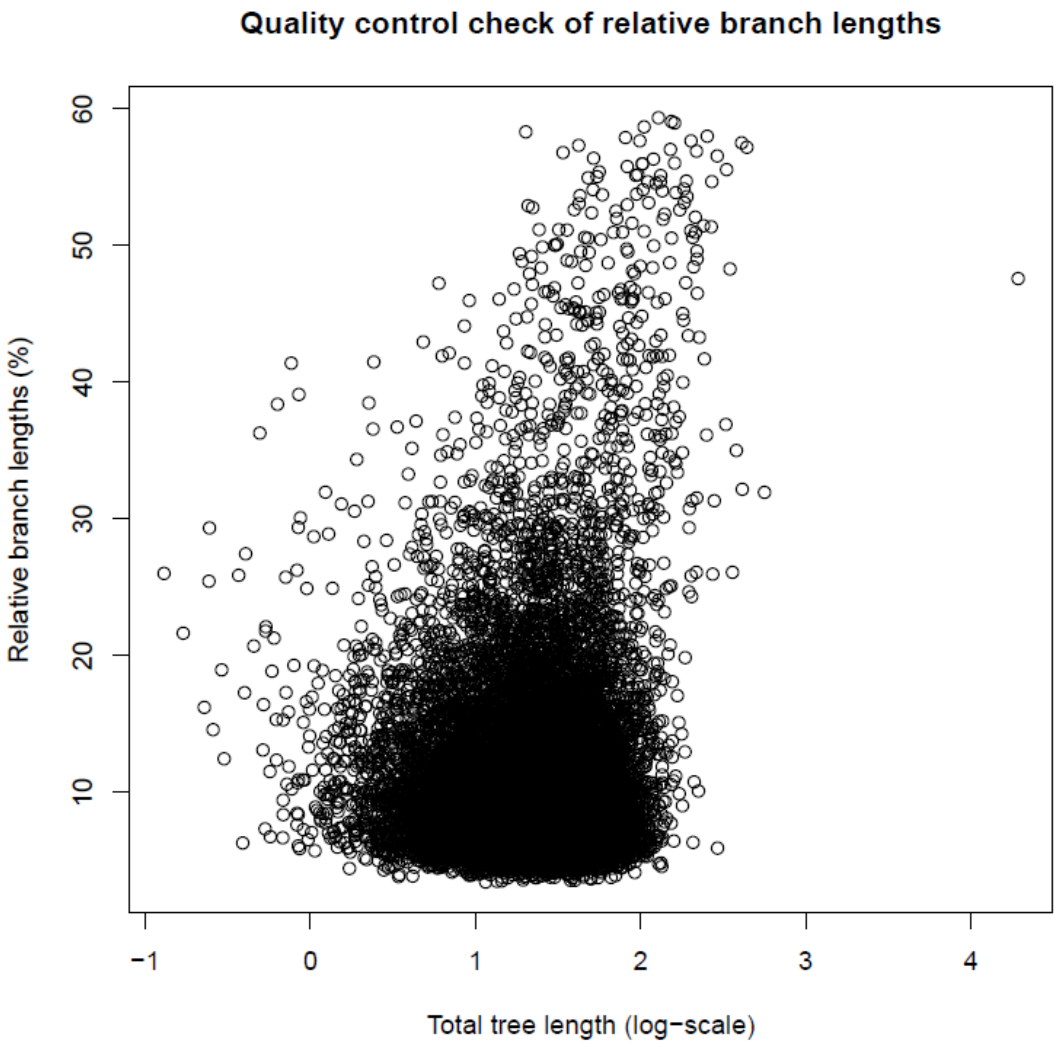

Figure S1: Quality control check of the estimated relative branch lengths (%) for each gene tree in comparison to the corresponding total tree length (log-scale). One of the criteria we had to keep a gene alignment was that the relative branch lengths (x-axis) could not be larger than or equal to 60% of the total length of the tree (y-axis). This plot shows how most of the gene trees have relative branch lengths that are 10-30% of the length of the tree, while few gene trees have relative branch lengths very close to the threshold (60%). Nevertheless, there is one outlier whose tree length in the log-scale is 4 units despite the relative branch length not accounting for more than 60% of the tree; there are at least two very long branch lengths in this gene tree. This plot is useful to visually identify which gene trees should be deleted according to the total log tree length that the relative branch lengths of each gene tree account for with regards to a specific threshold.

Table S1. Summary statistics for the 72-taxon gene alignments after each filtering step.

Filtering step	Raw	Initial filtering	Relative branch test	Pairwise distances	HMMER (dataset 2)
Number of genes left	15,904	15,569	15,436	15,431	15,268
Genes removed	0	335	133	5	163
% Removed	0	2.11	0.85	0.03	1.06
Cumulative genes removed	0	335	468	473	636
% Cumulative removed	0	2.11	2.94	2.97	4.00

Table S2. Number of taxa and orthologs, alignment length, corresponding site pattern counts, and missing data for each data subset and partition scheme. Partitions go from fastest-evolving (1) to slowest-evolving (4).

Data subset	No. taxa	No. orthologs	Alignment length (base pairs)	Site pattern counts	% Missing data
Partition 1	72	3,817	8,926,316	3,613,711	60.17
Partition 2	72	3,817	8,339,196	2,941,508	50.78
Partition 3	72	3,817	8,605,264	2,416,624	48.49
Partition 4	72	3,817	7,302,398	1,521,894	45.92

Table S3. Content of the mammal dataset after bioinformatics filtering.

Dataset	Data source	Data type	Dataset extended?	Range of taxa	No. genes
Dataset 1	Ensembl	Nuclear protein-coding	No	10-72	15,268
Dataset 2	ENA/HMM-profile RefSeq	Nuclear protein-coding	Yes, homology search	48-1,242	168
	RefSeq	Mitochondrial protein-coding	No	767	3
	ENA / HMM-profile		Yes, homology search	805-3,986	9
	ENA / HMM-profile	Mitochondrial non-coding rRNA	Yes, homology search	1,542-2,114	2

Table S4. Number of taxa (alignment length | site pattern counts) for mitochondrial subtrees and partitions. Monotremata is an outgroup in all subtrees.

Data subset	mit-12CP	mit-3CP	mit-RNA
Afrotheria	34 (7,226 | 2,298)	34 (3,613 | 3,352)	32 (2,786 | 1,486)
Euarchonta	452 (7,260 | 4,549)	452 (3,630 | 3,630)	289 (3,087 | 2,274)
Lagomorpha	82 (7,198 | 1,326)	82 (3,599 | 3,034)	46 (2,634 | 928)
Artiodactyla	419 (7,240 | 3,430)	419 (3,620 | 3,614)	293 (2,817 | 1,828)
Chiroptera (I)	216 (7,202 | 1,932)	216 (3,601 | 3,457)	133 (3,287 | 1,993)
Chiroptera (II)	566 (7,240 | 3,020)	566 (3,620 | 3,590)	328 (4,117 | 3,033)
Rest of Laurasiatheria	598 (7,320 | 3,710)	598 (3,660 | 3,640)	386 (3,402 | 2,436)
Marsupialia	260 (7,278 | 3,131)	260 (3,639 | 3,610)	215 (3,366 | 2,342)
Ctenohystrica	174 (7,224 | 2,535)	174 (3,612 | 3,375)	125 (2,897 | 1,709)
Sciuridae and related	215 (7,200 | 2,068)	215 (3,600 | 3,398)	100 (2,958 | 1,727)
Rest of Rodentia (I)	602 (7,366 | 3,712)	602 (3,694 | 3,663)	167 (3,072 | 2053)
Rest of Rodentia (II)	636 (7,320 | 2,826)	636 (3,662 | 3,568)	127 (2,927 | 1,581)
Xenarthra	32 (7,210 | 1,980)	32 (3,605 | 3,404)	33 (2,655 | 1,190)

Table S5. Number of taxa (alignment length | site pattern counts) for nuclear subtrees and partitions. Monotremata is an outgroup in all subtrees.

Data subset	nuc-12CP	nuc-3CP
Afrotheria	52 (166,190 | 6,853)	52 (83,095 | 6,786)
Euarchonta	253 (193,708 | 40,599)	253 (96,854 | 42,084)
Lagomorpha	43 (130,746 | 1,845)	43 (65,373 | 2,070)
Artiodactyla	189 (191,394 | 19,451)	189 (95,697 | 20,472)
Chiroptera (I)	163 (222,499 | 8,057)	163 (80,524 | 9,316)
Chiroptera (II)	448 (234,986 | 9,407)	448 (117,248 | 10,205)
Rest of Laurasiatheria	453 (198,006 | 45,479)	453 (177,439 | 43,565)
Marsupialia	249 (171,898 | 10,417)	249 (85,949 | 9,322)
Ctenohystrica	116 (33,287 | 8,980)	116 (16,778 | 7,043)
Sciuridae and related	118 (24,890 | 2,967)	118 (12,445 | 3,115)
Rest of Rodentia (I)	379 (423,700 | 11,881)	379 (94,825 | 12,671)
Rest of Rodentia (II)	505 (206,736 | 8,285)	505 (95,950 | 7,878)
Xenarthra	20 (102,226 | 2,513)	20 (51,113 | 2,487)

Table S6. Total number of taxa and alignment length (across all partitions) for each subtree. Monotremata is an outgroup in all subtrees.

Data subset	Number of taxa	Total alignment length
Afrotheria	60	262,910
Euarchonta	486	304,539
Lagomorpha	88	209,550
Artiodactyla	431	300,768
Chiroptera (I)	256	317,113
Chiroptera (II)	634	367,211
Rest of Laurasiatheria	659	389,827
Marsupialia	307	272,130
Ctenohystrica	210	63,798
Sciuridae and related	267	51,093

Rest of Rodentia (I)	630	532,657
Rest of Rodentia (II)	691	316,595
Xenarthra	33	166,809

Table S7. Missing data (%) for each subtree partition before (top) and after (bottom) removing missing taxa. The percentage of missing data is calculated by dividing the number of gaps in the alignment by the number of taxa times the alignment length. The number of taxa is shown within brackets. We note missing taxa are not used by `MCMCtree` during likelihood calculation.

Data subset	**mit-12CP**	**mit-3CP**	**mit-RNA**	**nuc-12CP**	**nuc-3CP**
Afrotheria	70.66 (60)	70.66 (60)	55.44 (60)	93.16 (60)	93.16 (60)
	48.22 (34)	48.22 (34)	16.46 (32)	92.11 (52)	92.11 (52)
Euarchonta	51.51 (486)	51.51 (486)	58.28 (486)	96.02 (486)	96.02 (486)
	47.86 (452)	47.86 (452)	29.84 (289)	92.35 (253)	92.35 (253)
Lagomorpha	65.24 (88)	65.24 (88)	68.55 (88)	96.57 (88)	96.57 (88)
	62.69 (82)	62.69 (82)	39.84 (46)	92.98 (43)	92.98 (43)
Artiodactyla	35.83 (431)	35.83 (431)	43.86 (431)	97.85 (431)	97.85 (431)
	33.99 (419)	33.99 (419)	17.42 (293)	95.10 (189)	95.10 (189)
Chiroptera (I)	82.48 (256)	82.48 (256)	69.59 (256)	98.33 (256)	97.69 (256)
	79.23 (216)	79.23 (216)	41.47 (133)	97.37 (163)	96.37 (163)
Chiroptera (II)	82.84 (634)	82.84 (634)	71.68 (634)	99.16 (634)	99.16 (634)
	80.78 (566)	80.78 (566)	45.26 (328)	98.81 (448)	98.81 (448)
Rest of Laurasiatheria	59.35 (659)	59.35 (659)	66.98 (659)	97.84 (659)	98.80 (659)
	55.20 (598)	55.20 (598)	43.62 (386)	96.86 (453)	98.25 (453)
Marsupialia	61.52 (307)	61.52 (307)	57.51 (307)	97.39 (307)	97.39 (307)
	54.56 (260)	54.56 (260)	39.33 (215)	96.79 (249)	96.79 (249)
Ctenohystrica	83.33 (210)	83.33 (210)	76.03 (210)	93.96 (210)	94.01 (210)
	79.88 (174)	79.88 (174)	59.74 (125)	89.06 (116)	89.15 (116)
Sciuridae and related	84.83 (267)	84.83 (267)	85.37 (267)	96.57 (267)	96.57 (267)
	81.16 (215)	81.16 (215)	60.95 (100)	92.24 (118)	92.24 (118)

Rest of Rodentia (I)	81.15 (630)	81.21 (630)	87.69 (630)	99.51 (630)	98.90 (630)
	80.27 (602)	80.33 (602)	53.54 (167)	99.18 (379)	98.16 (379)
Rest of Rodentia (II)	84.02 (691)	84.03 (691)	90.69 (691)	98.96 (691)	98.88 (691)
	82.64 (636)	82.65 (636)	49.35 (127)	98.57 (505)	98.46 (505)
Xenarthra	3.30 (33)	3.30 (33)	4.67 (33)	90.04 (33)	90.04 (33)
	0.28 (32)	0.28 (32)	4.67 (33)	83.57 (20)	83.57 (20)

Divergence Time Estimation

Tables and Figures cited in the “Methods” section *“Divergence Time Estimation”* can be found below. They are shown in the same order in which they are cited in the corresponding subsections.

Figure S2 (a) - T1

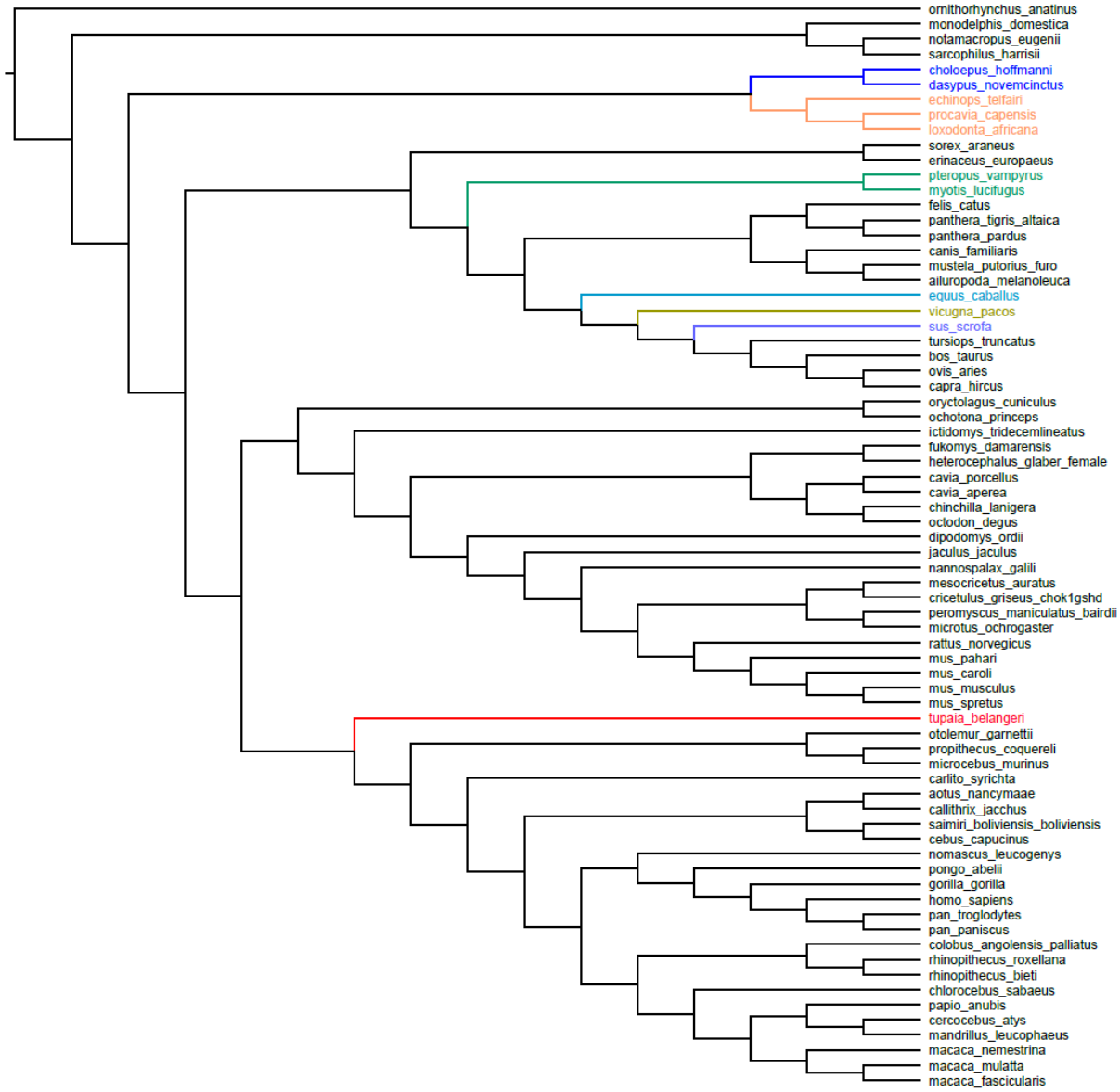

Figure S2 (b) - T2 *(main tree)*

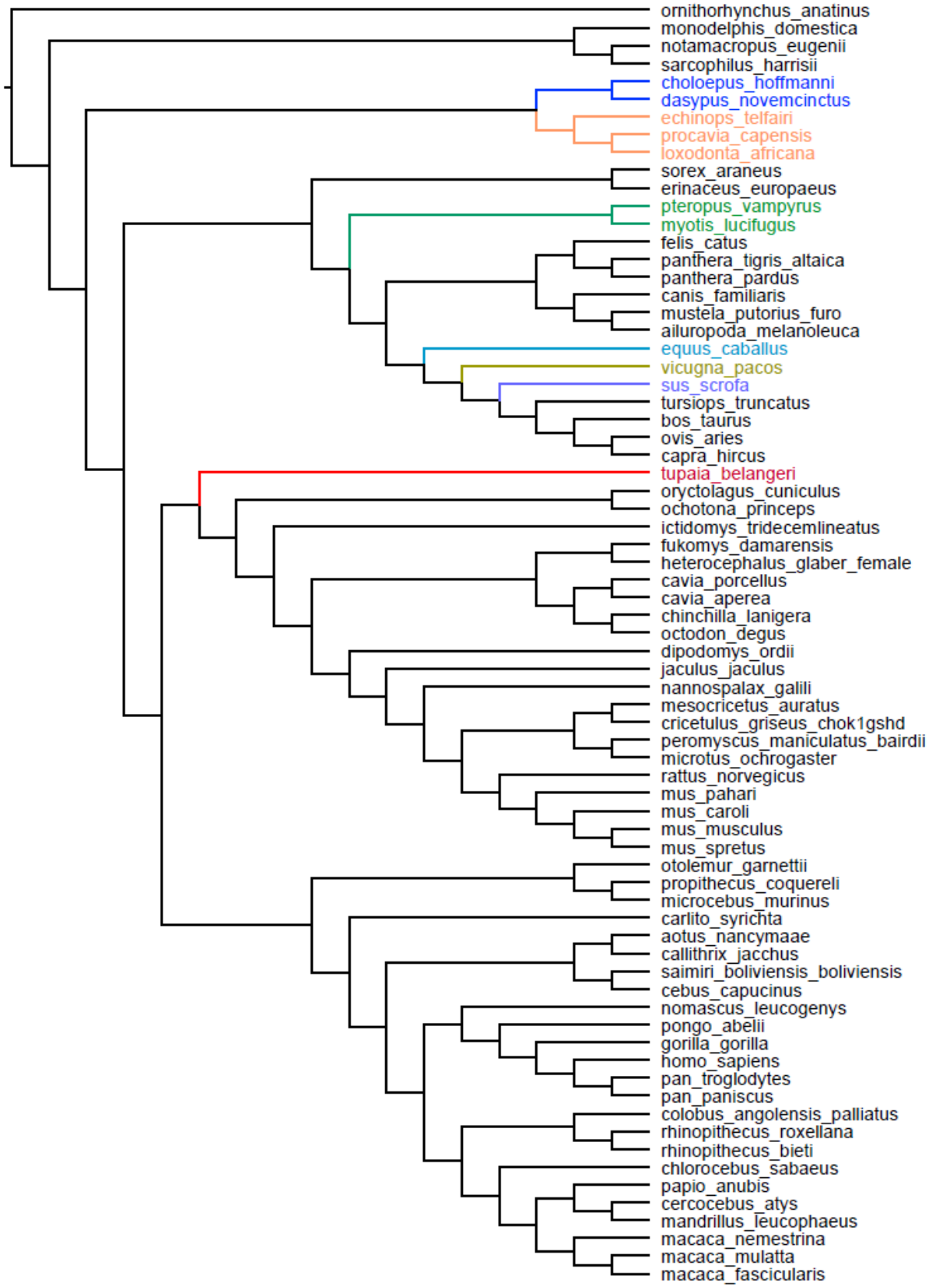

Figure S2 (c) - T3

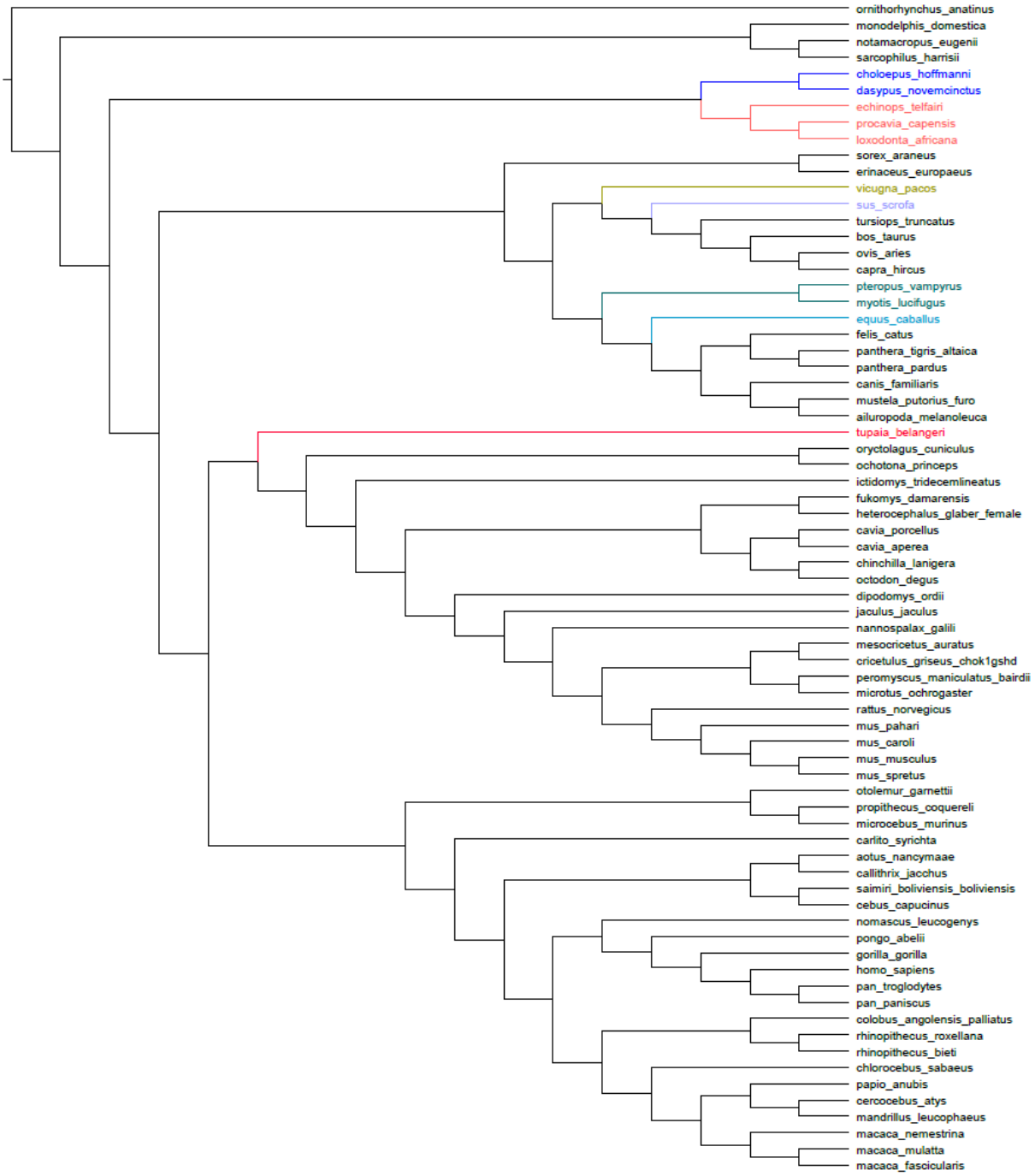

Figure S2 (d) - T4

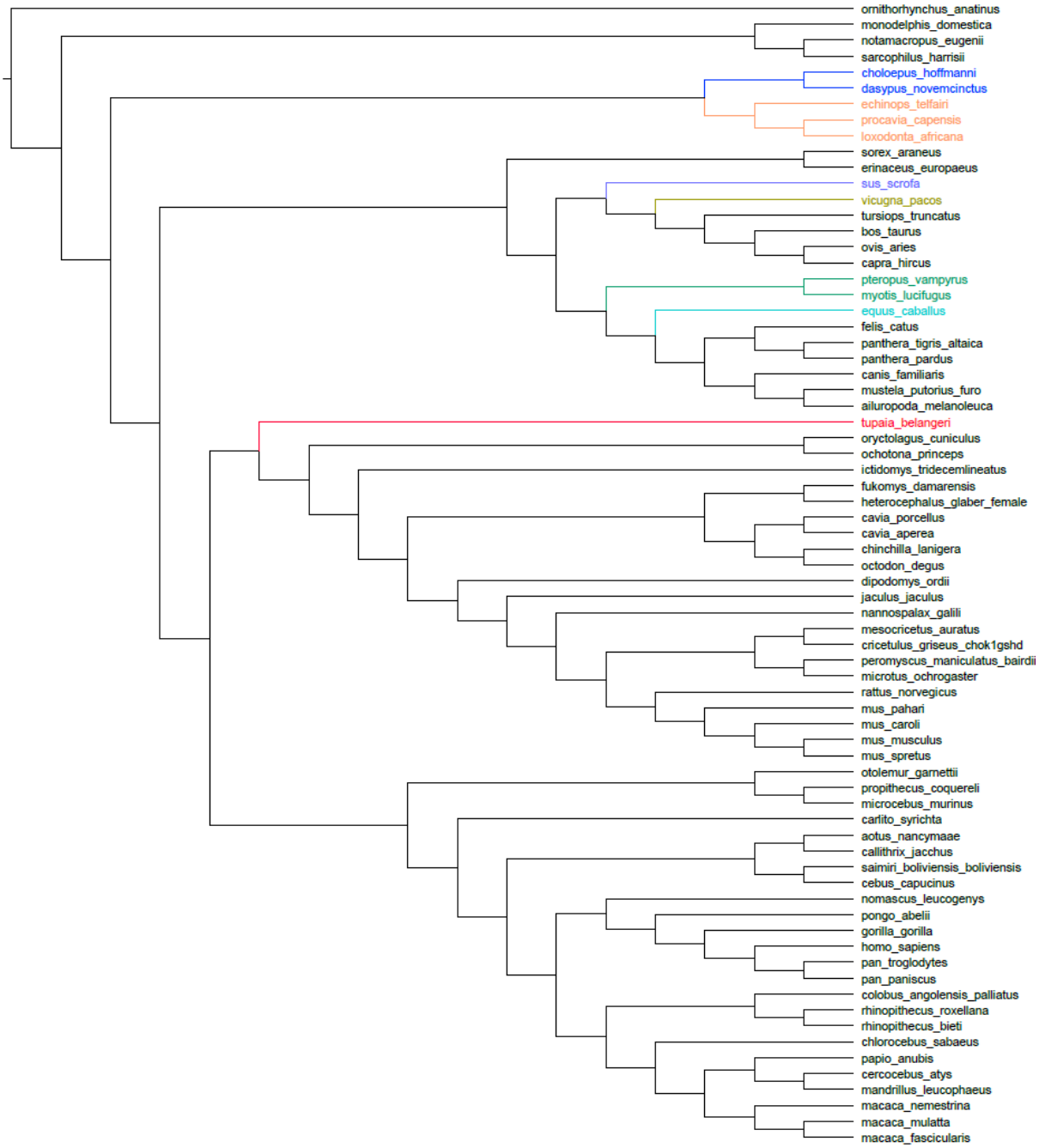

Figure S2 (e) - T5

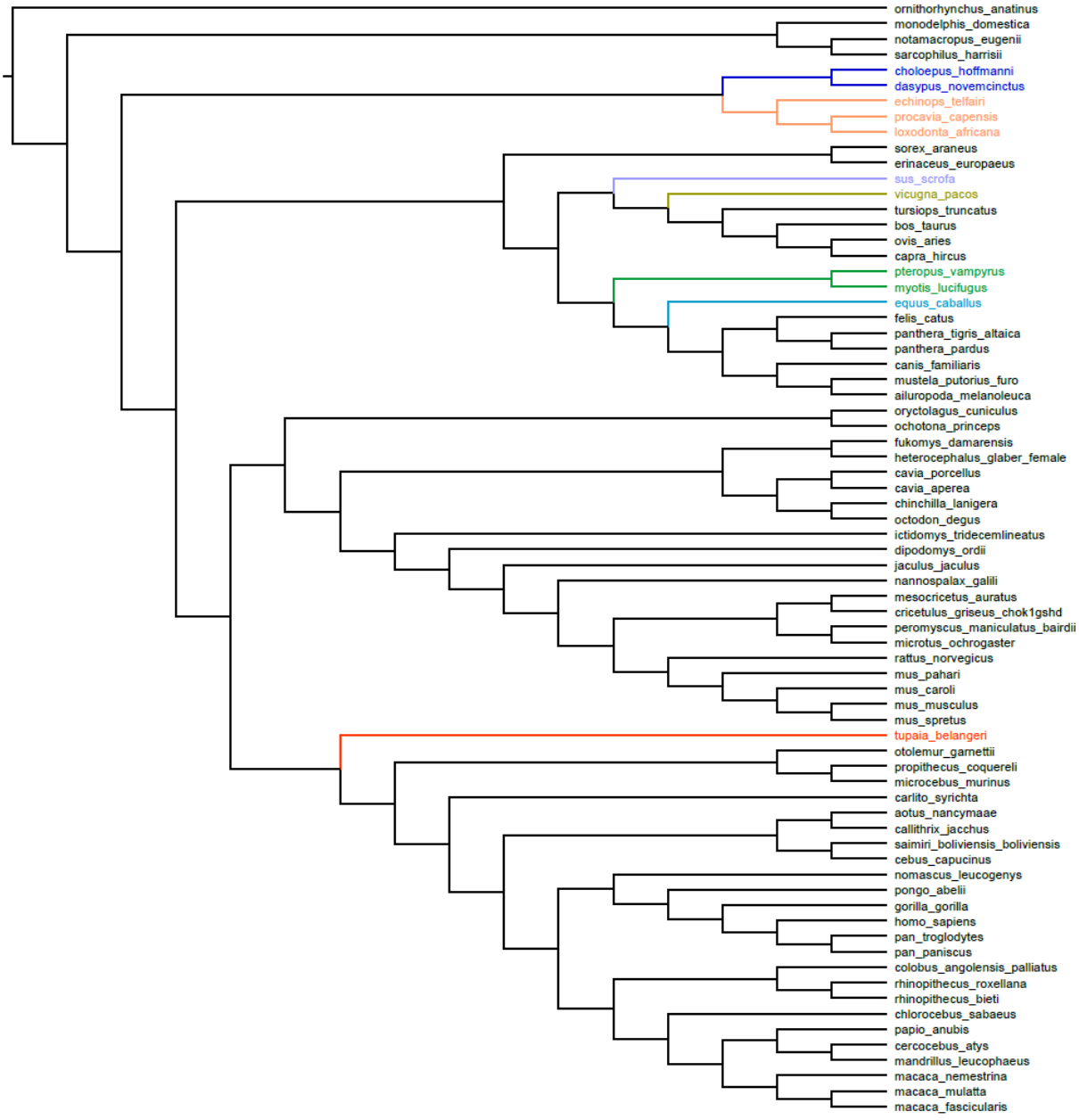

Figure S2 (f) - T6

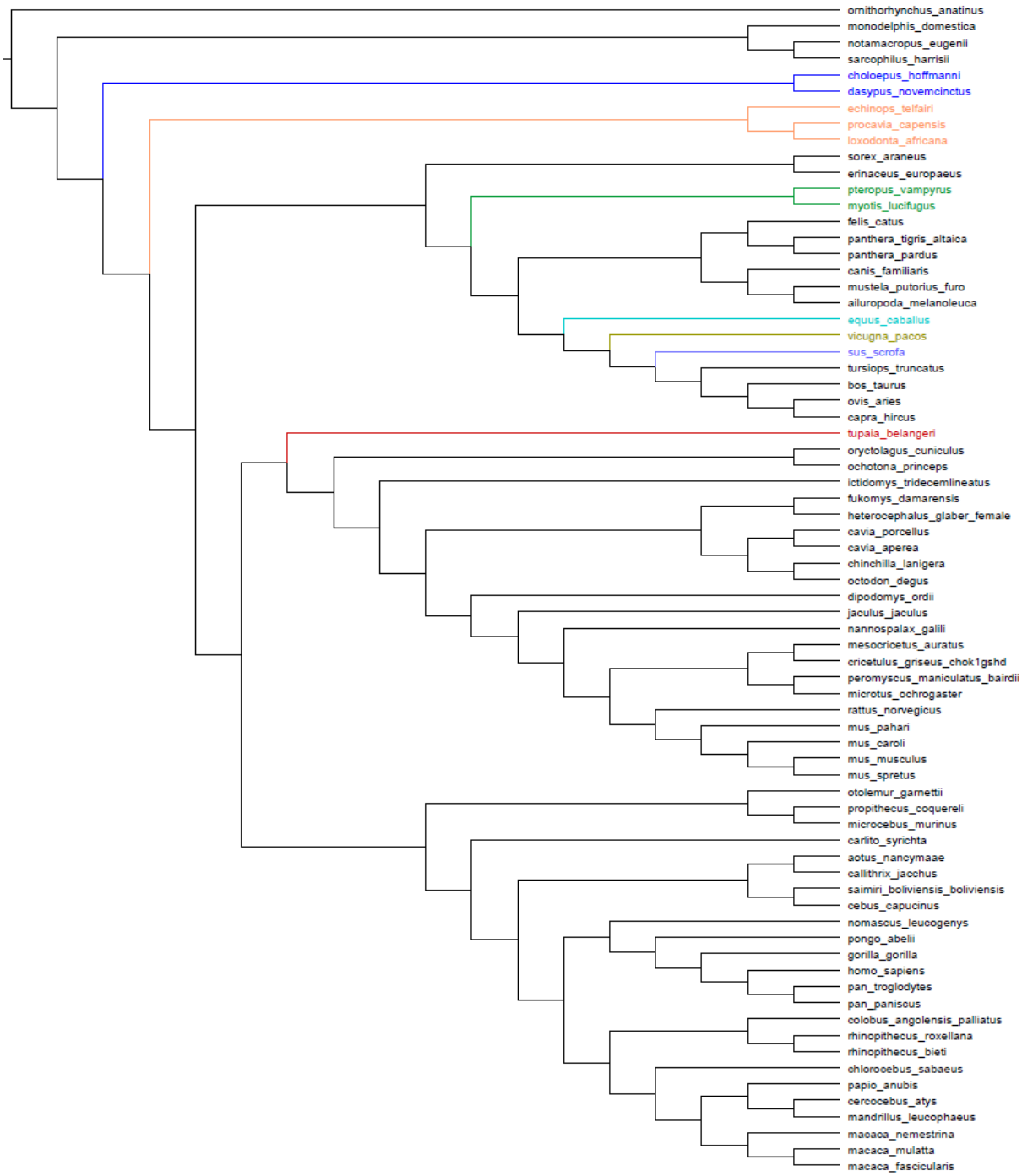

Figure S2 (g) - T7

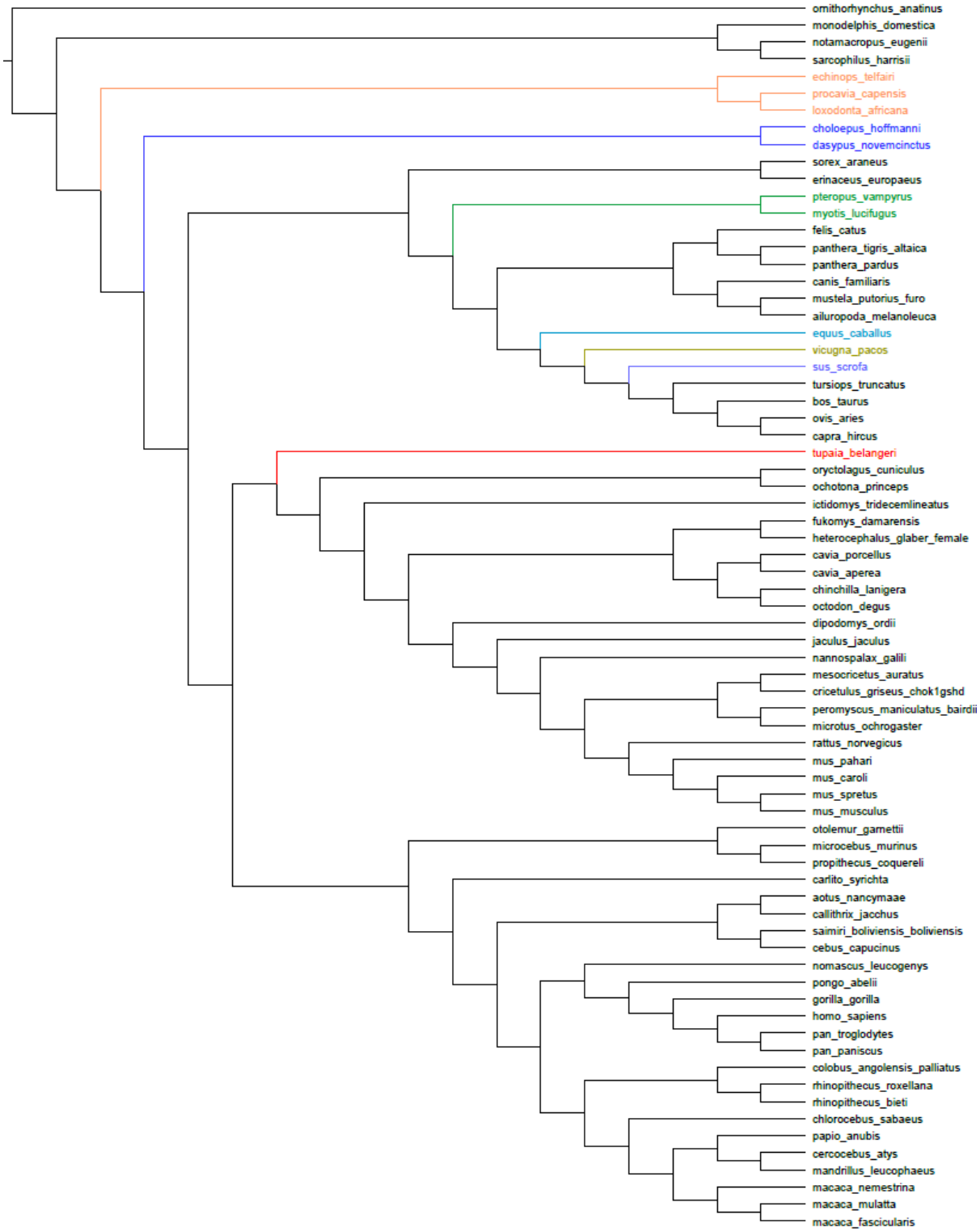

Figure S2: The seven mammal tree topologies analysed. a-T1, Atlantogenata rooting and *Tupaia belangeri* sister clade to Primates; **b-T2**, Atlantogenata rooting and *Tupaia belangeri* sister clade to Glires; **c-T3**, same as T1 but Chiroptera and *Equus caballus* are placed as sister clades to Carnivora; **d-T4**, same as T3 but *Vicugna pacos* and *Sus scrofa* exchange their placement; **e-T5**, same as T4 but *Tupaia belangeri* is sister clade to Primates; **f-T6**, Epitheria rooting and same placement for the other taxa as T2; **g-T7**, Exafroplacentalia rooting and same placement for the other taxa as T2. Taxa which topological placement changed are colored: (1, blue) Xenarthra, (2, orange) Afrotheria, (3, green) Chiroptera, (4, blue) *Equus caballus*, (5, yellow) *Vicugna pacos*, (6, purple) *Sus scrofa*, (7, red) *Tupaia belangeri*. The topologies in Newick format are available in the supplementary data.

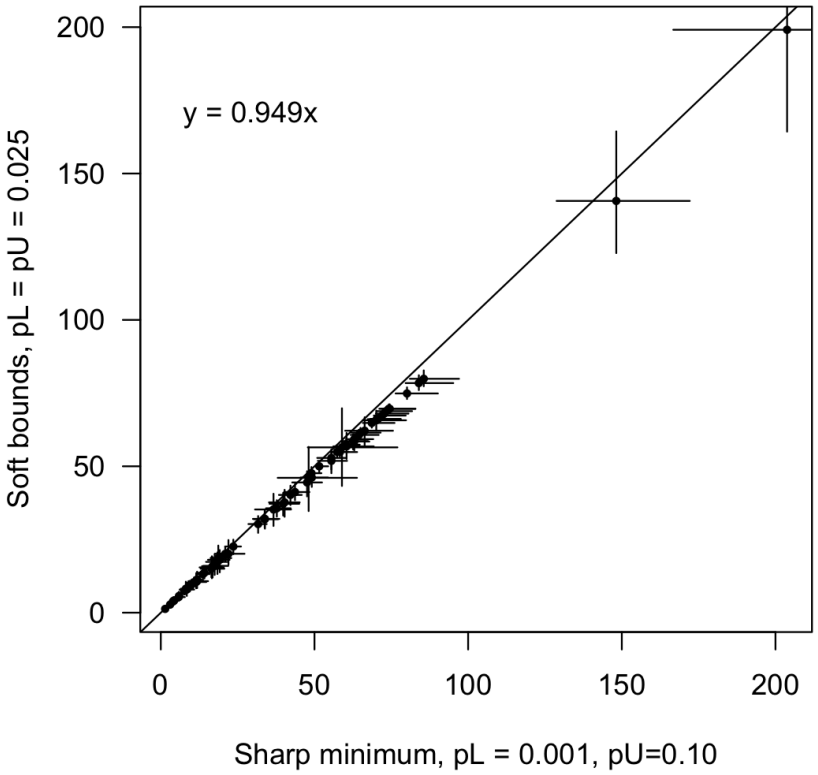

Figure S3: Comparison of posterior mean times (Ma) for the 72-genome phylogeny estimated using two different sets of bound violation probabilities. Points are plotted at the posterior mean ages. Error bars are 95% credibility intervals from the MCMC sample.

Table S8. Summary of the 32 fossil calibrations used in the 72-genome phylogeny.

Calibrated node	Old calibrations	Updated calibrations
Mammalia	B(1.649, 2.51254)	B(**1.641**, **2.522**)
Theria	B(1.2156, 1.696)	B(1.2156, **1.694**)
Placentalia	B(0.616, 1.646)	B(**0.6166**, **1.625**)
Euarchontoglires	B(0.616, 1.646)	B(**0.6166**, **1.625**)
Primates	B(0.56, 0.6611)	B(0.56, **0.6609**)
Anthropoidea	B(0.339, 0.6611)	B(0.339, **0.6609**)
Catarrhini	B(0.2444, 0.339)	B(0.2444, 0.339)
Hominidae	B(0.1163, 0.339)	B(**0.1165**, 0.339)
Homininae	B(0.0533, 0.339)	B(0.0533, 0.339)
Hominini	B(0.065, 0.1)	B(0.065, 0.1)
Cercopithecinae	B(0.0533, 0.34)	B(0.0533, **0.339**)
Papionini	B(0.053, 0.339)	B(**0.0533**, 0.339)

Strepsirrhini	B(0.339, 0.6611)	B(0.339, **0.6609**)
Glires	B(0.56, 1.646)	B(0.56, **1.625**)
Rodentia	B(0.56, 0.6611)	B(0.56, **0.6609**)
Nonsquirrel rodents[a]	B(0.476, 0.592)	B(**0.4807**, **0.5924**)
Dipodidae-Muroidea	B(0.407, 0.592)	B(**0.4103**, **0.5924**)
Murinae	B(0.072, 0.16)	B(**0.0725**, **0.1599**)
Lagomorpha	B(0.476, 0.6611)	B(**0.4807**, **0.6609**)
Euungulata[b]	B(0.524, 0.6611)	B(**0.507**, **0.6609**)
Artiodactyla	B(0.505, 0.6611)	B(**0.507**, **0.6609**)
Cetruminantia	B(0.505, 0.6611)	B(**0.507**, **0.6609**)
Bovidae	B(0.16, 0.281)	B(**0.1599**, **0.2729**)
Carnivora	B(0.373, 0.6611)	B(**0.3771**, **0.6609**)
Caniformia	B(0.373, 0.6611)	B(**0.3771**, **0.6609**)
Chiroptera	B(0.4760, 0.6611)	B(**0.4807**, **0.6609**)
Lipotyphla	B(0.6160, 1.6460)	B(**0.6166**, **1.625**)
Xenarthra	B(0.476, 1.646)	B(**0.4807**, **1.625**)
Afrotheria	B(0.56, 1.646)	B(0.56, **1.625**)
Paenungulata	B(0.56, 1.646)	B(0.56, **1.625**)
Marsupialia	B(0.4760, 1.313)	B(**0.4807**, **1.272**)
Eometatheria	B(0.2303, 0.56)	B(**0.2304**, 0.56)

Note: Calibrations are given in time unit = 100 Ma. Prior calibrations: soft-bound distributions are specified in `MCMCtree` format. The first number corresponds to the minimum age and the second to the maximum age in the soft-bound calibration, "B(max,min)". The second column, "Old calibrations", contains the calibrations used initially after the beginning of this project in 2016. The third column, "Updated calibrations", contains the geochronologically updated calibrations as of September 2021 (see changes in bold).
[a]Not included in tree hypothesis 5 due to taxa clustering differently.
[b]Not included in tree hypotheses 3, 4, and 5 due to taxa clustering differently.

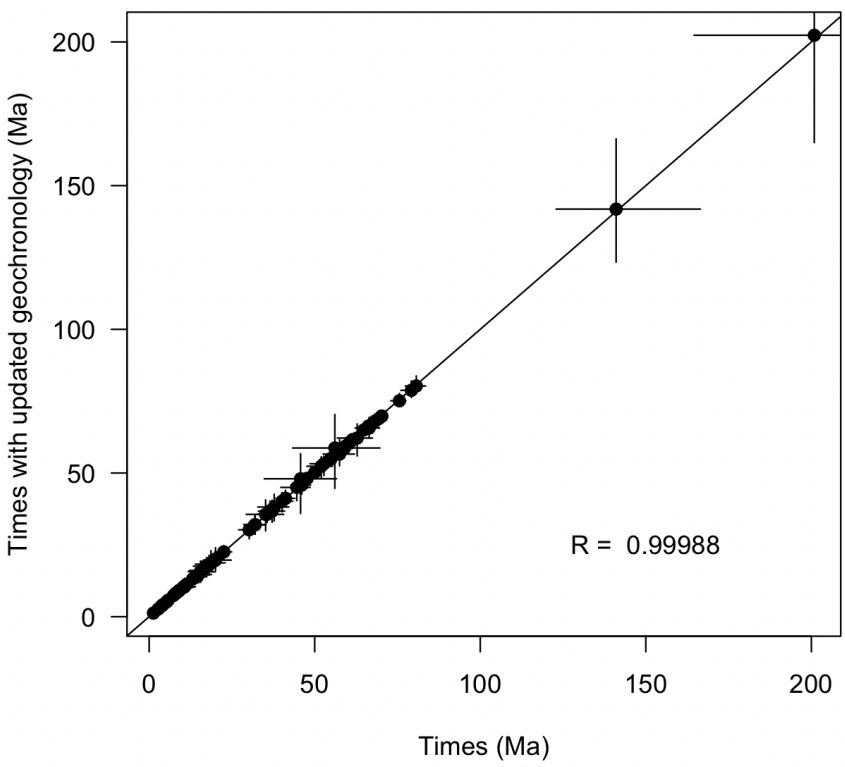

Figure S4: Comparison of posterior mean times (Ma) for the 72-genome phylogeny when using the original calibrations vs. the new calibrations with update geochronology (as of September 2021). Points are plotted at the posterior mean of node ages. Error bars are 95% credibility intervals from the MCMC. Solid line is *x* = *y*.

Table S9. Measures of effective sample size (ESS). For each tree (T1-T7), the ESS for bulk and tail quantiles together with the Rhat were measured for each parameter with the R package `rstan::monitor`. In addition, the ESS calculated with the `coda::effectiveSampleSize` has been included for comparison.

	MAIN (upd)[1]	**MAIN (old)[2]**	**T1**	**T3**	**T4**	**T5**	**T6**	**T7**
tail-ESS times (median)	232	929	2074	1839	2007	1118	2721	1362
tail-ESS times (min)	**61**	216	507	503	451	361	442	196
tail-ESS times (max)	3884	11669	22442	28525	27303	15411	29174	21129
bulk-ESS times (median)	180	374	1062	949	968	709	1295	751
bulk-ESS times (min)	**22**	**56**	142	**98**	177	125	193	103
bulk-ESS times (max)	2888	8358	16211	18054	19469	11241	19324	14015
Rhat (min)	0.9999884	1.000024	0.9999901	0.999998	0.9999954	0.9999916	0.9999919	1.000035
coda-ESS times (median)	426	1255	2495	2141	2301	1765	2634	2147
coda-ESS times (min)	62	179	285	353	373	330	355	266
coda-ESS times (max)	5722	9868	31305	34459	39686	21647	16136	28988
Number of samples	60003	160008	180009	200010	200010	180009	200010	160008

Note: An ESS for bulk and tail quantiles > 100 per chain is considered good. If Rhat $\leq$ 1.05, convergence is assumed. The ESS estimated with the coda package needs to be larger than or equal to 200.
[1] Values calculated with the posterior time estimates obtained when using the calibrations according to the geochronology updated as of September 2021.
[2] Values calculated with the posterior time estimates obtained when using the calibrations prior to September 2021.

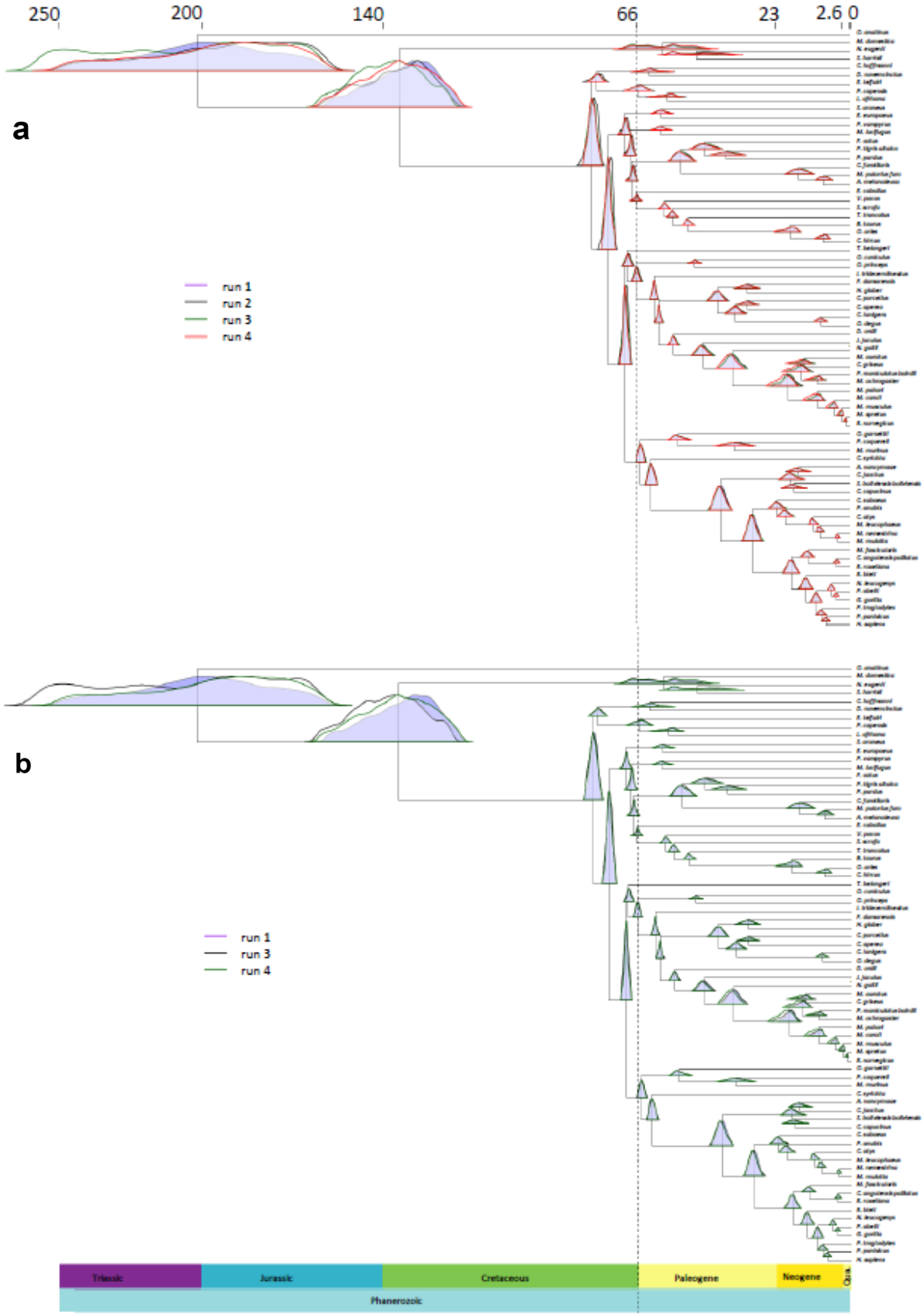

Figure S5. Posterior mean times for the MCMC chains that ran under the autocorrelated-rates clock model (GBM) using the main tree (T2) calibrated following the updated geochronology as of September 2021). The posterior distributions for the mean divergence times estimated in runs 1 to 4 are shown for the corresponding nodes in **a** (top), while **b** (bottom) does not include the results for chain 2 as they seem to have had convergence issues if compared to the mean time estimates obtained with the other chains. The tree with merged chains is available in Nexus format in the Supplementary Data. Abbreviations: Qua. = Quaternary.

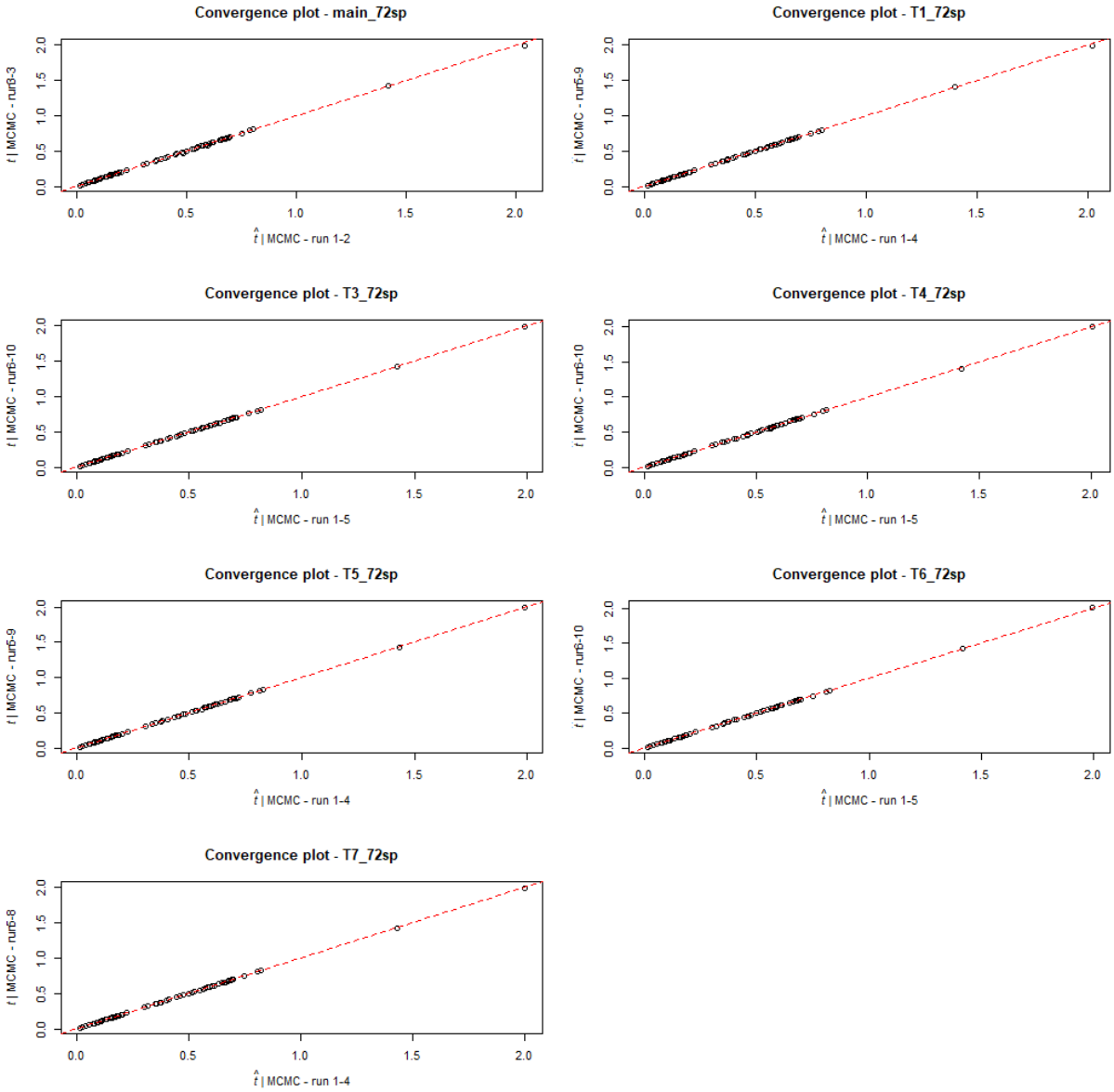

Figure S6. Scatterplot of the estimated posterior mean times for the MCMC runs under the autocorrelated-rates relaxed-clock model (GBM) model for each tree hypothesis. When comparing the mean estimates for half of the chains against the other half, they fall almost in a straight line (i.e., $x \simeq y$), thus visually showing that the chains have converged.

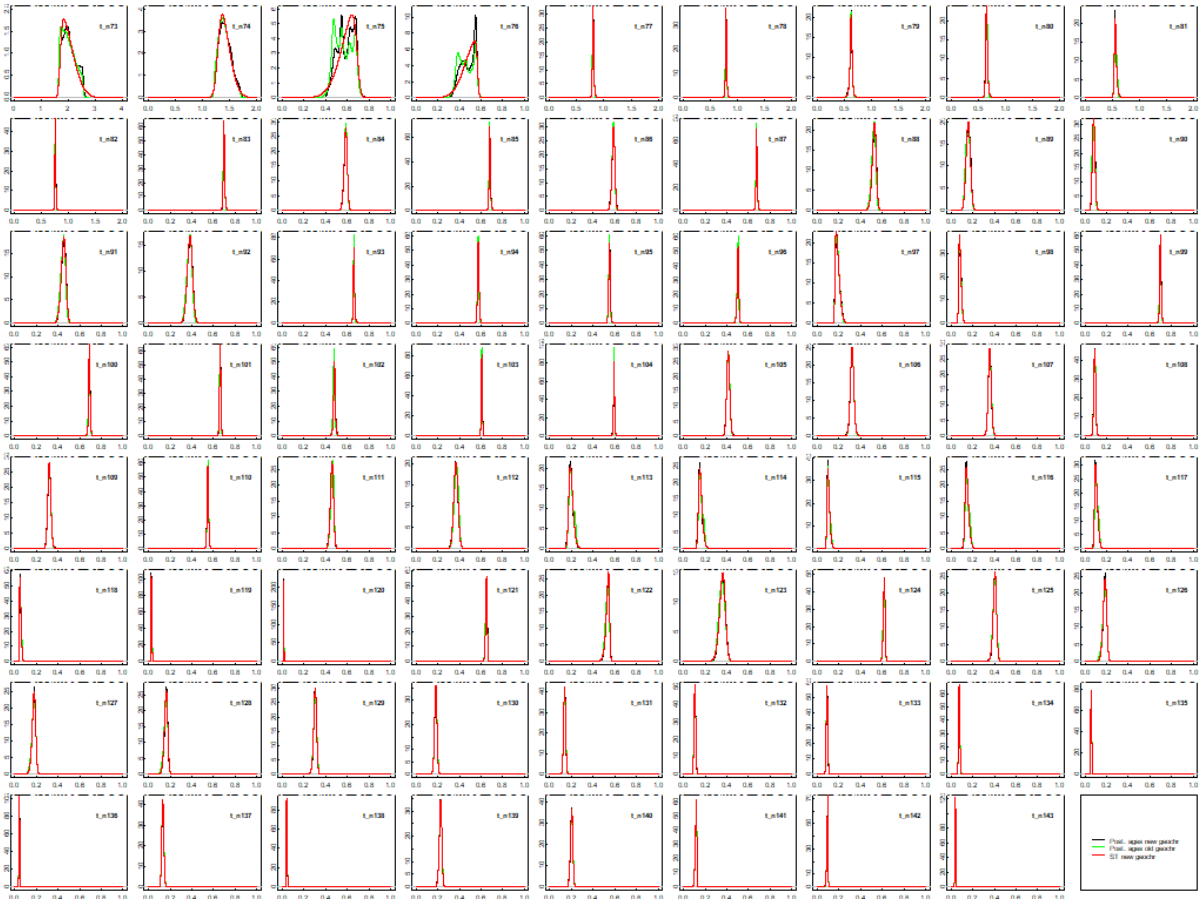

Figure S7. Assessment of the Skew-t (ST) distributions fitted to the internal nodes of the 72-species mammal tree. The ST distributions estimated with the `sn::st.mple` R function are plotted in red, those estimated when sampling from the posterior with `MCMCtree` when using the old set of calibrations in light green, and when sampling from the posterior with `MCMCtree` when using the calibrations with geochronology updates (as of September 2021) in black.

Table S10. Summary of soft-bound and low-bound calibrations used in molecular-clock dating of subtrees.

Calibrated node	Old calibrations
Cingulata	B(0.3485, 0.56)
Chlamyphoridae	B(0.339, 0.56)
Pilosa	B(0.3117, 0.56)
Folivora	B(0.1599, 0.56)
Vermilingua	B(0.1736, 0.56)
Chrysochloris asiatica - other chrysochlorids	B(0.036, 0.339)
Macroscelidea	B(0.2304, 0.56)
Proboscidea	B(0.0533, 0.2304)
Sirenia	B(0.4103, 0.6609)
Hyracoidea	B(0.0533, 0.339)
Paucituberculata	B(0, 0.1597)
Didelphidae	B(0.11608, 0.281)
Dasyuromorphia	B(0.1597, 0.33)[1]
Peramelidae	B(0.0436, 0.238)
Vombatiformes	B(0.255, 0.33)[1]
Phalangeridae - Burramyidae	B(0.25, 0.33)[1]
Petauridae - Pseudocheiridae	B(0.255, 0.33)[1]
Macropodoidea	B(0.247, 0.33)[1]
Platyrrhini	B(0.2045, 0.377)
Primatomorpha	B(0.64645, 0.68)
Scandentia	B(0.38, 0.66)
Suina	B(0.347, 0.53)[1]
Whippomorpha	B(0.478, 0.507) / L(0.507, 0, 0.01)[2]
Cetacea	B(0.3613, 0.56)
Mysticeti	B(0.1599, 0.48)[1]
Odontoceti	B(0.2304, 0.48)[1]
Delphinida	B(0.1599, 0.48)[1]
Phocoenidae - Monodontidae	B(0.076, 0.48)[1]

Hippopotamidae	B(0.0774, 0.48)[1]
Giraffidae	B(0.14, 0.48)[1]
Bovini	B(0.102, 0.16)[1]
Tragelaphini	B(0.0549, 0.16)[1]
Reduncini	B(0.05111, 0.16)[1]
Hippotragini - Alcelaphini	B(0.0648, 0.16)[1]
Alcelaphini	B(0.0505, 0.16)[1]
Caprinae	B(0.089, 0.16)[1]
Cervidae	B(0.17235, 0.284)
stem-Moschidae	B(0.195, 0.48)[1]
Neobalaeninae	B(0.2304, 0.339)
Balaenopteridae	B(0.073, 0.48)[1]
Physeteroidea	B(0.1382, 0.48)[1]
Perissodactyla	B(0.555, 0.6609)
Ceratomorpha	B(0.48078, 0.6609)
Prinodontidae - Felidae	B(0.281, 0.6609)
Herpestidae- Eupleridae	B(0.1597, 0.339)
Mustelidae-Procyonidae	B(0.2642, 0.33)[1]
Feliformia	B(0.19535, 0.48)[1]
Viverrinae - Genettinae	B(0.2044, 0.48)[1]
Lobodontini	B(0.0505, 0.33)[1]
Phocidae	B(0.1382, 0.33)[1]
Otarioidea	B(0.1597, 0.33)[1]
Pinnipedia	B(0.2045, 0.2729)
Hipposideridae - Rhinolophidae	B(0.38, 0.56)
Megadermatidae - Craseonycteridae	B(0.339, 0.478)
Molossidae - Vespertilionidae + Miniopteridae	B(0.38, 0.56)
Natalidae - Vespertilionidae + Miniopteridae + Molossidae	B(0.38, 0.56)
Sciuromorpha	B(0.4103, 0.5924)

Abrocomidae	B(0.01778, 0.1382)
Monotremata	B(0.24459, 1.332)
Tachyglossidae	B(0.0258, 1.332)

Note: Time unit is 100 Ma. Calibrations are specified in `MCMCtree` format, with "B(max, min)" giving the minimum and maximum bounds respectively and "L(min)" giving the minimum bound.
[1] The maximum ages of these calibrations are set to be the 2.5% quantile of the ST distributions on the corresponding ancestors. This adjustment is done to avoid truncation artefacts against the ST and soft-bound calibrations.
[2] The posterior age of the parent node, Cetruminantia (derived from the 72-taxon tree), is in conflict with its fossil calibration (Himalayacetus, 50.7 Ma, from the Yipressian deposits of the Subathu Formation, India), with the 2.5% quantile of the posterior close to ~48 Ma. This node, Whippomorpha, uses the same fossil constraint as its parent, thus creating a conflict with the ST calibration on its parent node. We deal with this conflict by dating the Artiodactyla subtree twice, once using the 50.7 Ma minimum, and again using a minimum of 47.8 Ma, which is the top of the Ypressian. The 'B' calibration results are used in the stitched tree of 4,705 taxa.

Table S11. Summary of ST/SN-fitted calibrations used in molecular-clock dating of subtrees.

Calibrated node	ST/SN calibrations	Subtree
Mammalia	ST(1.642, 0.425, 12.652, 1714.565)	Afrotheria
Afrotheria	ST(0.653, 0.017, 0.302, 11.274)	Afrotheria
Paenungulata	ST(0.55, 0.028, 1.247, 14.653)	Afrotheria
Mammalia	ST(1.642, 0.425, 12.652, 1714.565)	Euarchonta
Euarchontoglires	ST(0.695, 0.007, 0.32, 7.619)	Euarchonta
Primates	ST(0.655, 0.01, -1.355, 178.316)	Euarchonta
Strepsirrhini	ST(0.548, 0.026, -2.506, 66.983)	Euarchonta
Propithecus - Microcebus	ST(0.37, 0.033, -0.876, 275.655)	Euarchonta
Haplorrhini	ST(0.622, 0.011, -1.196, 166.803)	Euarchonta
Anthropoidea	ST(0.415, 0.021, -1.14, 156.796)	Euarchonta
Aotidae - Callitrichidae	ST(0.186 ,0.033, -1.856, 48.135)	Euarchonta
Cebidae	ST(0.189, 0.021, -1.722, 40.505)	Euarchonta
Catarrhini	ST(0.314, 0.018, -1.23, 314.095)	Euarchonta
Cercopithecoidea	ST(0.182, 0.012, -0.054, 88.157)	Euarchonta
Cercopithecinae	ST(0.136, 0.009, -1.159e-07, 10)	Euarchonta
Papionini	ST(0.1, 0.009, 0.641, 145.414)	Euarchonta

Papio - Mandrillus	ST(0.087, 0.007, 0.195, 50.335)	Euarchonta
Cercocebus atys - *Mandrillus leucophaeus*	ST(0.073, 0.006, 0.229, 40.768)	Euarchonta
Genus Macaca	ST(0.053, 0.007, 1.101, 200.596)	Euarchonta
Macaca fascicularis - *Macaca mulatta*	ST(0.039, 0.005, 1.207, 108.063)	Euarchonta
Colobinae	ST(0.127, 0.011, 0.584, 209.998)	Euarchonta
Genus Rhinopithecus	ST(0.038, 0.007, 1.525, 104.388)	Euarchonta
Hominoidea	ST(0.236, 0.016, -1.223, 135.248)	Euarchonta
Hominidae	ST(0.21, 0.015, -1.248, 109.524)	Euarchonta
Homininae	ST(0.122, 0.012, -4.859, 295.449)	Euarchonta
Hominini	ST(0.101, 0.01, -7.603, 93.226)	Euarchonta
Pan paniscus - *Pan troglodites*	ST(0.038, 0.003, -0.337, 47.276)	Euarchonta
Mammalia	ST(1.642, 0.425, 12.652, 1714.565)	Lagomorpha
Lagomorpha	SN(0.474, 0.008, 0.293)	Lagomorpha
Mammalia	ST(1.642, 0.425, 12.652, 1714.565)	Artiodactyla
Artiodactyla	ST(0.577, 0.007, -0.634, 7.509)	Artiodactyla
Artiofabula	ST(0.554, 0.008, -0.964, 7.343)	Artiodactyla
Cetruminantia	ST(0.507, 0.009, -1.513, 6.294) / ST(0.479, 0.016, -1.513, 6.294)	Artiodactyla
Bovidae	ST(0.149, 0.025, 5.863, 624.148) / ST(0.149, 0.025, 5.863, 624.148)	Artiodactyla
Ovis aries - *Capra hircus*	ST(0.059, 0.016, 3.225, 169.672) / ST(0.058, 0.014, 3.225, 169.672)	Artiodactyla
Mammalia	ST(1.642, 0.425, 12.652, 1714.565)	Chiroptera (I and II)
Chiroptera	ST(0.596, 0.016, -1.239, 13.572)	Chiroptera (I and II)
Mammalia	ST(1.642, 0.425, 12.652, 1714.565)	Rest of Laurasiatheria
Laurasiatheria	ST(0.694, 0.006, 0.431, 4.953)	Rest of Laurasiatheria
Erinaceidae - Soricidae	ST(0.596, 0.017, -1.243, 19.856)	Rest of Laurasiatheria
Scrotifera	ST(0.678, 0.006, 0.37, 4.464)	Rest of Laurasiatheria

Chiroptera	ST(0.596, 0.016, -1.239, 13.572)	Rest of Laurasiatheria
Fereungulata	ST(0.671, 0.005, 0.355, 4.329)	Rest of Laurasiatheria
Carnivora	ST(0.538, 0.027, -2.115, 70.375)	Rest of Laurasiatheria
Felidae	ST(0.14, 0.02, 0.417, 367.218)	Rest of Laurasiatheria
Pantherinae	ST(0.067, 0.015, 1.12, 331.497)	Rest of Laurasiatheria
Caniformia	ST(0.467, 0.031, -1.966, 117.012)	Rest of Laurasiatheria
Arctoidea	ST(0.397, 0.031, -1.415, 427.391)	Rest of Laurasiatheria
Euungulata	ST(0.660, 0.005, 0.341, 4.207)	Rest of Laurasiatheria
Artiodactyla	ST(0.577, 0.007, -0.634, 7.509)	Rest of Laurasiatheria
Mammalia	ST(1.642, 0.425, 12.652, 1714.565)	Marsupialia
Didelphimorphia - Australidelphia	ST(0.562, 0.08, 0.035, 299.837)	Marsupialia
Eometatheria	ST(0.459, 0.068, 0.025, 623.433)	Marsupialia
Mammalia	ST(1.642, 0.425, 12.652, 1714.565)	Ctenohystrica
Rodentia	ST(0.606, 0.005, 0.178, 5.22)	Ctenohystrica
Caviomorpha - Phiomorpha	ST(0.414, 0.014, -0.164, 18.225)	Ctenohystrica
Phiomorpha	ST(0.324, 0.016, -0.255, 17.835)	Ctenohystrica
Caviomorpha (Cavioidea - Erethizontoidea)	ST(0.356, 0.014, 0.022, 18.214)	Ctenohystrica
Cavia porcellus - *Cavia aperea*	ST(0.086, 0.01, 0.671, 36.22)	Ctenohystrica
Chinchilla lanigera - *Octodon degus*	ST(0.317, 0.014, 0.203, 19.215)	Ctenohystrica
Mammalia	ST(1.642, 0.425, 12.652, 1714.565)	Rest of Rodentia (I and II)
Dipodomys ordii - Myomorpha	ST(0.55, 0.006, -0.171, 6.759)	Rest of Rodentia (I)
Dipodidae-Muroidea	ST(0.473, 0.017, -1.282, 13.044)	Rest of Rodentia (I)
Nannospalax galili - Muridae	ST(0.382, 0.022, -0.67, 36.812)	Rest of Rodentia (I)
Muridae	ST(0.174, 0.035, 3.117, 381.97)	Rest of Rodentia (I and II)
Mesocricetus auratus - *Cricetulus griseus*	ST(0.081, 0.022, 3.756, 209.065)	Rest of Rodentia (I)

Peromyscus maniculatus - *Microtus ochrogaster*	ST(0.128, 0.029, 3.532, 404.416)	Rest of Rodentia (I)
Murinae	ST(0.094, 0.027, 3.794, 547.445)	Rest of Rodentia (I)
Murinae	ST(0.086, 0.021, 3.794, 547.445)	Rest of Rodentia (II)
Cricetidae	ST(0.137, 0.03, 3.464, 240.317)	Rest of Rodentia (II)
Mus pahari - rest of Mus	ST(0.043, 0.013, 3.575, 94.222)	Rest of Rodentia (II)
Mus caroli - rest of Mus	ST(0.022, 0.007, 3.426, 86.245)	Rest of Rodentia (II)
Mus spretus - *Mus musculus*	ST(0.0104, 0.003, 3.38, 83.529)	Rest of Rodentia (II)
Mammalia	ST(1.642, 0.425, 12.652, 1714.565)	Xenarthra
Xenarthra	ST(0.628, 0.019, -0.389, 4.88)	Xenarthra

Note: Time unit is 100 Ma. Calibrations are specified in `MCMCtree` format. ST calibrations are given as "ST(a, b, c, d)", with a, b, c, and b being the location, scale, shape and degrees of freedom respectively (see `MCMCtree`'s manual for details). Skew-normal distributions are given as "SN(a, b, c)", with parameters to be the same as in ST but without the degrees of freedom. For Cetruminantia, Bovidae, and *Ovies*-*Capra*, two versions are provided corresponding to the B and L calibrations on Whippomorpha, respectively (Table S10).

Table S12. Effective sample sizes (ESS) for each subtree. The ESS for bulk and tail quantiles together with the Rhat were measured for each parameter with the R package `rstan::monitor`. In addition, the ESS calculated with the `coda::effectiveSampleSize` has been included for comparison (part I).

	Afro.	**Eua.**	**Lag.**	**Art.**	**Chi-I**	**Chi-II**	**L.rest.**
tail-ESS times (median)	130906	4651	36837	14401	65955	1958	1573
tail-ESS times (min)	27957	305	9338	1713	461	112	171
tail-ESS times (max)	278303	17309	251588	51125	211161	10379	6221
bulk-ESS times (median)	68429	1527	11006	6102	26290	419	523
bulk-ESS times (min)	16209	167	4679	1066	329	**19**	**68**
bulk-ESS times (max)	244573	14074	136426	47870	172817	9045	5870
Rhat (min)	0.9999971	0.9999437	0.9999968	0.999981	0.9999965	0.9999122	0.9998421
coda-ESS times (median)	138179	3397	22876	12623	59814	1622	1223
coda-ESS times (min)	29675	476	10151	2397	409	**82**	**164**
coda-ESS times (max)	519552	27388	263722	96251	343651	17425	11988
No. samples	640032	35507	600030	104802	493192	21725	12572
No. taxa	60	486	88	431	256	634	659

Note: An ESS for bulk and tail quantiles > 100 per chain is considered good. If Rhat $\leq$ 1.05, convergence is assumed. The ESS estimated with the coda package needs to be larger than or equal to 200. **Abbreviations**: Afro. = Afrotheria, Eua. = Euarchonta, Lag. = Lagomorpha, Art. = Artiodactyla, Chi-I = Chiroptera (I), Chi-II = Chiroptera (II), L.rest. = Rest of Laurasiatheria. **No. taxa**: All subtrees include 3 taxa as outgroup. Some subtrees include common taxa in other subtrees to avoid issues with calibrations: Rest of Laurasiatheria = 4 repeated taxa, Chiroptera (I) = 1 repeated taxon, Chiroptera (II) = 1 repeated taxon.

Table S13. Effective sample sizes (ESS) for each subtree. The ESS for bulk and tail quantiles together with the Rhat were measured for each parameter with the R package `rstan::monitor`. In addition, the ESS calculated with the `coda::effectiveSampleSize` has been included for comparison (part II).

	Mar.	**Cte.**	**Sci.**	**Rod-I**	**Rod-II**	**Xen.**
tail-ESS times (median)	48352	94398	74820	1615	569	149875
tail-ESS times (min)	4047	13121	7537	247	**40**	28838
tail-ESS times (max)	135255	315674	260577	14387	2471	285304
bulk-ESS times (median)	20550	37585	29477	843	**95**	75308
bulk-ESS times (min)	123593	5727	7785	125	**14**	13837
bulk-ESS times (max)	4579	308325	201905	13662	2502	226337
Rhat (min)	0.999993	0.9999969	0.9999969	0.9999344	0.999821	0.999997
coda-ESS times (median)	43470	75039	61317	2113	329	150844
coda-ESS times (min)	7617	11372	13229	**53**	**29**	30200
coda-ESS times (max)	245808	634321	354877	26974	4951	439262
No. samples	284546	640032	639984	30169	11096	640032
No. taxa	307	210	267	630	691	33

Note: An ESS for bulk and tail quantiles > 100 per chain is considered good. If Rhat $\leq$1.05, convergence is assumed. The ESS estimated with the coda package needs to be larger than or equal to 200. **Abbreviations**: Mar. = Marsupialia, Cte. = Ctenohystrica, Sci. = Sciuridae and related, Rod-I = Rest of Rodentia (I), Rod-II = Rest of Rodentia (II), Xen. = Xenarthra. **No. taxa**: All subtrees include 3 taxa as outgroup. Some subtrees include common taxa in other subtrees to avoid issues with calibrations: Rest of Rodentia (II) = 2 repeated taxa, Rest of Rodentia (I) = 2 repeated taxa, Ctenohystrica = 1 repeated taxon.

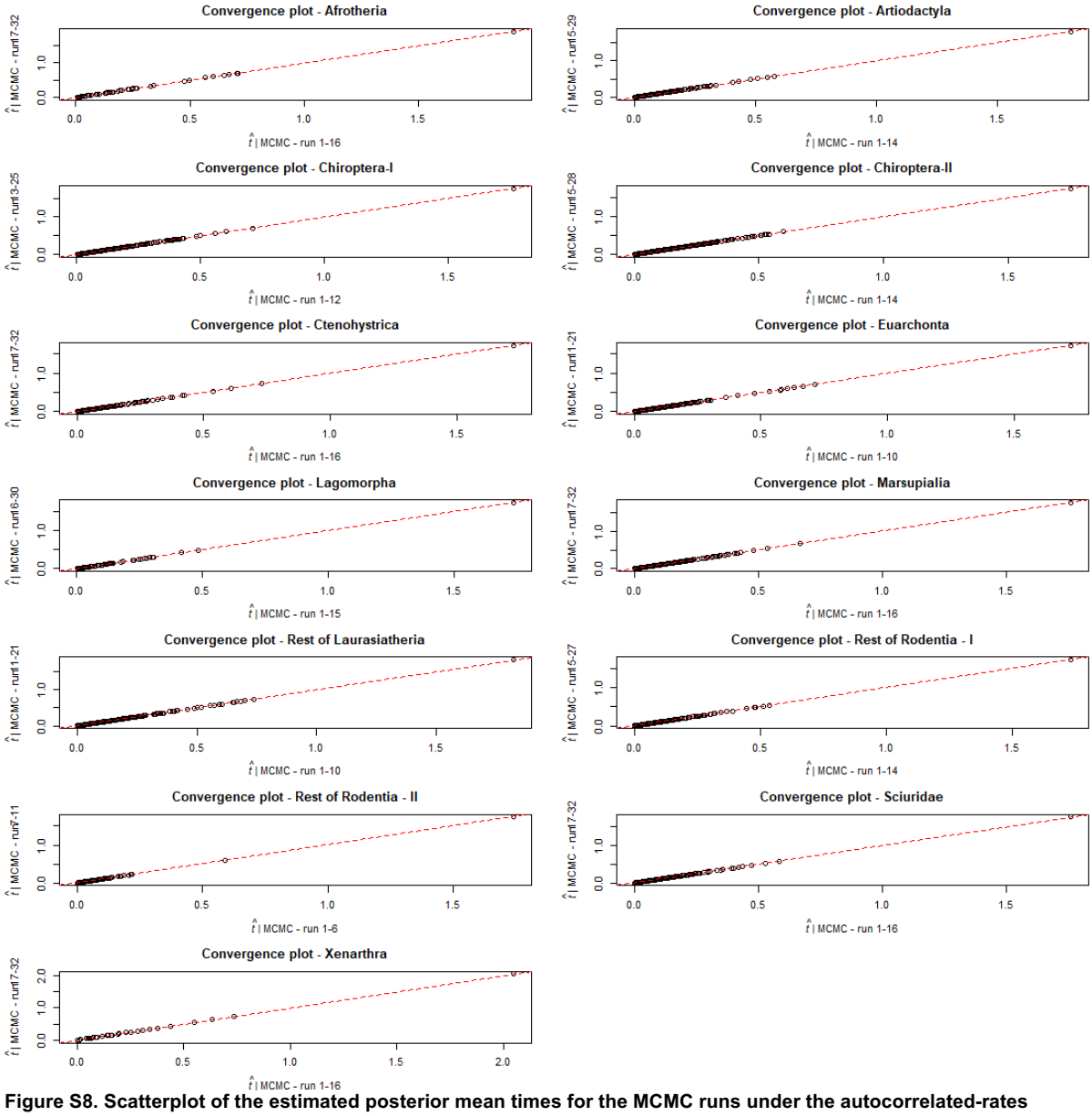

Figure S8. Scatterplot of the estimated posterior mean times for the MCMC runs under the autocorrelated-rates relaxed-clock model (GBM) model for each of the 13 subtrees. The mean estimates for half of the chains are plotted against the other half. They fall almost perfectly on the $x = y$ line, thus visually showing the two sets of chains have converged to the same distribution. Note that 32 MCMC chains were run for each subtree, but some of those did not pass quality filters (e.g., convergence) and were not included.

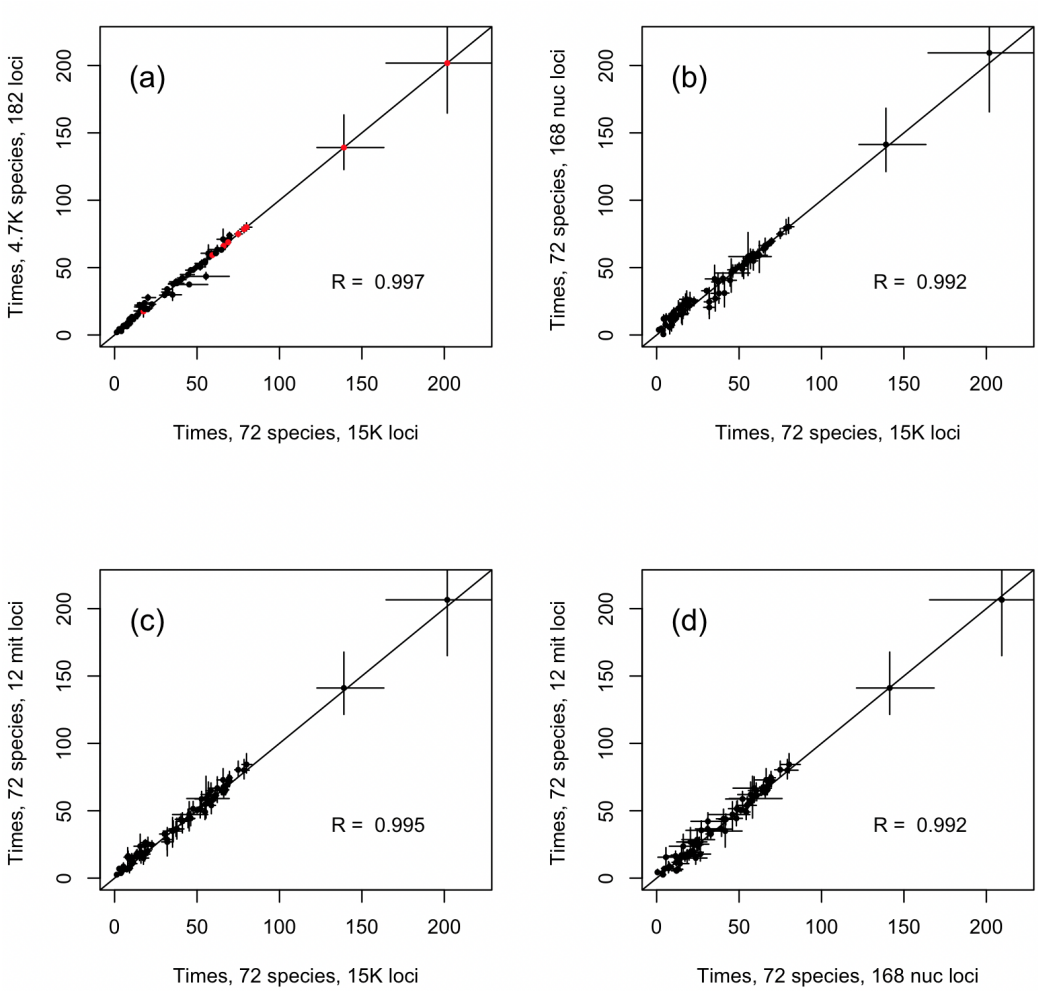

Figure S9. Integrity of divergence time estimates across dating steps and data partitions. a, Estimated posterior mean of divergence times from step I plotted against estimates from step II. Red dots are the nine nodes from the main 72-taxon tree that are not present in any subtree. The posterior time estimates for these nodes in the final stitched tree are the same as the estimates in the main tree. **b-c**, Estimates of posterior mean of divergence times on 72 taxa using the 182 loci step II dataset (with nuclear and mitochondrial loci analysed separately and using the original fossil calibrations), plotted against the estimates fusing 15K loci from step I. **d**, The estimates from the mitochondrial and nuclear loci plotted against each other. In all cases vertical and horizontal bars are the 95% CIs from the MCMC sample. Points are plotted at the posterior mean of node ages.

Integrity of time estimates across dating steps and data partitions

We assessed integrity of time estimates across dating steps and partitions. Figure S9 a shows the estimates of divergence times from step I (using the 72 genomes) vs those from step II (using 4,705 taxa) for the 71 nodes shared between the analyses. The posterior mean time estimates between the analyses are highly correlated. This does not appear surprising given the posterior of times in step I is used as the prior in step II. However, note the posterior means and 95% CIs do differ between the two analyses. This is a consequence of the increased taxon sampling in step II with corresponding use of additional fossil calibrations. We also assessed whether the nuclear and mitochondrial loci from the step II dataset produced similar time estimates. We extracted the 72 taxa from the 182 loci dataset and re-estimated the divergence times using the original fossil calibrations, with the mitochondrial and nuclear loci analysed separately (Figure S10 b-d). Time estimates are highly correlated and consistent when compared against the estimates from the 15K loci analysis (Figure S10 b-c) and when compared against each other (Figure S10 d).

Technical comment on the sequential Bayesian-subtree approach

The sequential Bayesian approach with subtree stitching used here is approximate. The joint posterior of divergence times on a phylogeny contains a correlation structure. This correlation structure is discarded when fitting the ST and SN densities to the marginal posteriors and when using these fitted densities as priors in the second step of the analysis[1]. A potential source of correlation may emerge from the constraint that nodes cannot be older than their ancestors. In divergence dating, this means the joint density of ages of nodes and their parents are truncated along the x = y diagonal[2]. For example, consider the sample from two joint independent normals with mean = 0 and s.d. = 0.5. If a truncation along the x = y line is applied so that samples in the x < y region are discarded, a positive correlation is generated on the remaining samples in the x > y region (Figure S10, left panel). On the other hand, if we sample from two joint independent normals with means 2 and –2, both with s.d. = 0.5, and apply the same truncation, no positive correlation is generated because the joint density is far from the x = y line and no data are discarded (Figure S10, right panel).

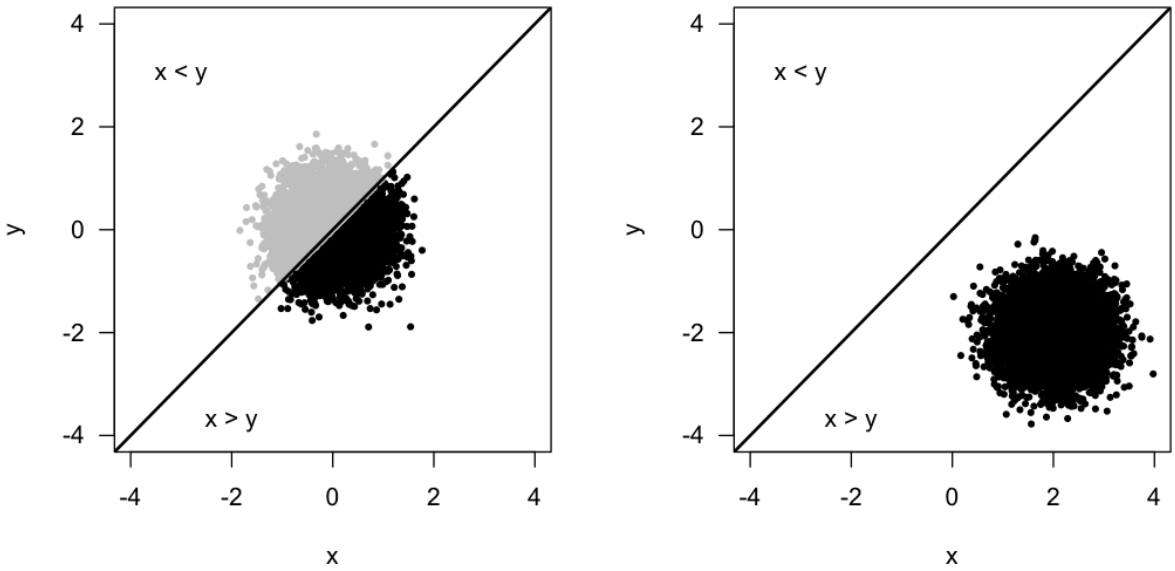

Figure S10. The effect of truncation on correlation. Left, a joint sample from two independent normal densities with mean = 0 and s.d. = 0.5 is generated, and a truncation along the x < y is applied. **Right**, a joint sample from two independent normal densities with means 2 and –2 and s.d. = 0.5 is generated, and the same truncation is applied. However, in this case, the truncation x = y line is far from the joint sample and no actual data are removed. Truncated (removed) samples are shown in light gray, and non-truncated samples are shown in black. Sample correlations after truncation are R = 0.468 (left) and R = 0.0126 (right).

If the marginal posterior densities on the ages of a node and its parent overlap, truncation means a positive correlation is present in the joint posterior, similar to the case of the left panel of Figure S10. Thus, when fitting ST or SN densities to the marginal posteriors, this correlation is discarded. In this case, the sequential Bayesian approach may not work well because the ST and SN calibrations will be a poorer approximation to the joint posterior of the corresponding node ages. On the other hand, if the marginal posterior densities of the ages of a node and its parent do not overlap (as in the right panel of Figure S10), then truncation is not an issue and the fitted ST and SN calibrations will provide an appropriate approximation.

Consequently, we recommend users examine the joint posterior of node ages in the first step of the sequential approach to assess whether truncation is present. If the marginal posterior density of the age of a node overlaps extensively with those of its ancestors, then truncation will be present and it will be substantial; using the sequential approach in this case may result in a poor approximation. In particular, if truncation is substantial and if the posterior of a daughter node's age is used to calibrate the root of a subtree, it may not be

possible to stitch the subtree back into the main tree because the mean posterior age of the subtree's root may, for example, be older than the posterior mean of the parent node in the main tree (a consequence of ignoring truncation and correlation).

Benchmarking

We performed a benchmarking analysis to calculate the computational time savings of our Bayesian sequential-subtree approach. We ran one MCMC chain for each subtree (using its appropriate fossil calibrations and rate prior, and approximate likelihood) with a burn-in of 150,000 iterations and a total of 10,000 samples collected every 100 iterations (note that, in `MCMCtree`, one iteration is one cycle in which all model parameters are sampled sequentially[3]). We then calculated the ESS of the divergence times per hour of computation (Figure S11). For example, the smallest subtree, Xenarthra (33 taxa), achieved a median ESS of 2,400 per hour. As the number of taxa increases, the computational efficiency decreases (Figure S11). The largest subtree, "Rest of Rodentia (II)" (691 taxa) has an expected median of only ESS of 0.903 per hour (Figure S11), a 2,657x reduction in sampling efficiency per time unit when compared to Xenarthra. Extrapolating these results to 4,705 taxa, we get an expected median ESS per hour of 7.8×10^{-3} (Figure S11). This means that obtaining a median ESS of 1,000 on the 4,705-taxon phylogeny would require running the MCMC chain for ~15 years (128K hours). Of course, the analysis could be parallelised, but this would require many months per chain and each chain would still need its own expensive burn-in period. In total, we estimate a 115x time saving when comparing the required MCMC lengths for our largest subtree against the full 4,705-taxon phylogeny.

Computational improvements are also due to the use of approximate likelihood calculation[4], which a previous benchmarking study[5] places very close to 1000x. Three of the most widely used Bayesian molecular-clock dating programs (`MrBayes`, `BEAST`, and `PhyloBayes`) implement exact likelihood only. Thus, if using exact likelihood, our largest subtrees would be expected to need over 1.12 M hours (126 years) of computation to achieve a median ESS of 1,000. This appears unfeasible, and thus subtrees would need to be made smaller (less taxa) and chains would have to run for shorter times to achieve an ESS in the order of 100 or less. Such small ESSs would sacrifice precision of MCMC parameter estimates. We note the ESS per hour may depend not only on the number of taxa in the tree, but also on the number of partitions, the clock model, the number of fossil calibrations used, the variance of the calibration densities, and whether the calibrations are in conflict or not. Thus, it may be possible to further adjust these to reduce computation time at the cost of information loss.

We estimate the totality of the approximate likelihood analysis here (excluding the clock model selection analysis which used exact likelihood) took ~80K hours or ~9 years of CPU time. Because 1 day of CPU computing emits ~5 Kg CO_2 (see [6]), this means our analysis emitted roughly 16.7K metric tonnes of CO_2. Without the subtree approach (i.e., attempting to estimate the times on the whole 4,705-taxon tree directly), the analyses would have required over 115x more CPU time and thus would have emitted over 1.9 million tonnes of CO_2. Without the use of approximate likelihood, computation times and CO_2 emissions would have increased by 1,000 fold.

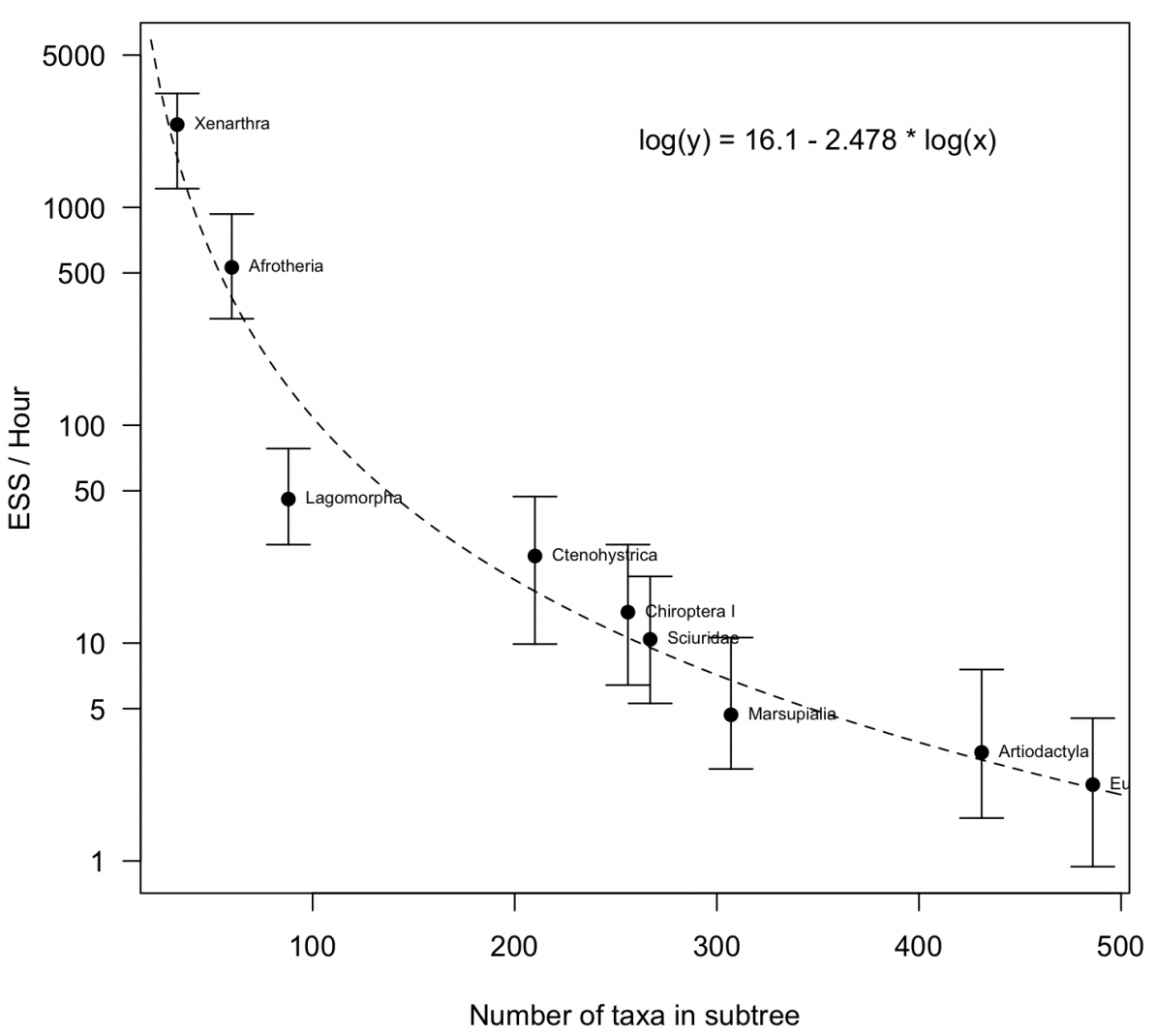

Figure S11. Benchmarking analyses. Each subtree was analysed with a single MCMC chain and the median ESS (for the divergence times, black circles) per hour calculated. The bars span the 25% and 75% quantiles of ESS values among the 71 node ages for the subtree. The dashed line is the fitted regression model log(y) = b + a x log(x). The four largest subtrees (all with >600 taxa) did not produce usable samples during the test period and thus are not included. However, the regression equation can be used to extrapolate to our largest subtree (Rest of Rodentia (II), 691 taxa) and also to the complete 4,705-taxon phylogeny, giving 0.903 ESS/h and 7.8 x 10^{-3} ESS/h, respectively.

Supplementary Data Structure

The data (available at DOI: 10.6084/m9.figshare.14885691) are released as a single zip file (~450 Mb) containing alignments, trees, and other files.

Alignments: Directory `aln/00_step_01/` contains the alignments for the 72 genomes in phylip format. Directory `aln/01_step_02/` contains the uncompressed, raw subtree alignments for the 4,705 taxa, with missing species represented as sequences of gaps (see Table S7). Directory `aln/01_step_02_patterns/` contains the same alignments after processing, that is, with missing species removed and with the alignments compressed into site patterns (see `MCMCtree` and `PAML` documentation for alignment formats). The processed alignments are the ones used by `MCMCtree` to calculate the likelihood during estimation of gradient and Hessian. Note each alignment file contains several alignment blocks, with each block corresponding to an alignment partition. If you load an alignment file into an alignment editor, make sure your editor allows you to see all partition blocks and not just the first one.

Approximate likelihood: Directory `inBV/` contains the estimated gradient and Hessian for each alignment partition, which are required to estimate the divergence times under the approximate likelihood method. This directory is subdivided into `step01` and `step02` subdirectories corresponding to the data for the 72 genomes and the 4,705-taxon subtrees respectively.

Phylogenetic trees: Directory `trees/` contains the trees with fossil calibrations in Newick format. As per above, subdirectories `step01` and `step02` contain the corresponding trees for the 72 genomes and 4,705 taxa respectively. These trees are required, together with the alignment and `in.BV` files to estimate the divergence times with `MCMCtree`. Directory `timetrees/` contains the estimated posterior timetrees in Nexus format. These are suitable for plotting with `FigTree` v1.3 (http://tree.bio.ed.ac.uk/software/figtree/). For the 4,705 taxa, both the separate subtrees and the fully stitched 4,705-taxon tree are provided.

Other files: Directory `clocktest/` contains the full results for the Bayesian selection of relaxed-clock model, while directory `paleodb/` contains the data mined from the Paleobiology Database. Note that all directories contain `README.md` files that provide additional information on the directory contents.

References

1 dos Reis M, Gunnell GF, Barba-Montoya J, Wilkins A, Yang Z, Yoder AD. Using phylogenomic data to explore the effects of relaxed clocks and calibration strategies on divergence time estimation: primates as a test case. *Syst Biol* 2018; **67**: 594–615.

2 Rannala B. Conceptual issues in Bayesian divergence time estimation. *Philos Trans R Soc Lond B Biol Sci* 2016; **371**. doi:10.1098/rstb.2015.0134.

3 Nascimento FF, dos Reis M, Yang Z. A biologist's guide to Bayesian phylogenetic analysis. *Nat Ecol Evol* 2017; **1**: 1446–1454.

4 dos Reis M, Yang Z. Approximate likelihood calculation on a phylogeny for Bayesian estimation of divergence times. *Mol Biol Evol* 2011; **28**: 2161–2172.

5 Battistuzzi FU, Billing-Ross P, Paliwal A, Kumar S. Fast and slow implementations of relaxed-clock methods show similar patterns of accuracy in estimating divergence times. *Mol Biol Evol* 2011; **28**: 2439–2442.

6 Zwart SP. The ecological impact of high-performance computing in astrophysics. *Nature Astronomy* 2020; **4**: 819–822.

ANNEX: Justification for Fossil Calibrations

For nodes without a maximum justification, the maximum is constrained to be the 2.5% quantile of the fitted ST/SN density in an ancestral node. This is done to avoid truncation artefacts between fossil calibration and fitted densities. Calibrations integrate geochronological updates as of September 2021.

Sort ID	Crown group	Dating step	Min (Ma)	Max (Ma)	Justification
1	Mammalia	1	164.1	252.2	**Node Calibrated.** Divergence of monotremes, marsupials, and placentals, following Tarver et al. [1]. **Fossil taxon and specimen**. Bathonian australosphenidans such as *Ambondro mahabo* (UA 10602 University of Antananarivo, Madagascar; Flynn et al. [2]). **Phylogenetic justification**. Puttick et al. [3] compared application of the Mk model in MrBayes to implied and equal-weights parsimony, and supported the interpretation of Jenkins et al. [4] and Luo et al. [5] that Triassic haramiyids fall outside of crown Mammalia. **Minimum Age**. 164.1 Ma. **Maximum Age**. 252.2 Ma. **Age Justification.** *Ambondro* comes from the upper part of the Isalo "Group" (middle Jurassic, Bathonian) of Madagascar [2]), dated as generally Bathonian, so we select the top of the Bathonian as the hard minimum calibration date, 165.3 Ma ± 1.1 Myr, or 164.1 Ma [6]. Following Tarver et al. [1] we revise our maximum calibration to allow for the possibility that the monotreme stem lineage really does extend into the upper Triassic [7,8]. Specifically, the soft maximum is set at the Permian-Triassic boundary, dated at the base of the Induan, 251.9 Ma ± 0.3 Myr [9] or 252.2 Ma. **Discussion.** Our calibration for this node contrasts to suggestions (e.g., [7,8,10]) that Triassic *Thomasia* and *Haramiyavia* are closely related to multituberculates and monotremes, which, in turn, implies membership of these Triassic species within crown Mammalia. We follow Luo et al. [5], Benton et al. [11], Puttick et al. [3] and Huttenlocker et al. [12] in excluding haramiyids from crown Mammalia and in using *Ambondro* for the minimum calibration.

2	Theria	1	121.56	169.4	**Node calibrated**. Divergence of marsupial and placental mammals. **Fossil taxon and specimen**. *Sinodelphys szalayi*. **Phylogenetic justification**. Resolved on stem to Placentalia, within Theria, by Bi et al. 2018 [13]. **Minimum age**. 121.56 Ma. **Maximum age**. 169.4 Ma. **Age justification**. Fossils from the Jehol biota of northeast China come from Barremian to Aptian-age deposits, although there is some ambiguity about their age [14]. Here we take the youngest age estimate from tuffs overlying the main fossil-bearing layers, dated to 121.96 Ma ± 0.5 Myr [15], thus 121.56 Ma. We conservatively use the age of the Barremian to define the ages of Jehol specimens, which has an upper margin of 125.0 Ma. Given the possibility that southern, tribosphenic mammals such as *Ambondro* are therian (cf. [16]), we set the soft maximum age for Theria in the Bathonian, 168.2 Ma ± 1.2 Myr so 169.4 Ma [6]. **Discussion**. Luo et al. [17] hypothesized that *Juramaia sinensis* from the late Jurassic was the geologically oldest therian mammal, more closely related to crown placentals than to other mammals and therefore eutherian (see also Bi et al. [13]). Some subsequent analyses have corroborated this result [5,8], but others have not, placing *Juramaia* instead on the stem to Theria (e.g., [10]). Other candidates for the oldest crown therians include *Sinodephys* [18] and *Eomaia* [19] originally argued to be on the stems to Marsupialia and Placentalia, respectively. Again, *Eomaia* in more recent studies has been placed on the therian stem [10,20], and *Sinodelphys* appears more consistently on the stem leading to either Placentalia [13] or Marsupialia [5,8,21]. Krause et al. [10] reconstruct *Sinodelphys* as a metatherian in at least their Bayesian topologies (their figs. S2, S4), although not with MP (their figs. S1, S3) or in Krause et al. [22]. Overall, *Sinodelphys* enjoys better support as a crown therian [12] than other taxa and we thus use it as a minimum constraint for Theria.
3	Placentalia	1	61.66	162.5	**Node calibrated**. The human-tenrec split is equivalent to the origin of the clade comprising Boreoeutheria (Laurasiatheria and Euarchontoglires) and Atlantogenata (Xenarthra and Afrotheria). Following Benton et al. [11] but with the geochronology revised following [23] and [6].
4	Euarchontoglires	1	61.66	162.5	**Node calibrated**. Euarchontoglires is composed of two clades, the Archonta and the Glires. Primates belong to the former, Rodentia to the latter, the common ancestor of which corresponds to the origin of Euarchontoglires. Following Benton et al. [11] but with the geochronology revised following [23] and [6].

5	Primates	1	56	66.09	**Node calibrated**. Crown-group Primates, or Euprimates, encompass living forms plus the extinct adapoids and omomyoids; the latter are more closely related to extant lemuriforms than to anthropoids [24-26]. Following Benton et al. [11] with the exception that the soft-maximum constraint, defined as the base of the Paleocene, is revised to 66.04 Ma ± 0.05 Myr [27], so 66.09 Ma.
6	Anthropoidea	1	33.9	66.09	**Node calibrated**. Last common ancestor of platyrrhine and catarrhine primates. Following Benton et al. [11] with the exception that the soft-maximum constraint, defined as the base of the Paleocene, is revised to 66.04 Ma ± 0.05 Myr [27], so 66.09 Ma.
7	Catarrhini	1	24.44	33.9	**Node calibrated**. The common ancestor of Old World monkeys (Cercopithecoidea) and apes (Hominoidea), which together form crown Catarrhini. Following Benton et al. [11] with the exception that the soft-maximum constraint, defined on the base of the Oligocene, is dated to 33.9 Ma [23].
8	Hominidae	1	11.65	33.9	**Node calibrated**. Last common ancestor of great apes, including human, chimp, gorilla, and orangutan. Following Benton et al. [11] with the exception that the minimum age constraint is revised The Chinji Formation of Pakistan corresponds to magnetic polarity chron 5Ar, estimated to be ca. 12 Ma before present [28]. This correlates to the Serravallian stage, the top of which is dated to 11.65 Ma [29].
9	Homininae	1	5.33	33.9	**Node calibrated**. Divergence of the human-chimp lineage from that of gorillas. **Fossil taxon and specimen**. *Chororapithecus abyssinicus* CHO-BT 4 from the Beticha locality, Chorora Fm, Ethiopia. **Phylogenetic justification**. Suwa et al. [30] identify shared, derived characters of their dental fossils with the lineage of *Gorilla*. **Minimum age**. 5.33 Ma. **Maximum age**. 33.9 Ma. **Age justification**. Katoh et al. [31] revised the geological context of this find, and concluded that it is not middle Miocene as originally reported, but upper Miocene, between 7-9 Ma in age, overlapping with the Tortonian and Messinian. The latter has an upper bound of 5.33 Ma [29]. The soft maximum is as for catarrhines, above. **Discussion**. The fossil lineage of habitually bipedal hominins is much better than that for great apes, and also has an oldest occurrence in the late Miocene (e.g., Brunet et al. [32]). No hominin fossils are known from deposits correlating with a marine stage older than the Messinian.
10	Hominini	1	6.5	10	**Node calibrated**. Chimpanzee-human. Following Benton et

					al. [11].
11	Cercopithecinae	1	5.33	33.9	**Node calibrated**. Divergence of vervet monkeys (*Chlorocebus*) from baboons and macaques (*Macaca* and *Papio*). **Fossil taxon and specimen**. *Macaca libyca*, YPM 21551 (Benefit et al. [33]: fig. 2) from Wadi Natrun, Egypt. **Phylogenetic justification**. Referred to the same genus as the living macaque by Benefit et al. [33]. **Minimum age**. 5.33 Ma. **Maximum age**. 33.9 Ma. **Age justification**. Cercopithecine fossils are known from As-Sahabi (Libya), Menacer (Algeria), Wadi Natrun (Egypt), and Toros-Menalla (Chad). All are late Miocene in age and overlap with the Messinian, with an upper bound of 5.33 Ma [29]. The soft maximum date is as for Catarrhini, above. **Discussion**. Cercopithecine fossils have been reported from the late Miocene of Europe [34] and North Africa [33]. Following Raaum et al. ([35]: fig. 3), the record of *Macaca* is slightly older than that of baboons, but Benefit et al. [33] summarize fossils of both lineages from North Africa. The lineage of vervet monkeys appears to be limited to the Plio-Pleistocene.
12	Papionini	1	5.33	33.9	**Node calibrated**. Divergence of baboons (e.g., *Papio*) from macaques (*Macaca*). **Fossil taxon and specimen**. Macaca libyca, YPM 21551 (Benefit et al. [33]: fig. 2) from Wadi Natrun, Egypt. **Phylogenetic justification**. As for cercopithecines, above. **Minimum age**. 5.33 Ma. **Soft maximum age**. 33.9 Ma. **Age justification**. As for catarrhines.
13	Strepsirhini	1	33.9	66.09	**Node calibrated**. The crown clade comprising lemurs, lorises, galagos, and other extant primates that possess a toothcomb [36]. Following Benton et al. [11] with the exception that we use the base of the Paleocene as the soft maximum, as for Primates, above.
14	Glires	1	56	162.5	**Node calibrated**. The last common ancestor of Rodentia and Lagomorpha. Following Benton et al. [11] with the exception that the soft-maximum constraint, defined as the base of the Oxfordian, is revised to 161.5 Ma ± 1.0 Myr [6], so 162.5 Ma.

15	Rodentia	1	56	66.09	**Node calibrated**. The common ancestor of the three major extant rodent clades: Muroidea (mouse-related), Sciuromorpha (squirrel-related), and Ctenohystrica (guinea-pig related). Following Benton et al. [11] with the exception that the soft maximum constraint, defined on the base of the Paleocene, is revised to 66.04 Ma ± 0.05 Myr [27], so 66.09 Ma.
16	Nonsquirrel rodentia	1	48.07	59.24	**Node calibrated**. The divergence of Myomorpha+ Ctenohystrica to the exclusion of Sciuromorpha (Fabre et al. [37]; [38]; high-level taxa defined in Asher et al. [38]). We acknowledge that there is uncertainty regarding the initial divergence within Rodentia (cf. Myomorpha reconstructed as sister to Ctenohystrica-Sciuromorpha in Swanson et al. [39]). **Fossil taxon and specimen**. Chapattimyidae such as *Birbalomys sondaari* (Geological Survey of Pakistan, Howard University Collection, H-GSP 92161 of Thewissen et al. [40]) from the Kuldana Formation of the Ganda Kas area, Pakistan. **Phylogenetic justification**. Phylogenetic analysis by Marivaux et al. [41] placed Eocene chapattimyids within the Ctenohystrica, close to hystricognaths and to the exclusion of diatomyids. They are therefore nested within the unnamed crown clade comprising Myomorphaand Ctenohystrica. **Minimum age**. 48.07 Ma. **Maximum age**. 59.24 Ma. **Age justification**. The Kuldana Formation of Pakistan has been dated as early–middle Eocene, and ages may differ in different regions of northern India, and mammals occur in different horizons. *Birbalomys* is noted as occurring at 51 Ma by Marivaux et al. ([41], p. 132), thus well within the Ypresian. Hence, we assign a minimum constraint for rodents excluding Sciuromorpha at the top of the Ypresian marine stage, hence 48.07 Ma [23]. The soft maximum constraint might be taken as equivalent to the age of *Paramys and Franimys* from the late Paleocene (base of the Thanetian) of North America and Europe, 59.24 Ma [23]. **Discussion**. Fossils associated with the mouse-related stem group are younger, including Eocene dipodids such as *Ulkenulastomys*, *Blentosomys*, and *Aksyiromys* from the Obayla Svita of the Zaysan Basin, Kazakhstan [42]. Lucas [43] assigned a younger, Irdinmanhan age to this site based on biostratigraphic comparisons, changing its previous stratigraphic interpretation from early Eocene to the base of the middle Eocene.

17	Dipodidae-Muroidea	1	41.03	59.24	**Node calibrated**. Divergence of dipodid from muroid(i.e., within the mouse-related clade) rodents. **Fossil taxon and specimen**. *Aksyiromys dalos*, IZ-NAS-RK 34/181 (Emry et al. [44]: fig. 3A). **Phylogenetic justification**. Following Fabre et al. [37] and Asher et al. [38], dipodids (jerboas, birch mice, et al.) comprise the sister taxon to Muroids. Marivaux et al. [41] reconstruct *Aksyiromys* as sister taxon to fossil dipodids (e.g., *Primisminthus*) and cricetids (e.g., *Pappocricetodon*), the latter a putative member of Muroidea. **Minimum age**. 41.03 Ma. **Maximum age**. 59.24 Ma. **Age justification**. Lucas [43] and Emry [45] note that the age of the fossils described by Shevyreva [42] is within the Irdinmanhan ALMA, as are their fossils from the Shinzaly fauna of eastern Kazakhstan [44]. The marine equivalent is likely the Lutetian, with an upper bound of 41.03 Ma [23]. The soft maximum is as for rodents minus the squirrel related clade, above. **Discussion**. Shevyreva [42] described *Aksyiromys, Ulkenulastomys,* and *"Blentosomys"* from middle Eocene deposits of Kazhakstan. dos Reis et al. [46] used *Ulkenulastomys* as a minimum calibration point for this clade. Emry et al. [44] described *Aksyiromys* as a zapodine dipodid rodent from the Shinzaly fauna of eastern Kazhakstan, equivalent in age to Obayla Svita, Zaysan Basin, Kazhakstan, where Shevyreva [42] first described *Aksyiromys.* Emry [45] noted that *Blentosomys* is likely a junior synonym of *Aksyiromys*. Because their description is more accessible in the literature than that of Shevyreva [42], and because of their publication of good quality figures with associated specimen numbers, we base our minimum calibration on *Aksyiromys* as described by Emry et al. [44], rather than other fossil dipodids of the same age.
18	Murinae	1	7.25	15.99	**Node calibrated**. Divergence of *Mus* from *Rattus.* Following Benton et al. [11]; note that their summary age constraints did not match their justification - we follow their justification and revise the age constraints following [29].
19	Lagomorpha	1	48.07	66.09	**Node calibrated**. The common ancestor of leporids (rabbits and hares) and ochotonids (pikas). Following Benton et al. [11] but with the geochronology revised following [23].

20	Euungulata	1	50.7	66.09	**Node calibrated**. Common ancestor of Perissodactyla and Artiodactyla. Following calibration for crown-Artiodactyla in Benton et al. [11] but with the geochronology revised following [23]. **Discussion**. dos Reis et al. [46] took *Lambdotherium* as the basis for a 62.5 Ma minimum date for perissodactyls, based on Benton et al. [47]. However, the 62.5 Ma date from Benton et al. [47] derived from a topology ("Zooamata", or Carnivora-Perissodactyla) that is no longer supported by larger datasets ([1]: figs S1, S3) and which was based on a carnivoran calibration: *Proticis* (Torrejonian NALMA). Instead, the 21.4 gigabase alignment of Tarver et al. ([1]: fig. S1) supports an artiodactyl-perissodactyl clade, or Euungulata. Two Paleocene genera often associated with perissodactyls are worth mention: *Radinskya* and *Lambdotherium* as possible minimum calibration points. Neither Holbrook [48] nor Rose et al. [49] unequivocally support *Radinskya* in a close sister-taxon relationship with perissodactyls. Rose et al. [49] does support *Lambdotherium* within tapiromorphs; Beard [50] emphasizes its affinities to perissodactyls, but the description of a Gashatan ALMA (Thanetian) specimen by Meng et al. ([51]: 176) is more circumspect: "other than its possible perissodactyl affinities, the fragmentary material precludes definitive taxonomic placement." There are many records of slightly younger, early Eocene perissodactyls (e.g., *Homogalax, Hyracotherium*) and among the best material is *Cambaytherium* from the Cambay Shale, India (ca. 54.5 Ma [49]). These correlate with the Ypresian, the top of which is 47.8Ma. The record of archaeocete whales (*Himalayacetus*, described below) is likely younger in absolute terms, but is found in deposits with intercalated marine deposits (NP zones 11-12, 52.4 Ma), and thus can be correlated with the marine record at an older age than early Eocene Asian and North American records of perissodactyls.
21	Artiodactyla	1	50.7	66.09	**Node calibrated**. Common ancestor of ruminants, tylopods, and "Suiformes", including the now well-established hippo-whale clade. Following Benton et al. [11] but with the geochronology revised following [23].
22	Cetruminantia	1	50.7	66.09	**Node calibrated**. Divergence of the common ancestor of ruminants and cetaceans, excluding suids and tylopods. Following the calibration for Whippomorpha-Ruminantia in Benton et al. [11] but with the geochronology revised following [23].
23	Bovidae	1	15.99	27.29	**Node calibrated**. The branching between the cow (Bos) and sheep (Ovis) is an intrafamilial split within the Family Bovidae. Bos is a member of the Tribe Bovini, and Ovis is a member of the Tribe Caprini, which belong respectively to the subfamilies Bovinae and Antilopinae [52]. Following the calibration for Bovinae-Antilopinae in Benton et al. [11] but with the geochronology revised following [29].
24	Carnivora	1	37.71	66.09	**Node calibrated**. Common ancestor of Caniformia (dogs, bears, raccoons, seals) and Feliformia (cats, mongooses, hyaenas), excluding stem carnivoramorphans sensu Wesley Hunt and Flynn [53]. Following Benton et al. [11] but

					with the geochronology revised following [23].
25	Caniformia	1	37.71	66.09	**Node calibrated**. Divergence of canids (dogs) and arctoids (musteloids, ursids, pinnipeds). **Fossil taxon and specimen**. *Hesperocyon gregarius* (SMNH P1899.6; [54]) from the Cypress Hills Formation, Duchesnian NALMA, Lac Pelletier local fauna, Saskatchewan. **Phylogenetic justification**. As for Carnivora. **Minimum age**. 37.71 Ma. **Maximum age**. 66.09 Ma. **Age justification**. As for Carnivora.
26	Chiroptera	1	48.07	66.09	**Node calibrated**. Divergence of Yinpterochiroptera and Yangochiroptera. **Fossil taxon and specimen**. *Eppsinycteris anglica* [55], BMNH M13776 from the Lessness Shell Bed, Blackheath Beds, Abbey Wood, Ypresian. **Phylogenetic justification**. As summarized by Eiting & Gunnell [56], the stem lineage of chiropterans extends to the basal Eocene of Europe [57], Australia [58]. *Eppsinycteris* from the early Eocene of the UK may be related to emballonurids [55]; *Honrovits* from the early Eocene of Wyoming may be related to natalids [59]; *Witwatia* and *Dizzya* from the early Eocene of Tunisia may be vespertilionoids [60,61]. We choose *Eppsinycteris* as the minimum constraint as it is represented by a well preserved jaw [55]. **Minimum age**. 48.07 Ma. **Maximum age**. 66.09 Ma. **Age justification**. The three oldest records for modern bat groups cited above all correspond to the Ypresian in age, which has an upper bound of 48.07 Ma [23]. The absence of any chiropterans during the Paleocene may point to a soft maximum constraint at the base of the Danian, 66.04 Ma ± 0.05 Myr [23], so 66.09 Ma. **Discussion**. Smith et al. [62] estimate that the earliest records of modern families are middle Eocene, and we agree that the evidence in the above cases is uncertain. Nonetheless, the presence of multiple identifications of modern groups in the early Eocene, as noted above, implies that crown Chiroptera existed at this time.
27	Lipotyphla	1	61.66	162.5	**Node calibrated**. common ancestor of modern soricids, talpids, erinaceids, and *Solenodon*. Following the calibration for crown-Lipotyphla in Benton et al. [11] but with the geochronology revised following [23] and [6].

28	Xenarthra	1	48.07	162.5	**Node calibrated**. Divergence of cingulates (armadillos) from Pilosa (i.e., sloths and anteaters). Following Benton et al. [11] but with the geochronology revised following [23] and [6].
29	Afrotheria	1	56	162.5	**Node calibrated**. Last common ancestor of proboscideans and tenrecids (i.e., all extant afrotheres). Following Benton et al. [11] but with the geochronology revised following [23] and [6].
30	Paenungulata	1	56	162.5	**Node calibrated**. Common ancestor of *Loxodonta* and *Procavia*. **Fossil taxon and specimen**. The extinct proboscidean *Eritherium azzouzorum* (MNHN PM69, Paris) from the Sidi Chennane quarries, phosphate bed IIa, lower bone-bed, Ouled Abdoun Basin of Morocco, regarded as upper Paleocene (early Thanetian [63]). **Phylogenetic justification**. See Afrotheria. **Minimum age**. 56 Ma. **Soft maximum age**. 162.5 Ma. **Age justification**. See Afrotheria. **Discussion**. The topology within paenungulates is less certain that most other inter-ordinal branches among mammals. Several recent studies support a proboscidean-hyrax clade to the exclusion of sirenians [64,65]; others support a proboscidean-sirenian clade to the exclusion of hyracoids [66,67]. Either way, the fossil record of Proboscidea remains the oldest, well-documented fossil lineage in Afrotheria.
31	Marsupialia	1	48.07	127.2	**Node calibrated**. Divergence of crown marsupials. Following Benton et al. [11] but with the geochronology revised following [23] and [27].

32	Eometatheria	1	23.04	56	**Node calibrated**. Divergence of dasyuromorphs (e.g., *Sarcophilus*) and diprotodonts (e.g., *Macropus*), i.e., the origin of crown Australasian australidelphians. **Fossil taxon and specimen**. *Perikoala robustus*, SAM P26552 from Turtle Quarry, Etadunna Fm., west side of Lake Palankarinna, South Australia [68]. **Phylogenetic justification**. Black et al. [69] reconstruct *Perikoala* closer to *Phascolarctos* than *Vombatus* (but did not test its affinities widely throughout marsupials). Combined with the identification by Wooburne et al. [68] of features diagnostic of vombatiforms, we accept their identification of this taxon within Diprotodontia. **Minimum age**. 23.04 Ma. **Maximum age**. 56.0 Ma. **Age justification**. Woodburne et al. [70], as summarized in Mitchell et al. [71], noted the presence of crown diprotodonts including likely pseudocheirids and phascolarctods from Zone A of the Etadunna Fm. Megirian et al. [72] assign an age of 24.9-25.3 Ma, equivalent to the Chattian, the top of which is 23.04 Ma [23]. Following Mitchell et al. [71], no crown australidelphian lineages are evident at Murgon (early Eocene, = Tingamarra local fauna), which samples the early Eocene at ca. 55Ma, justifying a soft maximum defined by the base of the Ypresian at 56.0 Ma [23]. **Discussion**. Other crown australidelphians from Riversleigh could also serve as the mimimum, including a potorine ("*Kyeema mahoneyi*") and a pseudocheirid from the Edadunna Faunal Zone "A" [73,74]. The term Eometatheria dates to Simpson [75], who used it as we do, to encapsulate Australasian marsupials. The term was subsequently used by Kirsch [76] and Asher et al. [77] to imply Australasian marsupials excluding peramelians, based on the now overturned idea [71,78,79] that peramelians are the basal-most australidelphians. Given this somewhat complicated history, Beck [79] and Mitchell et al. [71] used the taxon "Eomarsupialia" for this clade (australidelphians excluding *Dromiciops*) instead. Arguably, however, the importance of precedent and minimizing the introduction of novel taxa would favor retaining older terms that have been used to delineate broadly similar (and in the case of Simpson [75] identical) groups [80]. Although the content of Eometatheria has changed over time, this is also true of other high-level taxa (e.g., Primates, Dinosauria); we therefore prefer Eometatheria over alternatives to indicate the crown clade of Australasian australidelphian marsupials.

33	Cingulata	2	34.85	56.0	**Node calibrated**. Common ancestor of dasypodids and other cingulates. **Fossil taxon and specimen**. Dasypodid petrosal (PVL 6245) from the middle Member of the Geste Formation, Antofagasta de la Sierra, Catamarca Province, Argentina Babot et al. [81]. **Phylogenetic justification**. Ciancio et al. [82] discuss *Prostegotherium* with dermal remains from the Vacan (early Casamayoran) as a member of Dasypodinae, but this ID as a crown cingulate is I think not yet bolstered by a phylogenetic analysis. Babot et al. [81] do undertake a phylogenetic analysis and place a petrosal from the slightly younger Barrancan (late Casamayoran) Geste Fm closer to Dasypus than other cingulate genera. **Minimum age**. 34.85 Ma. **Soft maximum**. Age: 56.0 Ma. **Age justification**. The Geste Formation is conventionally interpreted as late Eocene (Barrancan subage of Casamayoran South American Land Mammal Age; SALMA [81]); however, this age interpretation is not clearly established [81]. Detrital zircons from Geste Formation establish a 37 Ma maximum age interpretation and a bracket of 37.3 Ma ± 1.5 Myr to 35.4 Ma ± 0.55 Myr [83]. The soft maximum is established on the Eocene (Itaboraian) of Itaborai, Brasil [84] based on presence of xenarthrans but absence of any undisputed crown taxa. Also relevant is absence of any xenarthra from localities older than Itaborai (e.g., Paleocene Tiupampa; see Woodburne et al. [84]: table 1). Woodburne et al. [84] and Speijer et al. [23] consider the Itaboraian SALMA to be Ypresian, its base equating to 56.0 Ma [23].

34	Chlamyphoridae	2	33.9	56.0	**Node calibrated**. Common ancestor of tolypeutines-chlamyphorines and euphractines. **Fossil taxon and specimen**. *Glyptatelus*, e.g., scutes assigned to *G. fractus* including MACN 10949 [85]. Following McKenna et al. ([86]: fig. 1), the jaw fragment AMNH 29483 is not *Glyptatelus* but likely the folivoran *Pseudoglyptodon* (see below). **Phylogenetic justification**. *Riostegotherium* is not convincingly a dasypodine but it is more conservatively regarded as a stem cingulate. Delsuc et al. [87] reconstruct glyptodonts within crown cingulates, closer to tolypeutines-chlamyphorines than to dasypodines or euphractines. *Pseudoglyptodon* from the Abanico Fm of Chile [86] is likely a stem folivoran (see below), but this is still younger (Tingurrician) than Mustersan fossils like *Glyptatelus*. McKenna et al. [86] assigned a jaw fragment Simpson thought was *Glyptatelus* (cingulate, AMNH 29483) to *Pseudoglyptodon* (folivoran) so affinities of that specimen remain ambiguous (although the part-skull assigned to *Pseudoglyptodon* by McKenna et al. [86] does appear to be a stem folivoran). Hence, Mustersan dermal scutes and fossil teeth are the oldest indicators of glyptodonts and therefore non-dasypodid cingulates. **Minimum age**. 33.9 Ma. **Soft maximum age**. 56.0 Ma. **Age justification**. Eocene (Mustersan SALMA), Musters Fm, Patagonia [85,87]. The 2012 Geologic Timescale interprets the Mustersan SALMA to straddle Bartonian-Priabonian boundary, with a minimum age c. 33.9 Ma [23]. The soft maximum constraint follows that of Cingulata.
35	Pilosa	2	31.17	56	**Node calibrated**. Common ancestor of folivorans (sloths) and vermilinguans (anteaters). **Fossil taxon and specimen**. *Pseudoglyptodon chilensis*, SGO PV 2995 ([86]: fig. 3). **Phylogenetic justification**. Folivoran ID of *Pseudoglyptodon* from McKenna et al. [86] is supported by Slater et al. [88] and Gaudin and Croft [89]. **Minimum age**. 31.17 Ma. **Maximum age**. 56.0 Ma. **Age justification**. *Pseudoglyptodon chilensis* was recovered from volcanoclastic strata within the Abanico Fm., Chile, and is considered early Oligocene in age as it forms part of the Tinguiririan fauna and its associated South American Land Mammal Age (SALMA) [86]. The minimum age constraint is established based on Ar40/Ar39 dating from within the Tinguiririan SALMA stratotype, the youngest range being 31.34 Ma ± 0.17 Myr [90], providing a minimum constraint of 31.17 Ma. The soft maximum constraint follows that of Cingulata.

36	Folivora	2	15.99	56	**Node calibrated**. Common ancestor of megalonychid sloths (including *Choloepus*) and *Bradypus*. **Fossil taxon and specimen**. *Imagocnus zazae*, holotype MNHNH P 3014 (MacPhee & Iturralde-Vinent [91]: fig. 1). **Phylogenetic justification**. *Octodontotherium* and *Desadognathus* from Salla (Bolivia) may be stem folivorans rather than *Choloepus* sister taxa (following discussion in Slater et al. [88]). Pujos et al. ([92]: fig. 5) show a consensus tree with *Octodontotherium* closer to *Choloepus* than *Bradypus*, but this was not an original phylogenetic analysis (and neither *Octodontotherium* nor *Deseadognathus* are mentioned by Gaudin and Croft [89]). Thus, we interpret *Imagocnus* as the oldest definitive crown folivoran. **Minimum age**. 15.99 Ma. **Maximum age**. 56.0 Ma. **Age justification**. The holotype of *Imagocnus zazae* was recovered from the Lagunitas Fm., Domo de Zaza, Cuba [91]. As a majority of the remains recovered were found in float that cannot be constrained stratigraphically, the minimum constraint is based on the age of the Formation, believed to be Burdigalian (Miocene) based on foraminifera indicative of the Miogypsina-Soritiidae zone (*Miopypsina antillea*, *Heterostegina antillea*, and *Sorites marginalis*) [93]. MacPhee et al. [93] also attempted to date 4 shelly horizons using Sr87/Sr86 analysis but decided the results were inconsistent as stratigraphically older horizons produced younger dates than the youngest horizons. The minimum age is thus the Upper Burdigalian-Lower Langhian boundary, dated at 15.97 Ma [29]. The soft maximum constraint follows that of Cingulata.

37	Vermilingua	2	17.36	56	**Node calibrated**. Common ancestor of *Cyclopes* and myrmecophagines (*Myrmecophaga-Tamandua*). **Fossil taxon and specimen**. *Protamandua rothi* from the Santacrucian of Argentina, represented by a partial skull (YPM-VPPU 15267) and postcrania (e.g., astragalus MACN-A 10901b and calcaneus MACN-A 11530; see Bargo et al. [94]: fig. 13.2). **Phylogenetic justification**. Following Gaudin & Bramhan ([95]: fig. 1) and Bargo et al. ([94]: fig. 13.1), *Protamandua* comprises the sister taxon of mymecophagines (extant *Myrmecophaga* and *Tamandua*) to the exclusion of *Cyclopes*. Skeletal elements now recognized as *Protamandua* were first assigned by Ameghino [96] to multiple species but later recognized as a single species (and perhaps individual) by Hirschfeld [97]. **Minimum age**. 17.36 Ma. **Maximum age**. 56.0 Ma. **Age justification**. These remains of *Protamandua rothi* were collected south of the Río Coyle correlated to the lower fossiliferous levels (FL 1-7) of the Estancia La Costa Member of the Santa Cruz Formation, which is generally considered to be of Miocene age [98]. Tephra analysis using Ar40/Ar39 methods suggest FL 1-7 are part of a conformable sequence and that there is no temporal distinction between FL 3 and 7 [99]. Ar40/Ar39 dating of tephra sample CO from above FL 1-7, correlated across the Estancia La Costa Member fossil localities (Puesto Estancia La Costa, Cañadón Silva, and Estancia La Costa) was dated as 17.41 Ma ±0.05 Myr [100], thus making the minimum age 17.36 Ma. The soft maximum constraint floors that of Cingulata.
38	*Chrysochloris asiatica* - other chrysochlorids	2	3.6	33.9	**Node calibrated**. Divergence of *Chrysochloris asiatica* from other chrysochlorids. **Oldest crown fossil**. Following Asher & Avery [101], two Pliocene chrysochlorids from Langebaanweg, South Africa (*Chrysochloris bronneri* and *C. arenosa*) are more closely related to the extant *C. asiatica* than to other extant chrysochlorids. Other extinct chrysochlorids such as *Chlorotalpa spelea* from Sterkfontein and *Amblysomus hamiltoni* from Makapansgat, South Africa [101-103] may also be crown taxa, but likely post-date the Pliocene. **Minimum age**. 3.6 Ma. **Maximum age**. 33.9 Ma. **Age justification**. *Chysochloris arenosa* and *C. bronneri* are from early Pliocene deposits at Langebaanweg, South Africa. Most fossils from this locality were not recovered in-situ and represent at least some time-averaging. Nonetheless, they are generally regarded as early Pliocene and thus older than fossils recovered from South African hominid sites. Hence the minimum constraint for crown chrysochlorids would be the Langebaanweg fossils, correlating to Zanclean with a top of 3.6Ma. We propose a soft maximum in the late Eocene given the abundance of African mammal fossils during that time but absence of uncontroversial crown chrysochlorids elsewhere [101,104].

39	Macroscelidea	2	23.04	56	**Node calibrated**. Divergence of *Rhynchocyon* from other macroscelidids. **Oldest crown fossil**. *Oligorhynchocyon songwensis*, RRBP 08086 (left p4) from the Songwe Member of Nsungwe Formation. **Minimum age**. 23.04 Ma. **Maximum age**. 56.0 Ma. **Age justification**. Stevens et al. [105] describe an isolated lower premolar from Tanzania, 25.2 Ma in age and diagnostic to Rhynchocyoninae. This falls within the Chattian marine stage the upper margin of which is 23.04 Ma [23]. As the soft maximum, we propose the base of the Eocene (Ypresian) dated to 56.0 Ma [23]. Various localities near and above the Paleocene-Eocene boundary have yielded numerous remains of afrotherians [63,106] without evidence for crown macroscelideans.
40	Proboscidea	2	5.33	23.04	**Node calibrated**. Common ancestor of *Elephas* and *Loxodonta,* following Benton et al. [11] but with the geochronology revised following [29] and [23].
41	Sirenia	2	41.03	66.09	**Node calibrated**. Common ancestor of *Dugong* and *Trichechus*. Following [11] excepting (i) that we use the top rather than base of the Lutetian to define the minimum age constraint, (ii) we include the dating errors in defining the soft maximum constraint, and (iii) with the geochronology revised following [23].
42	Hyracoidea	2	5.33	33.9	**Node calibrated**. Divergence of *Dendrohyrax* from other hyracoid genera. **Oldest crown fossil**. *Dendrohyrax validus* [107]. Pickford & Hlusko [107] describe many specimens of *Dendrohyrax cf. validus* from Lemudong'o, Narok, Kenya,, one of which is KNM-NK 36534 (left mandible with p4-m2)). **Minimum age**. 5.33 Ma. **Maximum age**. 33.9 Ma. **Age justification**. According to Pickford & Hlusko [107], fossils from Lemudong'o Locality 1, including *Dendrohyrax*, are ca. 6.1 Ma old. This is within the Messinian marine stage with an upper bound of 5.33 Ma [29]. *Heterohyrax auricampensis* from Berg Aukas, Namibia is presumably contemporaneous (see Rasmussen et al. [108]). Max bound would be better constrained by lack of crown hyracoid spp. in north African localities. As the soft maximum, we propose the base of the Oligocene, corresponding to the Rupelian [23]. Numerous localities from near this age show no evidence of the divergence of extant hyracoid genera.
43	Paucituberculata (Caenolestidae)	2	0	15.97	**Node calibrated**. Divergence of *Caenolestes*, *Rhyncholestes* and *Lestoros.*. Following Emerling et al. [109].

44	Didelphidae	2	11.608	28.1	**Node calibrated**. Divergence of didelphine and caluromyine marsupials. Following Emerling et al. [109].
45	Dasyuromorphia	2	15.97	-	**Node calibrated**. Divergence of *Thylacinus* from other dasyuromorphs. Following Emerling et al. [109].
46	Peramelidae	2	4.36	23.8	**Node calibrated**. Divergence of *Peroryctes* from other peramelids**.** Following Emerling et al. [109].
47	Vombatiformes	2	25.5	-	**Node calibrated**. Divergence of phascolarctids from other vombatiformes. Following Emerling et al. [109].
48	Phalangeridae-Burramyidae	2	25	-	**Node calibrated**. Divergence of *Phalanger* from *Burramys***.** Following Emerling et al. [109].
49	Petauridae - Pseudocheiridae	2	25.5	-	**Node calibrated**. Divergence of *Petaurus* from *Pseudocheirus***.** Following Emerling et al. [109].
50	Macropodoidea (=Macropodidae + Potoroidae)	2	24.7	-	**Node calibrated**. Divergence of *Macropus* from *Potorous***.** Following Emerling et al. [109].
51	Platyrrhini	2	20.45	37.7	**Node calibrated**. Divergence of cebids from other South American monkeys (Platyrrhini)**.** **Fossil taxon and specimen**. *Panamacebus transitus*, left upper M1 (UF 280128) from Lirio Norte, Panama Canal area, Panama [110]. **Phylogenetic justification**. Bloch et al. [110] resolved *Panamacebus transitus* as a member of crown-Cebinae based on parsimony analysis of a morphological dataset. **Minimum age**. 20.45 Ma. **Maximum age**. 37.7 Ma. **Age justification**. Bloch et al. (2016) report a “a precisely dated 20.9-Ma layer in the Las Cascadas Formation in the Panama Canal Basin, Panama” as the source of *Panamacebus*. This is just within the Aquitanian marine stage with an upper bound of 20.45 Ma. As a soft maximum we suggest the late Eocene, a time by which a number of localities globally have yielded abundant primate remains, but as yet without evidence for crown platyrrhines.

52	Primatomorpha	2	64.645	-	**Node calibrated**. Divergence of dermopterans from primates. **Fossil taxon and specimen**. *Purgatorius* UCMP 197509 isolated astragalus attributed to *Purgatorius* by Chester et al. [111] from the late Puercan Garbani Channel fauna, northeastern Montana, USA. **Phylogenetic justification**. Chester et al. (2015: fig. 2) place Purgatorius within a dermopteran-scandentian-primate clade. **Minimum age**. 64.645 Ma. **Age justification**. The late Puercan Garbani Channel fauna *Purgatorius* occurs within Puercan 2-3 [112], the top of which falls within Chron C28r [23], the top of which is dated to 64.645 Ma [23].
53	Scandentia	2	38	66.0	**Node calibrated**. Divergence of *Tupaia* from *Ptilocercus,* following Emerling et al. [109].
54	Suina	2	34.7	-	**Node calibrated**. Divergence of *Tayassu* from *Sus*. **Fossil taxon and specimen(s)**. *Perchoerus probus*; UMPE 0031: mandible fragment with m2-m3 and UMPE: upper canine from the Municipality of Santiago Yolomécatl, Tlaxiaco basin, northwestern Oaxaca, southern Mexico [113]. **Phylogenetic justification**. *Perchoreus probus* has been classified as either a crown tayassuid, suid or stem suoid in whole-scale analyses of Cetartiodactyla [114,115], however in suoid-level analyses [114,116,117] *Perchoerus* is nested within Tayassuidae due to a suite of cranial characters [118]. **Minimum age**. 34.7 Ma. **Age justification**. The minimum age constraint is based on the age of the Santiago Ylomécatl fauna. K-Ar dating of overlying volcanic rocks and the presence of *Miohippus assinoboiemsis* suggest the fauna is late Miocene in age, equivalent to the Chadronian North American Land Mammal Age [113]. K-Ar dating of the Cañada María Andesite overlying the mudstone outcrops from which the remains of the Santiago Ylomécatl fauna were recovered produced dates of 35.7 Ma ±1.0 Myr at the base and 32.9 Ma ±0.9 Myr further up the volcanic sequence [113]. The minimum age constraint therefore is 34.7 Ma.

55	Whippomorpha	2	50.7	-	**Node calibrated**. Clade containing Cetacea and Hippopotamidae according to [119]. **Fossil taxon and specimen**. *Himalayacetus subathuensis*; Holotype: specimen 2003, left dentary with molar teeth M2-3, Roorkee University Vertebrate Paleontology Laboratory (RUSB); from oyster-rich limestone near the base of the Subathu Formation, type section in Kuthar Nala, Simla Hills, Lesser Himalaya Range, Himachal Pradesh, India [120]. **Phylogenetic justification**. *Himalayacetus subathensis* is a representative of the extinct cetacean suborder Archaeoceti based on the absence of auditory specialisations within a small mandibular canal present in the type dentary and its possession of Pakicetus-like teeth [120]. **Minimum age**. 50.7 Ma. **Age justification**. *Himalayacetus subathensis* was found in zone IIIc from (Mathur 1978), associated with *Nummulites atacicus* from shallow benthic zone SB8 (zones II-IV) [120]. The minimum age constraint therefore is correlated to the top of nanoplankton zone NP11-12, which gives an updated minimum age constraint of 50.7 Ma (Benton, et al. 2015).

56	Cetacea	2	36.13	56	**Node calibrated**. The crown cetacean clade consisting of the suborders Odontoceti and Mysticeti to the exclusion of the extinct Archaeoceti [121]. **Fossil taxon and specimen**. *Mystacodon selenensis*; Holotype: MUSM 1917, partial skeleton including cranium, mandibles, teeth, cervical, thoracic, lumbar and caudal vertebrae, ribs, partial right and left forelimbs, and left innominate from the Yumaque Formation, Playa Media Luna, southern part of Pisco Basin, southern coast of Peru [122]. **Phylogenetic justification**. *Mystacodon* possesses derived mysticete characters including: a dorsoventrally thin lateral edge of maxilla on the rostrum, the presence of an antorbital process of the maxilla, the presence of a maxillary infraorbital plate, and triangular supraoccipital shield [122]. As a result *Mystacodon* is considered the oldest mysticete, part of the basal-most mysticete family Llanocetidae [123]. This group is characterised by large cheek teeth with two separate roots, and strong labial and lingual enamel ornament (uncertain in *Mystacodon*) [123]. **Minimum age**. 36.13 Ma. **Maximum age**. 56 Ma. **Age justification**. The *Mystacodon slenenensis* holotype was discovered 77 metres above the base of the Yumaque Formation, correlated to calcareous nanofosil zone NP19/20 of [124] in [122]. This corresponds to the *Isthmolithus recurvu*s Partial Range Zone CNE18, with an estimated age range of 37.46-36.13 Ma [125] The availability of this marine correlation for this fossil enables us to forego use of the corresponding marine stage (Ypresian). This gives a minimum age constraint of 36.13 Ma. We follow Benton et al. [11] in establishing the soft maximum constraint on the presence of a diverse, early Eocene artiodactyl record, including archaeocetes but no crown cetaceans during the Ypresian. Thus, the base of the Eocene serves as a soft maximum for the odontocete-mysticete divergence, dated at 56.0 Ma [23].

57	Mysticeti	2	15.99	-	**Node calibrated**. Clade consisting of the most recent common ancestor of the living baleen whale families Balaenidae, Balaenopteridae, Cetotheriidae, and Eschrichtiidae [126]. **Fossil taxon and specimen**. *Morenocetus parvus*; Holotype: MLP 5-11, incomplete cranium including the left periotic and incomplete right periotic in articulation with the basicranium but lacking the rostrum from El Castillo locality, Gaiman Formation, southern margin of the Lower Valley of the Chubut River, Chubut Province, central Patagonia, Argentina [127,128]. **Phylogenetic justification**. An unnamed stem balaenid from New Zealand dated to approximately 28 Ma was previously thought to be the oldest balaenid [129], however recent analyses have reported it outside Balaenidae [128]. Instead *Morenocetus parvu*s is now considered the oldest representative of Balaenidae, the oldest lineage of crown Mysticeti [128]. Identified as a balaenid due to the posterior margin of the zygomatic process of the squamosal and the lateral edge of the occipital forming a continuous lateral skull border, an anterolaterally directed zygomatic process of the squamosal, a squamosal that is higher dorsoventrally than long anteroposteriorly, and the body of the periotic lateral to the pars cochlearis is laterally and ventrally hypertrophied [128]. **Minimum age**. 15.99 Ma. **Age justification**. The lower Cerro Castillo beds of the lower part of the Gaiman Formation are considered Aquitanian-Burdigalian in age [128]. An Early Miocene age is supported by the Colhuehuapian mammal fauna from the underlying Trelew member of the Sarmiento Formation since it is dated to 21.0-20.5 Ma in age at Gran Barranca, Chubut Province, central Patagonia, Argentina [128,130]. The overlying Gaiman Formation shouldn't be older than this estimate, and the presence of marine vertebrates (fishes and penguins) indicate an early Miocene (Burdigalian) age [128]. The minimum constraint is then defined on the Burdigalian-Langhian boundary and the base of the Burdigalian, dated at 15.99 Ma [29].

58	Odontoceti	2	23.04	-	**Node calibrated**. Clade consisting of the most recent common ancestor of the living toothed whale families Delphinidae, Monodontidae, Phocoenidae, Iniidae, Pontoporiidae, Platanistidae, Lipotidae, Kogiidae, Physeteridae, and Zhiphidae. **Fossil taxon and specimen**. *Arktocara yakataga*; type specimen: USNM 214830, incomplete skull lacking the rostrum anterior of the antorbital notches, tympanoperiotics, dentition and mandibles from Poul Creek Formation, Yakutat City and Borough, Alaska, United States of America [131]. **Phylogenetic justification**. *Arktocara yakataga* belongs in Platanistoidea since the width of its maxilla is exceeds 50% of the width of the rostrum at the antorbital notch and it possesses affinities with members of Allodelphinidae that possess unequivocal synapomorphies of Platanistoidea [131]. Phylogenetic analysis supports this by placing Arktocara as the sister taxon to Allodelphis, meaning Arktocara yakataga is the oldest allodelphinid and oldest crown odontocete [131]. **Minimum age**. 23.04 Ma. **Age justification**. The *Arktocara yakataga* holotype (USNM 214830) was recovered from an unknown locality 400-500 metres below the top of the Poul Creek Formation [131]. The Poul Creek Formation is constrained to approximately 40-20 Ma in age, so, using a broadcast time of ~20 Ma and a thickness of ~2 km for the Poul Creek Formation, a constant rate of sedimentation gives an approximate age of 25 Ma to USNM 214830 (Late Eocene-Early Miocene) [131]. USNM 214830 is therefore Chattian in age (but with a possible species range extending into the Rupelian [131]). The minimum age constraint is therefore 23.04 Ma [23].

59	Delphinida	2	15.99	-	**Node calibrated**. Clade consisting of the most recent common ancestor of the living delphinoid odontocete families Lipotidae, Iniidae, Phocoenidae, Monodontidae and Delphinidae [132]. **Fossil taxon and specimen**. *Kentriodon pernix*; Type specimen: USNM 8060, fairly complete skeleton with skull, mandibles, tympanic bullae, periotics, right thyrohyal of the hyoids, and cervical and dorsal vertebrae in their natural positions; the left side displays 10 mostly incomplete ribs, an incomplete vertebral column with 7 cervicals, 10 dorsals, 4 lumbars with 3 transverse processes of others, 10 caudals with 1 epiphysis of another, and 4 chevrons; the right side displays 6 articulated and 4 disarticulated ribs; forelimbs are missing ; from greenish sandy clay of Shattuck's zone 5, Calvert formation, Chesapeake bay, Chesapeake Beach, Calvert County, Maryland, Virginia, United States of America [133]. **Phylogenetic justification**. *Kentriodon pernix* shares various anatomical similarities with the living porpoise genus Sotalia as described by [133]. **Minimum age**. 15.99 Ma. **Age justification**. Referred materials USNM 10670 (skull) and USNM 11400 (atlas) suggest that the stratigraphic range of *Kentriodon pernix* extends between zones 3 to 10 of the Calvert Formation [133]. The minimum age constraint is therefore based on the minimum age of zone C3 since it is the earliest stratigraphic occurrence of the *Kentriodon pernix*. Zone C3 has Sr87/Sr86 ages of 19.2-18.6 Ma with the best estimated range being 18.8-18.4 Ma [134]. This makes the minimum age constraint 18.4 Ma.
60	Phocoenidae-Monodontidae	2	7.6	-	**Node calibrated**. Divergence between porpoises (Phocoenidae) and narwhals (Monodontidae). **Fossil taxon and specimen**. *Salumiphocaena stocktoni*; Type specimen: UCMP 34576, a skull from Dacelite Quarry, Valmonte Diatomite Member, Monterey Formation, Palos Verdes Peninsula, California, United States of America [135,136]. **Phylogenetic justification**. *Salumiphocaena stocktoni* is considered the most basal phocoenid [137]. **Minimum age**. 7.6 Ma. **Age justification**. The minimum age constraint is based on the earliest recorded appearance of Salumiphocaena stocktoni in the Late Miocene Monterey Formation [137]. Barnes [136] described the age of the holotype to be between 11-10 Ma, while Xiong et al. [138] suggested 11.2-10 Ma, Chen et al. [139] suggested 11.2-10 Ma ±1.138 Myr, and Galatius et al. [140] suggested 11.2-7.246 Ma. However, the upper bound on the Valmonte Diatomite is constrained by the *Thalassiosira antiqua* Zone [141], the upper bound on which is 7.2 Ma [29].

61	Hippopotamidae	2	7.74	-	**Node calibrated**. Divergence of *Hippopotamus* from *Hexaprotodon*. **Fossil taxon and specimen**. *Cororatherium roobii*; Holotype: CHO-BT 68, partial right upper unerupted molar from Beticha locality, 3 km south of Chorora type locality, Chorora Formation, southern Afar Depression, Ethiopia [142]. **Phylogenetic justification**. *Chororatherium roobii* displays a hippopotamine trigonid defined by lacking a developed metacristid, an enlarged endometacristid and a postprotocristid reduced compared to the postparacristid, supporting a placement within the subfamily Hippopotaminae [142]. Phylogenetic analysis utilising the [143] data matrix recovers *Cororatherium roobii* as the basal-most hippopotamine based on various other dental characters. **Minimum age**. 7.74 Ma. **Age justification**. The minimum age constraint is based on the age of the Beticha locality. This was dated to between 8.02 Ma and 7.74 Ma through single crystal step-heating Ar40-Ar39 analysis undertaken by [31], though the remains are stated to be closer to 8.0 Ma in age [31,142].
62	Giraffidae	2	14	-	**Node calibrated**. Divergence of *Okapia* from *Giraffa* [144,145]. **Fossil taxon and specimen**. *Giraffokeryx punjabiensis*; PC-GCUF 163/19 (Pakistan Palaeontology Research Center, Faisalabad, Pakistan), partial skull roof with horn cores and incomplete upper dentition [146]. **Phylogenetic justification**. Danowitz et al. [145] follow Hamilton [147] and Solounias [148] in identifying *Giraffokeryx punjabiensis* as an ingroup member of the *Giraffa-Okapia* clade based on the presence of ossicones [149], among other characters (shortened back of skull, posteriorly positioned orbits, flexed skull, brachycephalic skulls, cheek teeth with high crowns). **Minimum age**: 14 Ma. **Age justification**. Samiullah et al. [146] describe cranial fossils of *G. punjabiensis* from the Chinji Fm. of Pakistan, dated to the middle Miocene, between 11.2 and 14.2 Ma. This would indicate a marine equivalent of either (from oldest to youngest) the Langhian, Serravallian, or Tortonian marine stages. The top of the youngest (Tortonian) is 7.25 Ma in age. However, Barry et al. [150] suggest that *G. punjabiensis* from the Chinji Fm. has a first appearance of 14 Ma, which we accept.

63	Bovini	2	10.2	-	**Node calibrated**. Bovini is the clade consisting of all extant and extinct species that share a common ancestor more closely related to Bovini than *Pseudoryx nghetinhensis* [151]. This node is equivalent to the Bovini + *Pseudoryx* clade when only considering extant taxa [151]. **Fossil taxon and specimen**. *Selenoportax vexillarius;* Holotype: AMNH 19748, cranium with right and left horn cores from Hasnot, Jhelum district, Punjab province, Nagri Formation, Siwalik Group, northern Pakistan [152]. **Phylogenetic justification**. *Selenoportax vexillarius* is the oldest bovid species to display derived morphological characters associated with the early evolution of Bovini according to Bibi [151]. These bovine synapomorphies include a great basal divergence of the horns, a low and wide cranium with an enlarged mastoid region, and the absence of a textured dorsal cranial depression present in fossil and living Boselaphini [153]. The consideration of this taxon as a representative of stem Bovini however is due to poorly developed bovine dental synapomorphies such as the complication of occlusal enamel surfaces, tall and wide entostyles and ectostylids involved in occlusion, and increased crown height [151]. **Minimum age**. 10.2 Ma. **Age justification**. The minimum age constraint is based on the species range of *Selenoportax vexillarius*, dated to be 10.2-9.8 Ma in age based on magnetostratigraphic dating of localities associated with the first and last occurrences of *Selenoportax vexillarius* [154]. The minimum age constraint is therefore set as 10.2 Ma since it is the earliest recorded appearance of *Selenoportax vexillarius* [154].
64	Tragelaphini	2	5.49	-	**Node calibrated**. The clade is defined by the most recent common ancestor of *Tragelaphus scriptus* and all living bovids more closely related to it than to *Boselaphus tragocamelu*s or *Bos primigenius* [151]. **Fossil taxon and specimen**. *Tragelaphus moroitu*; Holotype: ALA-VP-2/2, frontlet with almost complete left horn core, proximal half of right horn core, and occipital fragment from the Asa Koma Member, Adu-Asa Formation, Middle Awash, Ethiopia [155]. **Phylogenetic justification**. *Tragelaphus moroitu* possesses all the synapomorphies of Tragelaphini: horn cores rising upright, spiralling 270°, with three keels and a triangular cross-section throughout the core, with weak anteroposterior compression basally if at all, and simple mesodont teeth with relatively long premolar rows [151]. *Tragelaphus moroitu* however lacks any autapomorphies or apomorphies that ally it with any of the living lineages of tragelaphins, therefore it is considered ancestral to all tragelaphin lineages [151]. **Minimum age**. 5.49 Ma. **Age justification**. Bibi [151] suggested deriving the minimum age constraint from the age of the Asa Koma Member. The Witti Mixed Magmatic Tuff (WMMT, MA96-30) near the top of the Asa Koma Member was dated using Ar40/Ar39 dating methods, yielding an age of 5.57 Ma ±0.08 Myr [156], resulting in a minimum age constraint of 5.49 Ma.

65	Reduncini	2	5.111	-	**Node calibrated**. The clade is defined by the most recent common ancestor of *Redunca redunca* and *Kobus kob* [151]. **Fossil taxon and specimen**. *Redunca ambae*; Holotype: AME-VP-1/42, cranium from the Kuseralee Member, Sagantole Formation, Middle Awash, Ethiopia [155]. **Phylogenetic justification**. *Redunca ambae* is the first appearance of *Redunca* in the fossil record and thus the first crown reduncin [151]. **Minimum age**. 5.111 Ma. **Age justification**. The minimum age constraint is based on the minimum age of the Kuseralee Member. Basalt sample MA92-15 from the Gawto Member basalts overlying the Kuseralee Member was dated to 5.177 Ma ±0.066 Myr in age using Ar40/Ar39 step heating methods [157]. The minimum age constraint therefore is set at 5.111 Ma.
66	Hippotragini-Alcelaphini	2	6.48	-	**Node calibrated**. Divergence of Hippotragini and Alcelaphini [151]. **Fossil taxon and specimen**. *Tchadotragus sudrei*; Holotype: TM12-97-23, near complete skull lacking premaxillae, right nasal, zygomatic arches, and most of auditory region from the anthracotheriid unit of Toros-Menalla, Djurab region, northern Chad [158]. **Phylogenetic justification**. *Tchadotragus sudrei* possesses typical hippotragine features including long slender, curved horn cores, weak cranial flexure, large frontal sinuses, and hippotragine-like dentition [158]. It is thus considered a basal member of the tribe predating the *Oryx-Praedamalis* split [158]. **Minimum age**. 6.48 Ma. **Age justification**. The minimum age constraint is based on the minimum age constraint of the anthracotheriid unit. Be^{10}/Be^{9} atmospheric cosmogenic nuclide dating of the anthracotheriid unit resulted in a mean authigenic age of 6.88 Ma ±0.40 Myr above the ash tuff layer at TM 254 [159]. The minimum age constraint is based on the Be^{10}/Be^{9} authigenic mean above TM 254 and so is set as 6.48 Ma.

67	Alcelaphini	2	5.05	-	**Node calibrated**. This clade is defined by the most recent common ancestor of *Alcelaphus buselaphus, Connochaetes gnou, Damaliscus pygargus*, and *Beatragus hunteri* [151]. **Fossil taxon and specimen**. *Damalacra neanica*; Holotype: L7257, complete skull with horn cores and upper dentitions comprising P3-M3 on the right and broken M1-M3 on the left from bed 3aS, 'E' Quarry, Pelletal Phosphorite Member (PPM), Varswater Formation, Langebaanweg, South Africa [160]. **Phylogenetic justification**. *Damalacra neanica* is recognised as an alcelaphine based on a suite of cranial and dental characters as highlighted by Gentry [160]. This placement in crown Alcelaphini has been supported by morphological and molecular analyses done by Vrba [161] and Faith et al. [162]. **Minimum age**. 5.05 Ma. **Age justification**. The minimum age constraint is based on the minimum age of the Muishond Fontein Pelletal Phosphorite Members (MPPM). The fossils from the MPPM are considered slightly younger than sea level cycle T7 since they occur within a small interval between 26-30 metres above sea level (asl) within the Varswater Formation, which starts approximately 15 metres asl [163]. This gives an age estimate of 5.15 Ma ±0.1 Myr [163], establishing the minimum age constraint at 5.05 Ma.
68	Caprinae	2	8.9	-	**Node calibrated**. Clade that consists of all extant and extinct species that share a more recent common ancestor (MRCA) with *Capra ibex* than *Pantholops hodgsonii* [151]. **Fossil taxon and specimen**. *Aragoral mudejar*; Holotype: RO-2268,MPZ 96/54, frontal fragment with two horn cores from La Roma 2, Alfambra, Teruel, Aragón, Spain [164,165]. **Phylogenetic justification**. *Aragoral mudejar* is considered a member of Caprini due to the presence of hystodonty, reduced premolar rows, horn cores with well-developed pedicular sinuses, and short and robust metacarpals [166]. The greatly shortened and wide metacarpals is synapomorphy of Caprini [167], however the simple frontal sinuses in the pedicel and horn core base are a synapomorphy of the Caprini + Alcelaphini + Hippotragini clade justifying the consideration of Aragoral Mudejar as a stem caprine [151]. **Minimum age**. 8.9 Ma. **Age justification**. The minimum age constraint is based on the minimum age of the La Roma 2 locality, which is upper Vallesian in age [166]. This locality is correlated to Mammal Neogene zone MN10 and dated to 8.9 Ma using bio- and magnetostratigraphy [168,169].

69	Cervidae	2	17.235	28.4	**Node calibrated**. Clade consisting of all extant and extinct species that share a more recent common ancestor with Cervidae than any other living ruminant [151]. **Fossil taxon and specimen**. *Procervulus praelucidus*; Specimens: BSPG 1937 II 16841, BSPG 1937 II 16803, BSPG 1937 II 16794, BSPG 1937 II 16852, antlers from Wintershof-West, Germany [170,171]. **Phylogenetic justification**. *Procervulus praelucidus* is classified as a cervid as it possesses antlers with a proximal permanent pedicel and an upper deciduous antler [151]. *Procervulus praelucidus* is however considered a stem taxon as it retains the conserved character of antler burrs, suggesting a different method of antler development to the crown clade [151]. **Minimum age**. 17.235 Ma. **Maximum age**. 28.4 Ma. **Age justification**. The minimum age constraint is based on the minimum age of the type locality of Wintershof-West. This locality is the type locality for the Mammal Neogene zone MN3 [169], the top of which is dated to 17.235 Ma [172]. Due to a lack of phylogenetic resolution between late Oligocene ruminants and their living relatives Bibi [151] suggests utilising a soft maximum age constraint of 28.4 Ma.
70	stem-Moschidae	2	19.5	-	**Node calibrated**. Divergence of moschids from other pecoran artiodactyls. **Fossil taxon and specimen**. *Dremotherium feignouxi*; MNHN SG. 4304 (Museum national d'Histoire naturelle, Paris, France) and StG. 548 (Centre de Conservation et d'Etudes des Collections Lyon), from early Miocene deposits, Saint-Gérand-le-Puy, France [173]. **Phylogenetic justification**. *Dremotherium feignouxi*; was identified as a stem-Moschidae based on a morphological (skeletal) phylogenetic analysis by Janis and Scott [174] and this interpretation has been followed to justify calibrations for stem-Moschidae in Bibi [151] and Zusano et al. [144]. **Minimum age**. 19.5 Ma. **Age justification**. Saint-Gérand-le-Puy is a suite of localities, the stratigraphy of which is not very well constrained. However. Costeur [173] asserts an early Miocene age, Aquitanian, European Land Mammal Zone MN2. The MN2-3 boundary has been dated to 19.3 Ma [169].

71	Neobalaeninae	2	23.04	33.9	**Node calibrated.** Divergence of *Caperea* (pygmy right whale) from Balaenopteridae [175]. **Fossil taxon and specimen**. *Mauicetus parki*; OU 22545 (Otago University), from the Otekaike Limestone at Hakataramea Valley, South Canterbury, New Zealand [176]. **Phylogenetic justification**. Both Marx and Fordyce [177] and Lloyd and Slater [178] resolved *Mauicetus parki* as the oldest representative of Balaenopteridae and, therefore, Neobalaeninae, baked on total evidence and supertree methods. **Minimum age**. 23.04 Ma. **Maximum age**. 33.9 Ma. **Age justification**. Integrated biostratigraphy and isotope stratigraphy has established that the top of the Otekaike Limestone falls fully within the Chattian [179], the top of which is dated to 23.04 [23].
72	Balaenopteridae	2	7.3	-	**Node calibrated**. Divergence of crown Balaenopteridae (*Balaenoptera, Eschrichtius, Megaptera*). **Fossil taxon and specimen**. *Incakujira anillodefuego* GNHM Fs-098-1 (Gamagori Natural History Museum, Gamagori, Japan) from *Cosmopolitodus*-bearing horizons of the Pisco Formation, Aguada de Lomas, near Puerto de Lomas, approximately 80 km south of Nazca, Peru. **Phylogenetic justification**. Resolved as the oldest member of crown-Balaenopteridae by Marx and Kohno [180] based on a total evidence analysis. **Minimum age**. 7.3 Ma. **Age justification**. Marx and Kohno [180] quote a 7.3 Ma minimum constraint based on Sr isotope dating.
73	Physeteroidea	2	13.82	-	**Node calibrated**. Divergence of *Kogia* and *Physeter* [178]. **Oldest crown fossil**. *Idiophyseter merriami*; UCMP V75114 (University of California Museum of Paleontology, Berkeley, California) at Locality Templeton 2, San Luis Obispo County, California [181]. **Phylogenetic justification**. Collareta et al. [182] identified *Idiophyseter merriami* as the oldest member of the crown-clade defined by extant *Kogia* and *Physeter* based on a morphological phylogenetic analysis. **Minimum age**. 13.82 Ma. **Age justification**. The Palaeobiology Database asserts a Langhian age for *Idiophyseter merriami*, the top of which is dated to 13.82 Ma [29].

74	Perissodactyla	2	55.5	66.09	**Node calibrated**. The clade comprised of Equidae, Tapiridae and Rhinocerotidae. Following Emerling et al. [109] with the exception that the soft-maximum constraint, defined as the base of the Paleocene, is revised to 66.04 Ma ± 0.05 Myr [27], so 66.09 Ma.
75	Ceratomorpha	2	48.078	66.09	**Node calibrated**. Divergence of tapirids from rhinoceratids**.** **Fossil taxon and specimen**: *Cambaylophus*. IITR/SB/VLM 760, right maxilla fragment from the Cambay Shale, Vastan Lignite Mine, western India [183]. **Phylogenetic justification**. Kapur & Bajpai [183] reconstruct *Cambaylophus* as a tapiroid. Its relation to modern tapirids to the exclusion of rhinoceratids is also reflected in the analysis of Bai et al. [184]. **Minimum age**. 48.078 Ma. **Age justification**. Kapur & Bajpai [183] cite data from isotope stratigraphy and dinoflagellate biostratigraphy supporting the interpretation that Vastan fossils are between 54.5 (PETM) and 53.7 Ma (9 ETM2) in age. This provides for a minimum constraint defined on the Ypresian-Lutetian boundary which is dated at 48.07 Ma. The soft maximum, defined as the base of the Paleocene, is revised to 66.04 Ma ± 0.05 Myr [27], so 66.09 Ma.
76	Prinodontidae-Felidae	2	28.1	66.09	**Node calibrated**. Divergence of Prionodontidae from Felidae. Following Emerling et al. [109] with the exception that the soft-maximum constraint, defined as the base of the Paleocene, is revised to 66.04 Ma ± 0.05 Myr [27], so 66.09 Ma.
77	Herpestidae-Eupleridae	2	15.97	33.9	**Node calibrated**. The clade comprised of mongooses and Malagasy mongooses [64]. Following Emerling et al. [109].

78	Mustelidae-Procyonidae	2	26.42	-	**Node calibrated**. The split between mustelids (weasels) and procyonids (raccoons) [185]. **Fossil taxon and specimen**. *Pseudobassaris riggsi*; Holotype: YPM-PU 11455, skull from the Phosphorites du Quercy, France [186]. **Phylogenetic justification**. *Pseudobassaris riggsi* is considered the oldest know procyonid since it possesses procyonid suprameatal fossae and epitympanic recesses of the middle-ear [186,187]. *Pseudobassaris riggsi* is also stratigraphically older than the oldest known mustelid, *Plesictic plesictis* [185]. **Minimum age**. 26.42 Ma. **Age justification**. *Pseudobassaris riggsi* is from French localities Belgarric 1 and Belgarrite 4A and so the minimum age constraint is based on the minimum age of these localities [187]. These localities are correlated with European Paleogene reference levels MP 24 and MP 25 [185] the upper range of which is constrained with Chron C25r [188]; the upper bound of Chron C25r is dated to 26.42 Ma, providing the minimum age constraint.
79	Feliformia	2	19.535	-	**Node calibrated**. Most recent common ancestor of Felidae (cats), Prionodontidae (Asiatic lisangs), Herpestidae (mongooses), Eupleridae (Malagasy mongooses), Hyaenidae (Hyaenas) and Viverridae (civets and genets). **Fossil taxon and specimen**. *Proailurus lemanensis*; Holotype: MNHN SG 3509, skull from Saint-Gérard-le-Puy, France [189]. **Phylogenetic justification**. *Proailurus lemanensis* is placed within Feliformia based on its possession of an anteriorly positioned middle lacerate foramen (extreme in its case) [190], and was further identified as a felid based on a derived petrosal morphology that incorporates a uniquely bony flange on the medial border of the promontorium (a feature that is suppressed and/or reoriented in living felids) [191,192]. However, under more recent analysis *Proailurus lemanensis* falls outside Felidae and nests within Eupleridae, though it is still considered a feliform [193]. **Minimum age**. 19.535 Ma. **Age justification**. The minimum age constraint is based on the age of the early Miocene Saint-Gérard-le-Puy locality [194], correlated to Mammal Neogene zone MN2 [189]. The top of this zone is correlated to chron C6r [172], dated to 19.535 Ma [23].

80	Viverrinae-Genettinae	2	20.44	-	**Node calibrated**. Most recent common ancestor of Genetta and Viverra [195]. **Fossil taxon and specimen**. *Herpestides antiquus*; Specimen: MGL SG 3066, cranium and associated lower jaw from unknown locality, Sant Gérard, Allier basin, France [196]. **Phylogenetic justification**. Basicranial morphology of the auditory region has patterns similar to those found in living viverrids [196], however based on the differences in peculiarities of the dental morphotypes of Hemigalinae and Paradoxurinae [197] hypothesize *Herpestides* is a representative of a viverrine and genettine fossil lineage. **Minimum age**. 20.44 Ma. **Age justification**. Though the specific locality from which the 12 basicrania analysed by Hunt Jr [196] is unknown the regional geology is considered of Aquitanian age. The minimum age constraint is therefore based on the minimum age of the Aquitanian, dated to 20.45 Ma [29].
81	Lobodontini	2	5.05	-	**Node calibrated**. Common ancestor of *Ommatophoca*, *Lobodon*, *Leptonychotes* and *Hydruga* [198]. **Fossil taxon and specimen**. *Homiphoca capensis*; Holotype: SAM-PQl-15695, rostral segment of partial skull from the Muishond Fontein Pelletal Phosphorite Members (MPPM), Varswater Formation, Langebaanweg, republic of South Africa [199]. **Phylogenetic justification**. A phylogenetic analysis utilising 6 skulls attributed to *Homiphoca capensis* from the Varswater Formation resulted in the taxon nesting within Lobodontini [199]. **Minimum age**. 5.05 Ma. **Age justification**. The minimum age constraint is based on the minimum age of the Muishond Fontein Pelletal Phosphorite Members (MPPM). The MPPM is considered to be of early Pliocene Zanclean age [200], as the member overlies sea level cycle T7 within the Varswater Formation [201]. This gives a central age estimate of 5.15 Ma ±0.1 Myr for the MPPM [201], setting the minimum age constraint at 5.05 Ma.

82	Phocidae	2	13.82	-	**Node calibrated**. Divergence between the subfamilies Monachinae and Phocinae [198]. **Fossil taxon and specimen**. *Monotherium? wymani;* Holotype: MCZ 8741, left and right temporal bones from Shockoe creek ravine near the base of Church Hill, Calvert Formation, Richmond, Virginia, United States of America [202]. **Phylogenetic justification**. *Monotherium? wymani* is considered the oldest known monachine phocid according to [203-206]. **Minimum age**. 13.82 Ma. **Age justification**. The Calvert Formation spans an interval of time from the early to middle Miocene (Aquitanian-Langhian) [202], however Deméré et al. [205] cite *Monotherium? wymani* as exclusively Langhian in age, and phocid remains from zone 10 of the Calvert Formation outcropping at the Calvert Cliffs in Maryland are cited as early middle Miocene age [202]. The minimum age constraint is therefore defined by the upper bound of the Langhian, dated at 13.82 Ma [29].
83	Otarioidea	2	15.97	-	**Node calibrated**. Divergence between the families Otariidae (fur seals and sea lions) and Odobenidae (walruses) [198]. **Fossil taxon and specimen**. *Proneotherium repenningi*; Holotype: USNM 205334, nearly complete skull with all teeth except left I1, right P1, left P4, and right and left M1-2; missing part of right zygomatic arch from the “Iron Mountain bed”, Astoria Formation, Lincoln County, Oregon, United States of America [207]. **Phylogenetic justification**. A phylogenetic analysis utilising 24 cranial, dental and postcranial characters done by [207] supports the monophyly of Odobenidae with the genera Proneotherium and Prototaria as sister taxa and basal members of the group. Because of this Proneotherium repenningi can be considered the oldest odobenid taxon to date [205,208]. **Minimum age**. 15.99 Ma. **Age justification**. *Proneotherium repenningi* is of Burdigalian age [205], the top of which is dated to 15.99 Ma [29].

84	Pinnipedia	2	20.45	27.29	**Node calibrated**. Divergence between the super families Otarioidea (Otariidae+Odobenidae) and Phocoidea (Desmatophocidae+Phocidae). **Fossil taxon and specimen**. *Desmatophoca brachycephala*; Holotype: LACM 120199, incomplete cranium with crowns of left I1-3, parts of both canines, lacking other teeth and parts of the rostrum, and the right dorsolateral part of the braincase from locality LACM 4584, Astoria Formation, east of Knappton, Pacific County, Washignton State, United States of America [209]. **Phylogenetic justification**. *Desmatophoca brachycephala* is the oldest records of crown-Pinnipedia [206]. **Minimum age**. 20.45 Ma. **Maximum age**. 27.29 Ma. **Age justification**. *Desmatophoca brachycephala* is of Aquitanian age [205], the top of which is dated to 20.45 Ma [29]. The presence of stem pinnipeds such as *Enaliarctos tedfordi* extends no further than the late Oligocene Chattian age [64,206,210]. The soft maximum age constraint is thus set to the base of the Chattian age, dated at 27.29 Ma [23].
85	Hipposideridae-Rhinolophidae	2	38	56	**Node calibrated**. Divergence of Hipposideridae-Rhinolophidae. Following Emerling et al. [109].
86	Megadermatidae-Craseonycteridae	2	33.9	47.8	**Node calibrated**. Divergence of megadermatids from craseonycterids**.** Following Emerling et al. [109].
87	Molossidae - Vespertilionidae + Miniopteridae	2	38	56	**Node calibrated**. Divergence of Molossidae from Vespertilionidae + Miniopteridae. Following Emerling et al. [109].
88	Natalidae - Vespertilionidae + Miniopteridae + Molossidae	2	38	56	**Node calibrated.** Divergence of Natalidae from Molossidae plus Vespertilionidae plus Miniopteridae. Following Emerling et al. [109].

89	Sciuromorpha	2	41.03	59.24	**Node calibrated**. Common ancestor of the glirid-*Aplodontia*-sciurid clade within Sciuromorpha. **Fossil taxon and specimen**. *Eogliravus wildi*; Specimen: WDC-C-MG202, articulated skeleton from Messel, Germany (Storch and Seiffert 2007). **Phylogenetic justification:** *Eogliravus wildi* is thought to be the earliest appearance of the suborder Gliridae [211], since It possesses occlusal tooth morphology that links Eocene/Oligocene Glirid genera with Eocene ischyromyids [212]. **Minimum age.** 41.03 Ma. **Maximum age.** 59.24 Ma. **Age justification.** The minimum age constraint is based on the age of the Messel Formation. The Messel Formation is early-middle Eocene in age, correlated with Mammal Paleogene (MP) zone 11 [212]. This suggests that the Messel Formation is Lutetian in age and therefore the minimum age is set by the age of the Lutetian-Bartonian boundary [212]. This is dated to 41.03 Ma [23], giving a minimum age constraint of 40.7 Ma. The soft maximum age is based on the presence of *Paramys* in Thanetian age deposits. The base of the Thanetian is dated to 59.24 Ma [23] and serves as the soft maximum constraint.
90	Abrocomidae	2	1.778	13.82	**Node calibrated**. Most recent common ancestor of Abrocomidae (*Abrocoma*+*Cuscomys*). **Fossil taxon and specimen**. *Abracoma sp.*; MMP 1059-M: fragment of left maxillary with DP4-M1 from Punta San Andrés, San Andrés Formation [213]; and MACN 19722: right mandible with incisor and dp4-m2 from Santa Isabel, San Andrés Formation, between S2 and S3 [214]. **Phylogenetic justification**. *Abrocoma* is the oldest crown member of Abrocomidae (*Abrocoma*+*Cuscomys*) [215]. **Minimum age**. 1.778 Ma. **Maximum age**. 9.112 Ma. **Age justification**. The fossiliferous unit from which the San Andrés Formation rodents are recovered from is part of the Sanandresian substage of the upper Marplatan South American Land Mammal Age (SALMA) [213]. West [216] suggests that the Marplatan extends up until the end of chron C2, dated to 1.775 Ma by [29]. Verzi et al. [217] noted paleontological evidence for divergence within abrocomids through the middle and late Miocene, prior to the divergence of *Abrocoma* from *Cuscomys* (Verzi et al.[217]: fig. 10). We therefore define the soft maximum on the middle Miocene (base Serravallian), dated to 13.82 Ma [29].

91	Monotremata	2	24.459	133.2	**Node calibrated**. Divergence of *Platypus* from echidnas. **Fossil taxon ad specimen**. *Obdurodon insignis* SAM P18087 and AMNH 97228, (right upper molars) from University of California, Riverside Loc. RV-7247, SAM Quarry North, Unit 2 of Etadunna Formation, west side of Lake Palankarinna, South Australia [218]. **Minimum age**. 24.459 Ma. **Soft maximum age**. 133.2 Ma. **Age justification**. Woodburne et al. [73] identify Unit 2 of Etadunna Formation as falling within magnetozone C7r which is age constrained by the base of the succeeding C7n.2n, dated to 24.459 Ma [23]. Given the possibility that Cretaceous fossils such as *Teinolophos* from Flat Rocks, Australia, might be crown monotremes, more closely related to the extant *Ornithorhynchus* than to *Tachyglossus*, we use the maximum age of the Flat Rocks site to establish the soft maximum constraint. The age of the Flat Rocks site (Strzelecki Group) is usually considered Barremian-Aptian (e.g. [219]). However, the age of the Flat Rocks site has been subject to detailed palynological characterization finding that it falls fully within the range of the spore *Pilosisporites notensis* [220], the FAD of which coincides with the base of the *Foraminisporis wonhaggiensis* Zone, *Dictyotosporites speciosus* Zone and its *Cyclosporites hughesii* subzone [220]. The *Foraminisporis wonhaggiensis* Zone is interpreted to have a Hauterivian to Barremian age (Partridge (2011) in Holdgate, et al. [221]). A soft maximum can therefore be established on the base of the Hauterivian 132.6 Ma ± 0.6 Myr [27], thus 133.2 Ma.
92	Tachyglossidae	2	2.58	133.2	**Node calibrated**. Common ancestor of *Tachyglossus* and *Zaglossus*. **Fossil taxon and specimen**. Postcranial elements of tachyglossids from Chinchilla Sands [222], no specimen numbers given. **Phylogenetic Justification**. "*Zaglossus*" (*Megalibgwilia*) *robustus* from the Miocene of Gulgong, NSW may constrain age of crown echidnas, but this taxon is now referred to *Megalibgwilia robustus* and is not clearly demonstrated to be closer to *Zaglossus* than *Tachyglossus*. Following Pian et al. [223] there are no unequivocal pre-Pliocene echidnas and, following Musser [222], the oldest are *Tachyglossus* sp. from Pliocene of Chinchilla Sands. **Minimum age**. 2.58 Ma. **Maximum age**. 133.2 Ma. **Age justification**. The Chinchilla Sand fluviatile deposits near the town of Chinchilla, on the Darling Downs, Queensland. No direct dates have been obtained for this deposit but Tedford et al. [224] and Mackness et al. [225] in Dawson [226] argue for an early to middle Pliocene age interpretation based on correlation. Hence, we use the date of the Pliocene-Pleistocene boundary to inform the minimum age interpretation of this fossil, dated to 2.58 Ma [227]. The soft maximum follows that of Monotremata.

References for “Justification for Fossil Calibrations”

1 Tarver, J. E. *et al.* The interrelationships of placental mammals and the limits of phylogenetic inference. *Genome Biology and Evolution* **8**, 330-344, doi:10.1093/gbe/evv261 (2016).

2 Flynn, J. J., Parrish, J. M., Rakotosamimanana, B., Simpson, W. F. & Wyss, A. R. A Middle Jurassic mammal from Madagascar. *Nature* **401**, 57-60 (1999).

3 Puttick, M. N. *et al.* Uncertain-tree: discriminating among competing approaches to the phylogenetic analysis of phenotype data. *Proceedings of the Royal Society B: Biological Sciences* **284**, 20162290, doi:10.1098/rspb.2016.2290 (2017).

4 Jenkins, F. A., Gatesy, S. M., Shubin, N. H. & Amaral, W. W. Haramiyids and Triassic mammalian evolution. *Nature* **385**, 715-718 (1997).

5 Luo, Z. X., Gatesy, S. M., Jenkins, F. A., Amaral, W. W. & Shubin, N. H. Mandibular and dental characteristics of Late Triassic mammaliaform Haramiyavia and their ramifications for basal mammal evolution. *Proceedings National Academy of Sciences* **112**, E7101–E7109, doi:10.1073/pnas.1519387112 (2015).

6 Hesselbo, S. P., Ogg, J. G., Ruhl, M., Hinnov, L. A. & Huang, C. J. in *Geologic Time Scale 2020* 955-1021 (2020).

7 Zheng, X., Bi, S., Wang, X. & Meng, J. A new arboreal haramiyid shows the diversity of crown mammals in the Jurassic period. *Nature* **500**, 199-202, doi:10.1038/nature12353 (2013).

8 Bi, S., Wang, Y., Guan, J., Sheng, X. & Meng, J. Three new Jurassic euharamiyidan species reinforce early divergence of mammals. *Nature* **514**, 579-584, doi:10.1038/nature13718 (2014).

9 Li, M. *et al.* Astronomical tuning of the end-Permian extinction and the Early Triassic Epoch of South China and Germany. *Earth and Planetary Science Letters* **441**, 10-25, doi:10.1016/j.epsl.2016.02.017 (2016).

10 Krause, D. W. *et al.* First cranial remains of a gondwanatherian mammal reveal remarkable mosaicism. *Nature* **515**, 512-517, doi:10.1038/nature13922 (2014).

11 Benton, M. J. *et al.* Constraints on the timescale of animal evolutionary history. *Palaeontologia Electronica* **18**, 1-106 (2015).

12 Huttenlocker, A. K., Grossnickle, D. M., Kirkland, J. I., Schultz, J. A. & Luo, Z. X. Late-surviving stem mammal links the lowermost Cretaceous of North America and Gondwana. *Nature* **558**, 108-112, doi:10.1038/s41586-018-0126-y (2018).

13 Bi, S. *et al.* An Early Cretaceous eutherian and the placental–marsupial dichotomy. *Nature*, doi:10.1038/s41586-018-0210-3 (2018).

14 Meng, J., Hu, Y., Li, C. & Wang, Y. The mammal fauna in the Early Cretaceous Jehol Biota: implications for diversity and biology of Mesozoic mammals. *Geological Journal* **41**, 439-463 (2006).

15 Ogg, J. G., Agterberg, F. P. & Gradstein, F. M. in *A geologic time scale 2004* (eds F. M. Gradstein, J. G. Ogg, & A. Smith) 344-383 (Cambridge University Press, 2004).

16 Woodburne, M. O., Rich, T. H. & Springer, M. S. The evolution of tribospheny and the antiquity of mammalian clades. *Molecular Phylogenetics and Evolution* **28**, 360-385 (2003).

17 Luo, Z. X., Yuan, C. X., Meng, Q. J. & Ji, Q. A Jurassic eutherian mammal and divergence of marsupials and placentals. *Nature* **476**, 442-445, doi:10.1038/nature10291 (2011).

18 Luo, Z. X., Ji, Q., Wible, J. R. & Yuan, C. X. An early Cretaceous tribosphenic mammal and metatherian evolution. *Science* **302**, 1934-1940 (2003).

19 Ji, Q. *et al.* The earliest known eutherian mammal. *Nature* **416**, 816-822 (2002).

20 O'Leary, M. A. *et al.* The placental mammal ancestor and the post–K-Pg radiation of placentals. *Science* **339**, 662-667, doi:10.1126/science.1229237 (2013).

21 Yuan, C.-X., Ji, Q., Meng, Q.-J., Tabrum, A. R. & Luo, Z.-X. Earliest evolution of multituberculate mammals revealed by a new Jurassic fossil. *Science* **341**, 779-783 (2013).

22 Krause, D. W. *et al.* Skeleton of a Cretaceous mammal from Madagascar reflects long-term insularity. *Nature* **581**, 421-427, doi:10.1038/s41586-020-2234-8 (2020).

23 Speijer, R. P., Pälike, H., Hollis, C. J., Hooker, J. J. & Ogg, J. G. in *Geologic Time Scale 2020* 1087-1140 (2020).

24 Silcox, M. T., Bloch, J. I., Sargis, E. J. & Boyer, D. M. in *The rise of placental mammals : origins and relationships of the major extant clades* (eds K.D. Rose & J.D. Archibald) 127-144 (Johns Hopkins University Press, 2005).

25 Bloch, J. I., Silcox, M. T., Boyer, D. M. & Sargis, E. J. New Paleocene skeletons and the relationship of plesiadapiforms to crown-clade primates. *Proceedings of the National Academy of Sciences, USA* **104**, 1159-1164 (2007).

26 Seiffert, E. R., Perry, J. M., Simons, E. L. & Boyer, D. M. Convergent evolution of anthropoid-like adaptations in Eocene adapiform primates. *Nature* **461**, 1118-1121, doi:10.1038/nature08429 (2009).

27 Gale, A. S. *et al.* in *Geologic Time Scale 2020* 1023-1086 (2020).

28 Kappelman, J. *et al.* The earliest occurrence of Sivapithecus from the Middle Miocene of Chinji Formation of Pakistan. *Journal of Human Evolution* **21**, 61-73 (1991).

29 Raffi, I. *et al.* in *Geologic Time Scale 2020* 1141-1215 (2020).

30 Suwa, G., Kono, R. T., Katoh, S., Asfaw, B. & Beyene, Y. A new species of great ape from the late Miocene epoch in Ethiopia. *Nature* **448**, 921-924 (2007).

31 Katoh, S. *et al.* New geological and palaeontological age constraint for the gorilla-human lineage split. *Nature* **530**, 215-218, doi:10.1038/nature16510 (2016).

32 Brunet, M., Guy, F., Pilbeam, D., Mackay, H. T., Likius, A., Djimboumalbaye, A., et al. . A new hominid from the upper Miocene of Chad, central Africa. *Nature* **418**, 145-151 (2002).

33 Benefit, B. R., McCrossin, M., Boaz, N. T. & Pavlakis, P. New fossil cercopithecoids from the Late Miocene of As Sahabi, Libya. *Garyounis Scientific Bulletin* **Special Issue 5**, 265-282 (2008).

34 Alba, D. M. *et al.* First joint record of Mesopithecus and cf. Macaca in the Miocene of Europe. *J*

Hum Evol **67**, 1-18, doi:10.1016/j.jhevol.2013.11.001 (2014).

35 Raaum, R. L., Sterner, K. N., Noviello, C. M., Stewart, C. B. & Disotell, T. R. Catarrhine primate divergence dates estimated from complete mitochondrial genomes: concordance with fossil and nuclear DNA evidence. *J Hum Evol* **48**, 237-257, doi:10.1016/j.jhevol.2004.11.007 (2005).

36 Fleagle, J. G. *Primate adaptation and evolution*. (Academic Press, 1999).

37 Fabre, P.-H., Hautier, L., Dimitrov, D. & Douzery, E. A glimpse on the pattern of rodent diversification: a phylogenetic approach. *BMC Evol Biol* **12**, 88 (2012).

38 Asher, R. J., Smith, M. R., Rankin, A. & Emry, R. J. Congruence, fossils and the evolutionary tree of rodents and lagomorphs. *Royal Society Open Science* **6**, doi:10.1098/rsos.190387 (2019).

39 Swanson, M. T., Oliveros, C. H. & Esselstyn, J. A. A phylogenomic rodent tree reveals the repeated evolution of masseter architectures. *Proceedings. Biological sciences / The Royal Society* **286**, 20190672, doi:10.1098/rspb.2019.0672 (2019).

40 Thewissen, J. G. M., Williams, E. M., Roe, L. J. & Hussain, S. T. Skeletons of terrestrial cetaceans and the relationship of whales to artiodactyls. *Nature* **413**, 277-281 (2001).

41 Marivaux, L., Vianey-Liaud, M. & Jaeger, J.-J. High-level phylogeny of early Tertiary rodents: dental evidence. *Zoological Journal of the Linnean Society* **142**, 105-134 (2004).

42 Shevyreva, N. S. in *Flora i fauna Zaysanskoi vpadiny [Flora and fauna of Zaysan Basin]* (ed L. K. Gabuniya) 77–114 (Akademiya Nauk Gruzinskoy SSR, 1984).

43 Lucas, S. G. in *Late Paleocene–Early Eocene climatic and biotic events in the marine and terrestrial records* (eds M. P. Aubry, S. G. Lucas, & W. A. Berggren) 451-500 (Columbia University Press, 1998).

44 Emry, R. J., Tyutkova, L. A., Lucas, S. G. & Wang, B. Rodents of the middle Eocene Shinzhaly fauna of Eastern Kazakstan. *Journal of Vertebrate Paleontology* **18**, 218-227 (1998).

45 Emry, R. J. The Middle Eocene North American myomorph rodent *Elymys*, her Asian sister *Aksyiromys*, and other Eocene myomorphs. *Bulletin of the Carnegie Museum of Natural History* **39**, 141-150 (2007).

46 dos Reis, M. *et al.* Phylogenomic datasets provide both precision and accuracy in estimating the timescale of placental mammal phylogeny. *Proceedings of the Royal Society B: Biological Sciences* **279**, 3491-3500, doi:10.1098/rspb.2012.0683 (2012).

47 Benton, M. J., Donoghue, P. C. J. & Asher, R. J. in *The timetree of Life* (eds S. B. Hedges & S. Kumar) 35-86 (Cambridge University Press, 2009).

48 Holbrook, L. T. On the skull of *Radinskya* (Mammalia) and its phylogenetic position. *Journal of Vertebrate Paleontology* **34** (2014).

49 Rose, K. D. *et al.* Early Eocene fossils suggest that the mammalian order Perissodactyla originated in India. *Nat Commun* **5**, 5570, doi:10.1038/ncomms6570 (2014).

50 Beard, K. C. East of Eden: Asia is an important center of taxonomic origination in mammalian evolution. *Bulletin of the Carnegie Museum of Natural History* **34**, 5-39 (1998).

51 Meng, J., Zhai, R. J. & Wyss, A. R. The late Paleocene Bayan Ulan fauna of Inner Mongolia,

China. *Bulletin of the Carnegie Museum of Natural History* **34**, 148-185 (1998).

52 Hassanin, A. *et al.* Pattern and timing of diversification of Cetartiodactyla (Mammalia, Laurasiatheria), as revealed by a comprehensive analysis of mitochondrial genomes. *C R Biol* **335**, 32-50, doi:10.1016/j.crvi.2011.11.002 (2012).

53 Wesley-Hunt, G. D. & Flynn, J. J. Phylogeny of the Carnivora: Basal relationships among the carnivoramorphans, and assessment of the position of 'Miacoidea' relative to Carnivora. *Journal of Systematic Palaeontology* **3**, 1-28, doi:10.1017/s1477201904001518 (2005).

54 Bryant, H. The Carnivora of the Lac Pelletier Lower Fauna (Eocene: Duchesnean), Cypress Hills Formation, Saskatchewan. *Journal of Paleontology* **66**, 847-855 (1992).

55 Hooker, J. J. A primitive emballonurid bat (Chiroptera, Mammalia) from the earliest Eocene of England. *Palaeovertebrata* **25**, 287-300 (1996).

56 Eiting, T. P. & Gunnell, G. F. Global completeness of the bat fossil record. *Journal of Mammalian Evolution* **16**, 151-173, doi:10.1007/s10914-009-9118-x (2009).

57 Tabuce, R., Telles Antunes, M. & Sigé, B. A new primitive bat from the earliest Eocene of Europe. *Journal of Vertebrate Paleontology* **29**, 627-630 (2009).

58 Hand, S., Novacek, M., Godthelp, H. & Archer, M. First Eocene bat from Australia. *Journal of Vertebrate Paleontology* **14**, 375-381, doi:10.1080/02724634.1994.10011565 (1994).

59 Beard, K. C., Sigé, B. & Krishtalka, L. A primitive vespertilionoid bat from the early Eocene of central Wyoming. *Comptes rendus de l'Académie des sciences. Série 2, Mécanique, Physique, Chimie, Sciences de l'univers, Sciences de la Terre* **314**, 735-741 (1992).

60 Sigé, B. Morphologie dentarre lactéaled'un Chiroptère de l'Éocène inférieur-moyen d'Europe. *Geobios* **24**, 231-236 (1991).

61 Ravel, A. *et al.* New philisids (Mammalia, Chiroptera) from the Early–Middle Eocene of Algeria and Tunisia: new insight into the phylogeny, palaeobiogeography and palaeoecology of the Philisidae. *Journal of Systematic Palaeontology* **13**, 691-709, doi:10.1080/14772019.2014.941422 (2014).

62 Smith, T., Habersetzer, J., Simmons, N. B. & Gunnell, G. F. in *Evolutionary History of Bats: Fossils, Molecules and Morphology* (eds G. F. Gunnell & N. B. Simmons) 23-66 (Cambridge University Press, 2012).

63 Gheerbrant, E. Paleocene emergence of elephant relatives and the rapid radiation of African ungulates. *Proceedings of the National Academy of Sciences* **106**, 10717-10721, doi:10.1073/pnas.0900251106 (2009).

64 Meredith, R. W. *et al.* Impacts of the Cretaceous Terrestrial Revolution and KPg extinction on mammal diversification. *Science* **334**, 521-524, doi:10.1126/science.1211028 (2011).

65 McCormack, J. E. *et al.* Ultraconserved elements are novel phylogenomic markers that resolve placental mammal phylogeny when combined with species-tree analysis. *Genome Res* **22**, 746-754, doi:10.1101/gr.125864.111 (2012).

66 Asher, R. J. A web-database of mammalian morphology and a reanalysis of placental phylogeny. *BMC Evol Biol* **7**, 108, doi:10.1186/1471-2148-7-108 (2007).

67 Springer, M. S. *et al.* Interordinal gene capture, the phylogenetic position of Steller's sea cow based on molecular and morphological data, and the macroevolutionary history of Sirenia. *Mol Phylogenet Evol* **91**, 178-193, doi:10.1016/j.ympev.2015.05.022 (2015).

68 Woodburne, M. O., Pledge, N. S. & Archer, M. in *Possums and Opossums: Studies in Evolution* (ed M. Archer) 581-602 (Surrey Beatty and Sons, 1987).

69 Black, K. H., Archer, M. & Hand, S. J. New Tertiary koala (Marsupialia, Phascolarctidae) from Riversleigh, Australia, with a revision of phascolarctid phylogenetics, paleoecology, and paleobiodiversity. *Journal of Vertebrate Paleontology* **32**, 125-138 (2012).

70 Woodburne, M. O. *et al.* Land mammal biostratigraphy and magnetostratigraphy of the Etadunna Formation (late Oligocene) of South Australia. *Journal of Vertebrate Paleontology* **13**, 483-515, doi:10.1080/02724634.1994.10011527 (1994).

71 Mitchell, K. J. *et al.* Molecular phylogeny, biogeography, and habitat preference evolution of marsupials. *Mol Biol Evol* **31**, 2322-2330, doi:10.1093/molbev/msu176 (2014).

72 Megirian, D., Prideaux, G., Murray, P. & Smit, N. An Australian land mammal age biochronological scheme. *Paleobiology* **36**, 658-671 (2010).

73 Woodburne, M. O. *et al.* Land mammal biostratigraphy and magnetostratigraphy of the Etadunna Formation (late Oligocene) of South Australia. *Journal of Vertebrate Palaeontology* **13**, 483-515 (1993).

74 Janis, C. M. *et al.* Palaeoecology of Oligo-Miocene macropodoids determined from craniodental and calcaneal data. *Memoirs of Museum Victoria* **74**, 209-232 (2016).

75 Simpson, G. G. The Argyrolagidae, extinct South American marsupials. *Bulletin of the Museum of Comparative Zoology* **139**, 1-86 (1970).

76 Kirsch, J. A. W., Lapointe, F.-J. & Springer, M. S. DNA-hybridisation studies of marsupials and their implications for metatherian classification. *Australian Journal of Zoology* **45**, 211-280 (1997).

77 Asher, R. J., Horovitz, I. & Sanchez-Villagra, M. R. First combined cladistic analysis of marsupial mammal interrelationships. *Mol Phylogenet Evol* **33**, 240-250, doi:10.1016/j.ympev.2004.05.004 (2004).

78 Phillips, M. J., McLenachan, P. A., Down, C., Gibb, G. C. & Penny, D. Combined mitochondrial and nuclear DNA sequences resolve the interrelations of the major Australasian marsupial radiations. *Syst Biol* **55**, 122-137, doi:10.1080/10635150500481614 (2006).

79 Beck, R. M. An 'ameridelphian' marsupial from the early Eocene of Australia supports a complex model of Southern Hemisphere marsupial biogeography. *Naturwissenschaften* **99**, 715-729 (2012).

80 Asher, R. J. & Helgen, K. M. Nomenclature and placental mammal phylogeny. *BMC Evolutionary Biology* **10**, 102 (2010).

81 Babot, J., López, D. A. G. & Gaudin, T. J. The most ancient xenarthran petrosal: morphology and evolutionary significance. *Journal of Vertebrate Paleontology* **32**, 1186-1197, doi:10.1080/02724634.2012.686466 (2012).

82 Ciancio, M., Herrera, C., Aramayo, A., Payrola, P. & Babot, M. Diversity of cingulates (Mammalia, Xenarthra) in the middle-late Eocene of Northwestern Argentina. *Acta Palaeontologica Polonica*

61, doi:10.4202/app.00208.2015 (2016).

83 DeCelles, P. G., Carrapa, B. & Gehrels, G. E. Detrital zircon U-Pb ages provide provenance and chronostratigraphic information from Eocene synorogenic deposits in northwestern Argentina. *Geology* **35**, doi:10.1130/g23322a.1 (2007).

84 Woodburne, M. O. *et al.* Revised timing of the South American early Paleogene land mammal ages. *Journal of South American Earth Sciences* **54**, 109-119, doi:10.1016/j.jsames.2014.05.003 (2014).

85 Simpson, G. G. *Menatotherium*, Eocene mammal from France. *American Journal of Science* **246**, 165, doi:10.2475/ajs.246.3.165 (1948).

86 McKenna, M. C., Wyss, A. R. & Flynn, J. J. Paleogene pseudoglyptodont xenarthrans from central Chile and Argentine Patagonia. *American Museum Novitates* **3536**, 1-18 (2006).

87 Delsuc, F. *et al.* The phylogenetic affinities of the extinct glyptodonts. *Current biology : CB* **26**, R155-156, doi:10.1016/j.cub.2016.01.039 (2016).

88 Slater, G. J. *et al.* Evolutionary Relationships among Extinct and Extant Sloths: The Evidence of Mitogenomes and Retroviruses. *Genome Biol Evol* **8**, 607-621, doi:10.1093/gbe/evw023 (2016).

89 Gaudin, T. J. & Croft, D. A. Paleogene Xenarthra and the evolution of South American mammals. *Journal of Mammalogy* **96**, 622-634, doi:10.1093/jmammal/gyv073 (2015).

90 Flynn, J. J., Wyss, A. R., Croft, D. A. & Charrier, R. The Tinguiririca Fauna, Chile: biochronology, paleoecology, biogeography, and a new earliest Oligocene South American Land Mammal 'Age'. *Palaeogeography, Palaeoclimatology, Palaeoecology* **195**, 229-259, doi:10.1016/s0031-0182(03)00360-2 (2003).

91 MacPhee, R. D. & Iturralde-Vinent, M. First Tertiary land mammal from Greater Antilles: an Early Miocene sloth. *3094* (1994).

92 Pujos, F., Gaudin, T. J., De Iuliis, G. & Cartelle, C. Recent Advances on Variability, Morpho-Functional Adaptations, Dental Terminology, and Evolution of Sloths. *Journal of Mammalian Evolution* **19**, 159-169, doi:10.1007/s10914-012-9189-y (2012).

93 MacPhee, R. D., Iturralde-Vinent, M. & Gaffney, E. S. Domo de Zaza, an Early Miocene vertebrate locality in south-central Cuba, with notes on the tectonic evolution of Puerto Rico and the Mona Passage. *American Museum Novitates* **3394**, 1-42 (2003).

94 Bargo, M. S., Toledo, N. & Vizcaíno, S. F. in *Early Miocene paleobiology in Patagonia. High latitude paleocommunities of the Santa Cruz Formation* (eds S. F. Vizcaíno, R. F. Kay, & M. S. Bargo) 216-242 (Cambridge University Press, 2012).

95 Gaudin, T. J. & Branham, D. G. The phylogeny of the Myrmecophagidae (Mammalia, Xenarthra, Vermilingua) and the relationship of Eurotamandua to the Vermilingua. *Journal of Mammalian Evolution* **5**, 237-265 (1998).

96 Ameghino, F. Nuevas especies de mamíferos cretáceos y terciarios de la República Argentina. *Anales Soc. Cient. Arg.* **56-58** (1904).

97 Hirschfeld, S. E. A new fossil anteater (Edentata, Mammalia) from Colombia, S.A. and evolution of the Vermilingua. *Journal of Paleontology* **50**, 419-432 (1976).

98 Kay, R. F., Vizcaíno, S. F. & Bargo, M. S. in *Early Miocene paleobiology in Patagonia: High-latitude paleocommunities of the Santa Cruz Formation* (eds S. F. Vizcaíno, R. F. Kay, & M. S. Bargo) 331-365 (Cambridge University Press, 2012).

99 Fleagle, J. G. *et al.* in *Early Miocene paleobiology in Patagonia: High-latitude paleocommunities of the Santa Cruz Formation* (eds S. F. Vizcaíno, R. F. Kay, & M. S. Bargo) 41-58 (Cambridge University Press, 2012).

100 Perkins, M. E. *et al.* in *Early Miocene paleobiology in Patagonia: High-latitude paleocommunities of the Santa Cruz Formation* (eds S. F. Vizcaíno, R. F. Kay, & M. S. Bargo) 23-40 (Cambridge University Press, 2012).

101 Asher, R. J. & Avery, D. M. New golden moles (Afrotheria, Chrysochloridae) from the early Pliocene of South Africa. *Paleontologia Electronica* **13**, 13.11.13A (2010).

102 Butler, P. M. Macroscelidea, Insectivora, and Chiroptera from the Miocene of East Africa. *Palaeovertebrata* **14**, 117-200 (1984).

103 Broom, R. On two Pleistocene golden moles. *Annals of the Transvaal Museum* **20**, 215-216 (1941).

104 Asher, R. J. Recent additions to the fossil record of tenrecs and golden moles. *Afrotherian Conservation* **15**, 4-13 (2019).

105 Stevens, N. J., O'Connor, P. M., Mtelela, C. & Roberts, E. M. Macroscelideans (Myohyracinae and Rhynchocyoninae) from the late Oligocene Nsungwe formation of the Rukwa Rift Basin, southwestern Tanzania. *Historical Biology*, 1-7, doi:10.1080/08912963.2021.1938565 (2021).

106 Tabuce, R. New remains of *Chambius kasserinensis* from the Eocene of Tunisia and evaluation of proposed affinities for Macroscelidea (Mammalia, Afrotheria). *Historical Biology* **30**, 251-266, doi:10.1080/08912963.2017.1297433 (2017).

107 Pickford, M. & Hlusko, L. J. Late Miocene procaviid hyracoids (Hyracoidea: *Dendrohyrax*) from Lemudong'o, Kenya. *Kirtlandia* **56**, 106-111 (2007).

108 Rasmussen, D. T. & Gutiérrez, M. in *Cenozoic mammals of Africa* (eds L. Werdelin & W. J. Sanders) 123-146 (University of California Press, 2010).

109 Emerling, C. A., Huynh, H. T., Nguyen, M. A., Meredith, R. W. & Springer, M. S. Spectral shifts of mammalian ultraviolet-sensitive pigments (short wavelength-sensitive opsin 1) are associated with eye length and photic niche evolution. *Proceedings. Biological sciences / The Royal Society* **282**, doi:10.1098/rspb.2015.1817 (2015).

110 Bloch, J. I. *et al.* First North American fossil monkey and early Miocene tropical biotic interchange. *Nature* **533**, 243-246, doi:10.1038/nature17415 (2016).

111 Chester, S. G., Bloch, J. I., Boyer, D. M. & Clemens, W. A. Oldest known euarchontan tarsals and affinities of Paleocene Purgatorius to Primates. *Proceedings of the National Academy of Sciences* **112**, 1487-1492 (2015).

112 Clemens, W. A. Purgatorius (Plesiadapiformes, Primates?, Mammalia), a Paleocene immigrant into northeastern Montana: stratigraphic occurrences and incisor proportions. *Bulletin of Carnegie Museum of Natural History* **2004**, 3-13 (2004).

113 Jiménez-Hidalgo, E., Smith, K. T., Guerrero-Arenas, R. & Alvarado-Ortega, J. The first Late Eocene continental faunal assemblage from tropical North America. *Journal of South American Earth Sciences* **57**, 39-48, doi:10.1016/j.jsames.2014.12.001 (2015).

114 Orliac, M., Boisserie, J.-R., MacLatchy, L. & Lihoreaum, F. Early Miocene hippopotamids (Cetartiodactyla) constrain the phylogenetic and spatiotemporal settings of hippopotamid origin. *Proceedings of the National Academy of Sciences* (2010).

115 Frantz, L. *et al.* The evolution of Suidae. *Annu Rev Anim Biosci* **4**, 61-85, doi:10.1146/annurev-animal-021815-111155 (2016).

116 Liu, L. *Chinese fossil Suoidea: Systematics, evolution, and paleoecology*. (University of Helsinki, 2003).

117 Boisserie, J. R., Lihoreau, F. & Brunet, M. The position of hippopotamidae within cetartiodactyla. *Proceedings of the National Academy of Sciences of the United States of America* **102**, 1537-1541 (2005).

118 Prothero, D. R. The early evolution of the North American peccaries (Artiodactyla: Tayassuidae). *Museum of Northern Arizona Bulletin* **65**, 509-541 (2009).

119 Waddell, P. J., Okada, N. & Hasegawa, M. Towards resolving the interordinal relationships of placental mammals. *Systematic Biology* **48**, 1-5 (1999).

120 Bajpai, S. & Gingerich, P. D. A new Eocene archaeocete (Mammalia, Cetacea) from India and the time of origin of whales. *Proceedings of the National Academy of Sciences, USA* **95**, 15464-15468 (1998).

121 Fordyce, R., Perrin, W., Würsig, B. & Thewissen, J. Encyclopedia of marine mammals. (2009).

122 Lambert, O. *et al.* Earliest mysticete from the Late Eocene of Peru sheds new light on the origin of Baleen Whales. *Current biology : CB* **27**, 1535-1541 e1532, doi:10.1016/j.cub.2017.04.026 (2017).

123 Fordyce, R. E. & Marx, F. G. Gigantism precedes filter feeding in baleen whale evolution. *Current biology : CB* **28**, 1670-1676 e1672, doi:10.1016/j.cub.2018.04.027 (2018).

124 Martini, E. in *Second Planktonic Conference,*. 739–785.

125 Agnini, C. *et al.* Biozonation and biochronology of Paleogene calcareous nannofossils from low and middle latitudes. *Newsletter in Stratigraphy* **47**, 131-181 (2014).

126 Tsai, C. H. & Fordyce, R. E. Archaic baleen whale from the Kokoamu Greensand: earbones distinguish a new late Oligocene mysticete (Cetacea: Mysticeti) from New Zealand. *Journal of the Royal Society of New Zealand* **46**, 117-138, doi:10.1080/03036758.2016.1156552 (2016).

127 Cabrera, A. Cetáceos fósiles del Museo de La Plata. *Revista del Museo de la Plata* **29**, 363-411 (1926).

128 Buono, M. R., Fernández, M. S., Cozzuol, M. A., Cuitiño, J. I. & Fitzgerald, E. M. G. The early Miocene balaenid Morenocetus parvus from Patagonia (Argentina) and the evolution of right whales. *PeerJ*, e4148, doi:10.7717/peerj.4148 (2017).

129 Fordyce, R. E. Oligocene origin of skim–feeding right whales: a small archaic balaenid from New

Zealand. *Journal of Vertebrate Paleontology* **22**, 54(A) (2002).

130 Dunn, R. E. *et al.* A new chronology for middle Eocene-early Miocene South American Land Mammal Ages. *Geological Society of America Bulletin* **125**, 539-555, doi:10.1130/b30660.1 (2012).

131 Boersma, A. T. & Pyenson, N. D. *Arktocara yakataga*, a new fossil odontocete (Mammalia, Cetacea) from the Oligocene of Alaska and the antiquity of Platanistoidea. *PeerJ* **4**, e2321, doi:10.7717/peerj.2321 (2016).

132 Geisler, J. H., McGowen, M. R., Yang, G. & Gatesy, J. A supermatrix analysis of genomic,morphological, and paleontological data from crown Cetacea. *BMC Evolutionary Biology* **11**, 112 (2011).

133 Kellogg, R. Kentriodon pernix, a Miocene porpoise from Maryland. *Proceedings of the U. S. National Museum* **69**, 1-72 (1927).

134 Browning, J. V. *et al.* Quantification of the effects of eustasy, subsidence, and sediment supply on Miocene sequences, mid-Atlantic margin of the United States. *Geological Society of America Bulletin* **118**, 567-588, doi:10.1130/b25551.1 (2006).

135 Wilson, L. E. A delphinid (Mammalia, Cetacea) from the Miocene of Palos Verdes Hills, California. *University of California Publications in Geological Sciences* **103**, 1-34 (1973).

136 Barnes, L. G. Evolution, taxonomy and antitropical distributions of the porpoises Phocoenidae, Mammalia). *Marine Mammal Science* **1**, 149-165 (1985).

137 Fajardo-Mellor, L., Berta, A., Brownell, R. L., Boy, C. C. & Natalie P. Goodall, R. The phylogenetic relationships and biogeography of true porpoises (Mammalia: Phocoenidae) based on morphological data. *Marine Mammal Science* **22**, 910-932, doi:10.1111/j.1748-7692.2006.00080.x (2006).

138 Xiong, Y., Brandley, M. C., Xu, S., Zhou, K. & Yang, G. Seven new dolphin mitochondrial genomes and a time-calibrated phylogeny of whales. *BMC Evol Biol* **9**, 20, doi:10.1186/1471-2148-9-20 (2009).

139 Chen, Z., Xu, S., Zhou, K. & Yang, G. Whale phylogeny and rapid radiation eventsrevealed using novel retroposed elements andtheir flanking sequences. *BMC Evolutionary Biology* **11**, 314 (2011).

140 Galatius, A. *et al.* Raising your voice: evolution of narrow-band high-frequency signals in toothed whales (Odontoceti). *Biological Journal of the Linnean Society* **126**, 213-224 (2019).

141 Rowell, H. C. in *The Monterey Formation and related siliceous ricks of California* (eds R. E. Garrison *et al.*) 56-70 (SEPM, 1981).

142 Boisserie, J.-R. *et al.* Basal hippopotamines from the upper Miocene of Chorora, Ethiopia. *Journal of Vertebrate Paleontology* **37**, doi:10.1080/02724634.2017.1297718 (2017).

143 Lihoreau, F., Boisserie, J. R., Manthi, F. K. & Ducrocq, S. Hippos stem from the longest sequence of terrestrial cetartiodactyl evolution in Africa. *Nat Commun* **6**, 6264, doi:10.1038/ncomms7264 (2015).

144 Zurano, J. P. *et al.* Cetartiodactyla: Updating a time-calibrated molecular phylogeny. *Mol*

Phylogenet Evol **133**, 256-262, doi:10.1016/j.ympev.2018.12.015 (2019).

145 Danowitz, M., Vasilyev, A., Kortlandt, V. & Solounias, N. Fossil evidence and stages of elongation of the Giraffa camelopardalis neck. *R Soc Open Sci* **2**, 150393, doi:10.1098/rsos.150393 (2015).

146 Samiullah, K. *et al.* A new discovery of a *Giraffokeryx* skull and associated fossil assemblage of Ruminants from the Middle Miocene deposits of the Siwaliks. *Historical Biology*, 1-25, doi:10.1080/08912963.2021.1946529 (2021).

147 Hamilton, W. R. Fossil giraffes from the Miocene of Africa and a revision of the phylogeny of the Giraffoidea. *Philosophical Transactions of the Royal Society B-Biological Sciences* **283**, 165-229 (1973).

148 Solounias, N. I. in *The evolution of artiodactyls* (eds D. R. Prothero & S. E. Foss) 257-277 (Johns Hopkins University Press, 2007).

149 Solounias, N. & Moelleken, S. M. C. Evidence for the presence of ossicones in *Giraffokeryx punjabiensis*. *Journal of Mammalogy* **72**, 215-217 (1991).

150 Barry, J. C., Johnson, N. M., Raza, S. M. & Jacobs, L. L. Neogene mammalian faunal change in southern Asia: correlations with climatic, tectonic, and eustatic events. *Geology* **13**, 637-640 (1985).

151 Bibi, F. A multi-calibrated mitochondrial phylogeny of extant Bovidae (Artiodactyla, Ruminantia) and the importance of the fossil record to systematics. *BMC Evolutionary Biology* **13**, 1-15 (2013).

152 Pilgrim, G. E. & Brown, B. Siwalik antelopes and oxen in the American Museum of Natural History. *Bulletin of the American Museum of Natural History* **72**, 729-874 (1937).

153 Bibi, F. Origin, paleoecology, and paleobiogeography of early Bovini. *Palaeogeography, Palaeoclimatology, Palaeoecology* **248**, 60-72, doi:10.1016/j.palaeo.2006.11.009 (2007).

154 Badgley, C. *et al.* Ecological changes in Miocene mammalian record show impact of prolonged climatic forcing. *Proc Natl Acad Sci U S A* **105**, 12145-12149, doi:10.1073/pnas.0805592105 (2008).

155 Haile-Selassie, Y., Vrba, E. S. & Bibi, F. in *Ardipithecus kadabba: Late Miocene Evidence from the Middle Awash, Ethiopia* (eds Y. Haile-Selassie & G. WoldeGabriel) 277-330 (University of California Press, 2007).

156 WoldeGabriel, G. *et al.* Geology and palaeontology of the Late Miocene Middle Awash valley, Afar rift, Ethiopia. *Nature* **412**, 175-178 (2001).

157 Renne, P. R., WoldeGabriel, G., Hart, W. K., Heiken, G. & White, T. D. Chronostratigraphy of the Miocene–Pliocene Sagantole Formation, Middle Awash Valley, Afar rift, Ethiopia. *GSA Bulletin* **111**, 869-885 (1999).

158 Geraads, D. *et al.* New hippotragini (Bovidae, Mammalia) from the Late Miocene of Toros-Menalla (Chad). *Journal of Vertebrate Paleontology* **28**, 231-242, doi:10.1671/0272-4634(2008)28[231:Nhbmft]2.0.Co;2 (2008).

159 Lebatard, A. E. *et al.* Cosmogenic nuclide dating of Sahelanthropus tchadensis and Australopithecus bahrelghazali: Mio-Pliocene hominids from Chad. *Proc Natl Acad Sci U S A*

105, 3226-3231, doi:10.1073/pnas.0708015105 (2008).

160 Gentry, A. W. Fossil Bovidae (Mammalia) from Langebaanweg, South Africa. *Annals of the South African Museum* **79**, 213-337 (1980).

161 Vrba, E. S. New fossils of Alcelaphini and Caprinae (Bovidae: Mammalia) from Awash, Ethiopia, and phylogenetic analysis of Alcelaphini. *Palaeont. afr.* **34**, 127-198 (1997).

162 Faith, J. T., Choiniere, J. N., Tryon, C. A., Peppe, D. J. & Fox, D. L. Taxonomic status and paleoecology of Rusingoryx atopocranion (Mammalia, Artiodactyla), an extinct Pleistocene bovid from Rusinga Island, Kenya. *Quaternary Research* **75**, 697-707, doi:10.1016/j.yqres.2010.11.006 (2017).

163 Roberts, D. L. *et al.* Regional and global context of the Late Cenozoic Langebaanweg (LBW) palaeontological site: West Coast of South Africa. *Earth-Science Reviews* **106**, 191-214, doi:10.1016/j.earscirev.2011.02.002 (2011).

164 Adrover, R., Alcalá, L., Paricio, J., Mein, P. & Moissenet, F. Dos nuevos yacimientos de vertebrados terciarios continentales: La Roma II (Alfambra, Teruel) y Búnker de Valdecebro (Teruel). *Teruel* **67**, 7-21 (1982).

165 Alcalá, L. *Macromammíferous neógenos de la fose de Alfambra-Teruel*. (Instituto de Estudios Terulenses-Museo National de Ciencias Naturales, 1994).

166 Alcalá, L. & Morales, J. A primitive caprine from the Upper Vallesian of La Roma 2 (Alfambra, Teruel, Aragon, Spain). *Comptes Rendus de l'Académie des Sciences - Series IIA - Earth and Planetary Science* **324**, 947-953 (1997).

167 Vrba, E. S. & Schaller, G. *Antelopes, deer, and relatives: fossil record, behavioral ecology, systematics, and conservation*. (Yale University Press, 2000).

168 Van Dam, J. A. *et al.* The upper Miocene mammal record from the Teruel-Alfambra region (Spain). The MN system and continental stage/age concepts discussed. *Journal of Vertebrate Paleontology* **21**, 367-385, doi:10.1671/0272-4634(2001)021[0367:Tummrf]2.0.Co;2 (2001).

169 Hilgen, F. J., Lourens, L. J. & Van Dam, J. A. in *The Geologic Times Scale 2012* (eds F. M. Gradstein, J. G. Ogg, M. Schmitz, & G. Ogg) 923-978 (Elsevier, 2012).

170 Rössner, G. E. Odontologische und schädelanatomische Untersuchungen an Procervulus (Cervidae, Mammalia). *Münchner geowissenschaftliche Abhandlungen, Reihe A* **29**, 1-127 (1995).

171 Rössner, G. E. Systematics and palaeoecology of Ruminantia (Artiodactyla, Mammalia) from the Miocene of Sandelzhausen (southern Germany, Northern Alpine Foreland Basin). *Paläontologische Zeitschrift* **84**, 123-162, doi:10.1007/s12542-010-0052-2 (2010).

172 Agustí, J. *et al.* A calibrated mammal scale for the Neogene of Western Europe. State of the art. *Earth-Science Reviews* **52**, 247-260, doi:https://doi.org/10.1016/S0012-8252(00)00025-8 (2001).

173 Costeur, L. A partial skull of *Dremotherium feignouxi* from the Aquitanian of France (MN2, Saint-Gérand-le-Puy, Allier). *Acta Geologica Slovaca* **3**, 105-111 (2011).

174 Janis, C. M. & Scott, K. M. The interrelationships of higher ruminant families: with special emphasis on the members of the Cervoidea. *American Museum Novitates* **2893**, 1-85 (1987).

175 Fordyce, R. E. & Marx, F. G. The pygmy right whale Caperea marginata: the last of the cetotheres. *Proceedings. Biological sciences / The Royal Society* **280**, 20122645, doi:10.1098/rspb.2012.2645 (2013).

176 Fordyce, E. New specimen of archaic baleen whale Mauicetus parki (Late Oligocene, New Zealand) elucidates early crown-mysticeti. *Journal of Vertebrate Paleontology* **25**, 58A-58A (2005).

177 Marx, F. G. & Fordyce, R. E. Baleen boom and bust: a synthesis of mysticete phylogeny, diversity and disparity. *R Soc Open Sci* **2**, 140434, doi:10.1098/rsos.140434 (2015).

178 Lloyd, G. T. & Slater, G. J. A total-group phylogenetic metatree for Cetacea and the importance of fossil data in diversification analyses. *Syst Biol*, doi:10.1093/sysbio/syab002 (2021).

179 Graham, I. J., Morgans, H. E., Waghorn, D. B., Trotter, J. A. & Whitford, D. J. Strontium isotope stratigraphy of the Oligocene-Miocene Otekaike Limestone (Trig Z section) in southern New Zealand: age of the Duntroonian/Waitakian Stage boundary. *New Zealand Journal of Geology and Geophysics* **43**, 335-347 (2000).

180 Marx, F. G. & Kohno, N. A new Miocene baleen whale from the Peruvian desert. *R Soc Open Sci* **3**, 160542, doi:10.1098/rsos.160542 (2016).

181 Kellogg, R. Two physeteroid whales from California. *Contributions to Palaeontology from the Carnegie Institution of Washington* **348**, 1-35 (1925).

182 Collareta, A., Lambert, O., de Muizon, C., Urbina, M. & Bianucci, G. Koristocetus pescei gen. et sp. nov., a diminutive sperm whale (Cetacea: Odontoceti: Kogiidae) from the late Miocene of Peru. *Fossil Record* **20**, 259-278, doi:10.5194/fr-20-259-2017 (2017).

183 Kapur, V. V. & Bajpai, S. Oldest South Asian tapiromorph (Perissodactyla, Mammalia) from the Cambay Shale Formation, western India, with comments on its phylogenetic position and biogeographic implications. *The Palaeobotanist* **64**, 95-103 (2015).

184 Bai, B., Meng, J., Janis, C. M., Zhang, Z. Q. & Wang, Y. Q. Perissodactyl diversities and responses to climate changes as reflected by dental homogeneity during the Cenozoic in Asia. *Ecology and Evolution* **10**, 6333-6355 (2020).

185 Sato, J. J. *et al.* Deciphering and dating the red panda's ancestry and early adaptive radiation of Musteloidea. *Molecular Phylogenetics and Evolution* **53**, 907-922 (2009).

186 Wolsan, M. & Lange-Badré, B. An arctomorph carnivoran skull from the Phosphorites du Quercy and the origin of procyonids. *Acta Palaeontologica Polonica* **41**, 277-298 (1996).

187 Sato, J. J. *et al.* Phylogenetic relationships and divergence times among mustelids (Mammalia: Carnivora) based on nucleotide sequences of the nuclear interphotoreceptor retinoid binding protein and mitochondrial cytochrome b genes. *Zoological Science* **20**, 243-264 (2003).

188 Vandenberghe, N., Hilgen, F. J. & Speijer, R. P. in *The geologic timescale 2012* (eds F. M. Gradstein, J. G. Ogg, M. Schmitz, & G. Ogg) 855-921 (Elsevier, 2012).

189 Werdelin, L., Yamaguchi, N., Johnson, W. E. & O'Brien, S. J. Phylogeny and evolution of cats (Felidae). *Biology and conservation of wild felids*, 59-82 (2010).

190 Flynn, J. J. & Wesley-Hunt, G. D. in *The rise of placental mammals: origins and relationships of*

the major extant clades (eds K. D. Rose & J. D. Archibald) 175-198 (Johns Hopkins University Press, 2005).

191 Hunt Jr, R. M. Evolution of the aeluroid Carnivora. Diversity of the earliest aeluroids from Eurasia (Quercy, Hsanda-Gol) and the origin of felids. American Museum novitates; no. 3252. (1998).

192 Barycka, E. Evolution and systematics of the feliform Carnivora. *Mammalian Biology* **72**, 257-282 (2007).

193 Phillips, M. J. & Fruciano, C. The soft explosive model of placental mammal evolution. *BMC Evol Biol* **18**, 104, doi:10.1186/s12862-018-1218-x (2018).

194 Janis, C. M., Damuth, J. & Theodor, J. M. Miocene ungulates and terrestrial primary productivity: where have all the browsers gone? *Proceedings of the National Academy of Sciences* **97**, 7899-7904 (2000).

195 Patou, M.-L. *et al.* Phylogenetic relationships of the Asian palm civets (Hemigalinae & Paradoxurinae, Viverridae, Carnivora). *Molecular Phylogenetics and Evolution* **47**, 883-892 (2008).

196 Hunt Jr, R. M. Evolution of the aeluroid Carnivora. Viverrid affinities of the Miocene carnivoran Herpestides. American Museum novitates; no. 3023. (1991).

197 Gaubert, P. & Cordeiro-Estrela, P. Phylogenetic systematics and tempo of evolution of the Viverrinae (Mammalia, Carnivora, Viverridae) within feliformians: implications for faunal exchanges between Asia and Africa. *Molecular Phylogenetics and Evolution* **41**, 266-278 (2006).

198 Fulton, T. L. & Strobeck, C. Multiple fossil calibrations, nuclear loci and mitochondrial genomes provide new insight into biogeography and divergence timing for true seals (Phocidae, Pinnipedia). *Journal of Biogeography* **37**, 814-829 (2010).

199 Govender, R. Preliminary phylogenetics and biogeographic history of the Pliocene seal, Homiphoca capensis from Langebaanweg, South Africa. *Transactions of the Royal Society of South Africa* **70**, 25-39 (2015).

200 Govender, R. Fossil cetaceans from Duinefontein (Koeberg) an early Pliocene site on the southwestern Cape, South Africa. *Palaeontologia Electronica* **22**, 1-21 (2019).

201 Roberts, D. L. *et al.* Regional and global context of the Late Cenozoic Langebaanweg (LBW) palaeontological site: West Coast of South Africa. *Earth-Science Reviews* **106**, 191-214 (2011).

202 Dewaele, L., Lambert, O. & Louwye, S. A critical revision of the fossil record, stratigraphy and diversity of the Neogene seal genus Monotherium (Carnivora, Phocidae). *R Soc Open Sci* **5**, 171669, doi:10.1098/rsos.171669 (2018).

203 Ray, C. E. Geography of phocid evolution. *Systematic Zoology* **25**, 391-406 (1976).

204 Repenning, C., Ray, C. & Grigorescu, D. (Oregon State University Press, Corvallis, OR, 1979).

205 Deméré, T. A., Berta, A. & Adam, P. J. Chapter 3: Pinnipedimorph evolutionary biogeography. *Bulletin of the American Museum of Natural History*, 32-76 (2003).

206 Yonezawa, T., Kohno, N. & Hasegawa, M. The monophyletic origin of sea lions and fur seals (Carnivora; Otariidae) in the Southern Hemisphere. *Gene* **441**, 89-99 (2009).

207 Deméré, T. A. & Berta, A. A reevaluation of Proneotherium repenningi from the Miocene Astoria Formation of Oregon and its position as a basal odobenid (Pinnipedia: Mammalia). *Journal of Vertebrate Paleontology* **21**, 279-310 (2001).

208 Berta, A. in *Encyclopedia of marine mammals* 712-722 (Elsevier, 2018).

209 Barnes, L. G. An early Miocene pinniped of the genus Desmatophoca (Mammalia: Otariidae) from Washington. *Contributions in Science* **382**, 1-20 (1987).

210 Berta, A. New Enaliarctos (Pinnipedimorpha) from the Oligocene and Miocene of Oregon and the role of "enaliarctids" in pinniped phylogeny. (1991).

211 Norris, R. Phylogenetic relationships and divergence times in rodents based on both genes and fossils. (2009).

212 Storch, G. & Seiffert, C. Extraordinarily preserved specimen of the oldest known glirid from the middle Eocene of Messel (Rodentia). *Journal of Vertebrate Paleontology* **27**, 189-194 (2007).

213 Verzi, D. H. & Quintana, C. A. The caviomorph rodents from the San Andrés Formation, east-central Argentina, and global Late Pliocene climatic change. *Palaeogeography, Palaeoclimatology, Palaeoecology* **219**, 303-320 (2005).

214 Teruggi, M. E., Andreis, R. R., Mazzoni, M. M., Dalla Salda, L. H. & Spalletti, L. A. in *Anales del LEMIT.*

215 Patterson, B. D. & Upham, N. S. A newly recognized family from the Horn of Africa, the Heterocephalidae (Rodentia: Ctenohystrica). *Zoological Journal of the Linnean Society* **172**, 942-963 (2014).

216 West, A. R. *Multidisciplinary investigations on the origins and evolution of the extinct ungulate order Notoungulata (Mammalia: Placentalia) and the extinct muskox genus Bootherium (Mammalia: Artiodactyla: Bovidae)*. (Columbia University, 2017).

217 Verzi, D. H., Olivares, A. I., Morgan, C. C. & Álvarez, A. Contrasting phylogenetic and diversity patterns in octodontoid rodents and a new definition of the family Abrocomidae. *Journal of Mammalian Evolution* **23**, 93-115 (2016).

218 Woodburne, M. O. & Tedford, R. H. The first Tertiary monotreme from Australia. *American Museum Novitates* **2588**, 1-11 (1975).

219 Poropat, S. F. *et al.* Early Cretaceous polar biotas of Victoria, southeastern Australia—an overview of research to date. *Alcheringa: An Australasian Journal of Palaeontology* **42**, 157-229, doi:10.1080/03115518.2018.1453085 (2018).

220 Seegets-Villiers, D. E. & Wagstaff, B. E. Morphological variation of stratigraphically important species in the genus *Pilosisporites* Delcourt & Sprumont, 1955 in the Gippsland Basin, southeastern Australia. *Memoirs of Museum Victoria* **74**, 81-91 (2016).

221 Holdgate, G. R., Wallace, M. W. & Forbes, S. Pre-Cenozoic geology of the Latrobe Valley Area—onshore Gippsland Basin, S.E. Australia. *Australian Journal of Earth Sciences*, 1-22, doi:10.1080/08120099.2015.1085901 (2015).

222 Musser, J. M. in *Evolution and biogeography of Australasian vertebrates* (eds J. Merrick, M. Archer, G. Hickey, & M. S. Y. Lee) 523-550 (Auscipub, 2006).

223 Pian, R., Archer, M., Hand, S. J., Beck, R. M. & Cody, A. The upper dentition and relationships of the enigmatic Australian Cretaceous mammal Kollikodon ritchiei. *Memoirs of Museum Victoria* **74**, 97-105 (2016).

224 Tedford, R., Wells, R. & Barghoorn, S. Tirari formation and contained faunas, Pliocene of the Lake Eyre basin, South Australia. *Beagle: Records of the Museums and Art Galleries of the Northern Territory, The* **9**, 173-193 (1992).

225 Mackness, B., Wroe, S., Muirhead, J., Wilkinson, C. & Wilkinson, D. First fossil bandicoots from the Pliocene. *Australian Mammalogy* **22**, 133-136 (2000).

226 Dawson, L. A new Pliocene tree kangaroo species (Marsupialia, Macropodinae) from the Chinchilla Local Fauna, southeastern Queensland. *Alcheringa* **28**, 267-273 (2004).

227 Gibbard, P. L. & Head, M. J. in *Geologic Time Scale 2020* Vol. 2 (eds F. M. Gradstein, J. G. Ogg, Schmitz. M. D., & G. M. Ogg) 1217-1255 (Elsevier, 2020).